Digital HF communications

for autonomous instrumentation in the polar regions

Thesis submitted for the degree of
Doctor of Philosophy
at the University of Leicester

by

Michael Prior-Jones, MEng (York)
Department of Engineering,
University of Leicester

October 2010

Abstract

Autonomous instrumentation is used to collect scientific data in very remote locations, especially in the polar regions. Retrieving data from these instruments is often done by the use of satellite communications or by manual retrieval, the latter often requiring the use of an aircraft. This research focussed on the use of HF radio (i.e frequencies of 3-30MHz) as a cheaper technology for data communications in the polar regions and concentrated on three main areas of work:

- the development of a channel simulator for high-latitude HF channels based on work by Warrington, Siddle and Stocker (2006) and using it for performance tests of existing HF modems
- work on HF modem waveforms, including Polynomial Cancellation Coding OFDM (PCC-OFDM) and conventional OFDM, to try and create waveforms suitable for the more demanding high-latitude channels
- an oblique propagation study using an OFDM waveform between Halley and Rothera stations in Antarctica, a 1600km sub-auroral link run for twelve months close to solar minimum.

This work has shown that existing military HF modems (MIL-STD-188-110B) perform reasonably well in all but the most demanding high-latitude HF channels simulated. The oblique propagation study showed that a total annual data volume of around 400MB could be transmitted over the Halley-Rothera link, showing that HF can carry sufficient data to be useful for data retrieval. Data volumes were at their highest in the austral summer, but limited communications were possible year-round.

Acknowledgements

I have been fortunate over the course of the last three years to have a large number of people give of their time and expertise to assist me in my work.
I would particularly like to thank Mike Pinnock, Mike Rose and Chris Hill for their encouragement and support during the whole project. I am also grateful for assistance from many other people at BAS, including Alan Rodger, Hoc Ewing, Beverley Gummer, Alison Teague and Peter Fretwell. The Halley and Rothera communications managers were invaluable in installing equipment in Antarctica, so my particular thanks go to Mike Clarke, Ian Sisson, Andrew Webster and Karen Fowler for all their help. Considerable thanks are also due to Mike Warrington for his support and assistance as my academic supervisor.
Section 3.2 contains material supplied by Dr Janusz Mlynarczyk of the AGH Technical University in Krakow, and I extend to him my profound thanks for all his assistance.
Most of the work described in Chapter 5 was carried out at the Communications Research Centre in Ottawa, and I am extremely grateful to all the CRC staff for making me so welcome and allowing me the use of their laboratory and equipment. In particular I should like to thank Tricia Willink, Nur Serinken, Don Haines, Sergei Bantseev and Benoit Gagnan. I would also like to thank Mark Jorgenson at Rockwell-Collins and Bill Furman at Harris.
The T Index data in chapter 6 was supplied by Dave Neudegg, Garth Patterson and Phil Wilkinson at the Ionospheric Prediction Service in Sydney, Australia, and I would like to thank them for their valuable assistance.
I would like to express my gratitude to Jonathan Stott, Andrew Murphy and Oliver Haffenden of the BBC and also to James Briggs of VT Merlin Communications for their information on the finer points of OFDM and the DRM standard.
I should also thank Jean Armstrong and Kusha Panta for information on PCC-OFDM.
My thanks are also extended to Paul Cannon, Matt Angling and David Brown at Qinetiq for their advice and for the loan of two modems.
I must also give considerable thanks to Francesco Lanza for supplying the source code to the WinDRM software, and for all his hard work in developing it.

Personal thanks are due to a large number of friends and colleagues who have supported me over the last three years, but I should particularly like to thank Mike Lee and my parents, Bill and Christine Prior-Jones, for listening to my rants with such patience.

Finally, I must extend thanks to NERC and the Royal Academy of Engineering (and through them the taxpayers of the UK) for funding my research.

“To the taxpayer, who made it all possible!” - Sir Vivian Fuchs

Contents

1. Introduction

Scientists working in the polar regions have collected time-series measurements since the earliest expeditions. These series are invaluable for research, but are extremely expensive to collect, especially where data is collected manually by staff living on a research station. With improvements in instrumentation technology and the development of solid-state digital storage media, it is possible to make measurements in remote locations using autonomous instrument platforms, which are capable of making several years' measurements without any manual intervention.

Retrieving the data from these instrument platforms can be difficult. Satellite communications systems capable of working at the poles are expensive and offer limited bandwidth, so many instruments have a regular "servicing visit" from a technician. This visit involves checking that the instrument is in working order and changing the memory card on which the data is stored. These visits usually require the use of an aircraft, making them expensive, and there is no way of checking on the operation of the instrument between visits.

This project was proposed as a result of seeing how HF radio ("High Frequency", i.e. 3-30MHz) is successfully used for voice communications in Antarctica. With good propagation conditions, field parties using portable transceivers are capable of communicating with a manned research station over distances of at least 2000km. It was therefore suggested that HF might be used for data communications with autonomous instrument platforms in a similar manner.

However, since HF signals propagate via the ionosphere, steps would need to be taken to mitigate the effects of the rapidly-changing high-latitude ionosphere on the received signal. Power consumption was also identified as a key issue, since autonomous platforms must provide their own electricity from solar panels and wind generators.

Early in the project it was recognized that implementing a complete system was unlikely to be achievable with the time and resources available, so this thesis presents several important components that lead towards a complete system.

Chapter 2 introduces the different kinds of communications technology that can be used in the polar regions, and explains why HF has been chosen as the subject for this study.

Chapter 3 then explains the physics behind the high-latitude ionosphere and how HF radio waves propagate through it.

Chapter 4 gives the requirements for a communications system for autonomous instrument platforms in the polar regions, introduces some of the possible techniques that may be used, and goes on to develop an outline design for such a system.

The next three chapters present the practical work that has been done to work towards this system design. Chapter 5 describes the development of a high-latitude HF channel simulator and gives the results of performance tests of several different modems carried out using it. Chapter 6 gives an account of an oblique-propagation study carried out in Antarctica using WinDRM as a testbed, and gives an indication as to how much data may reasonably be carried by such a system over the course of a year. Finally, in chapter 7, the results are summarized, conclusions drawn and recommendations made for future work.

2. Communications technology for the polar regions

2.1. Historical background

Radio communication is a vital part of modern polar exploration and research, not least because it provides a way to summon help in an emergency. The earliest polar expeditions were undertaken without it, and explorers would leave each other hand-written messages in caches (Cherry-Garrard 1922).

The first radio system in Antarctica was installed in 1912, by the Australian scientist and explorer Douglas Mawson. His expedition established radio stations (using 1kW spark transmitters operating at 100kHz) at the Commonwealth Bay base in Adelie Land and on Macquarie Island, the latter acting as a relay station to Sydney (Mawson 1914).

HF was first used in Antarctica on the Wilkins-Hearst expedition in 1928 (Wilkins 1929) and much more extensively on the first US Antarctic Expedition, led by Richard Byrd that same year. Byrd's team included five radio engineers and a total of 24 transmitters and 31 receivers, and maintained regular contact with the outside world as well as with all flights and field parties (Byrd 1931).

The Royal Navy's "Operation Tabarin" established the first permanent British Antarctic bases in 1943. These communicated with the Government offices in Stanley (in the Falkland Islands) using HF. All communication between the bases and Stanley was in Morse code, with messages being forwarded on from Stanley by telegram. British bases were upgraded to use radiotelex instead of Morse in the 1960s, and first gained satellite connectivity in the early 1980s.

2.2. Types of radio link used in the polar regions

2.2.1. Line-of-sight links

Radio waves at frequencies above 30MHz – such as VHF radio, cellular phone systems and microwave links - propagate by line-of-sight from transmitter to receiver, and are thus constrained by the landscape. A single VHF repeater station on a mountaintop may provide communications over a radius of as much as 100km, but using this technology for long distance communications involves establishing a chain of repeaters, which for best coverage may need to be on mountaintops only accessible by expensive helicopter operations. This is particularly impractical in most of Antarctica, where the terrain is almost entirely flat, and crevasse fields and snow accumulation restrict the possibility of erecting masts for repeater stations in remote regions.

2.2.2. Tropospheric scatter communications

Turbulent mixing in the troposphere can produce irregularities that scatter radio waves. This scattering permits communications beyond the horizon: a powerful signal is directed into the scattering region, where a small percentage of the power is scattered forward towards a highly sensitive receiver. The received signal power increases with the size of the scattering volume. Using high gain antennas will reduce the beamwidth and hence the scattering volume, so these systems use antennas with moderate gain and very powerful transmitters. Tropospheric scatter (troposcatter) may be operated from 300MHz to 3GHz or more, and was used to provide secure military communications before the advent of satellites, such as the links between the Distant Early Warning Line radar stations in the Canadian Arctic (Strom and Kunze 1959).

The major disadvantage of troposcatter is the need for very powerful transmitters and very large receiving antennas in order to obtain good performance (Raab et al. 2002).

For example, the AN/TRC-170 tactical troposcatter system used by the US military ((US Marine Corps n.d.) requires over 10kW of electrical power for a maximum link range of 100 nautical miles (=185km). Such power consumption is well beyond the capacity of any field-deployable renewable energy system.

2.2.3. Ionospheric scatter communications

Radio waves at low VHF frequencies (around 50MHz) are scattered by irregularities at the boundary between the D and E layers of the ionosphere. This effect may also be used for communications links - in a similar manner to troposcatter - and has the same shortcomings (Hunsucker and Hargreaves 2003).

2.2.4. Meteor burst communications

Meteors burning up in the atmosphere cause intense ionisation at around 80-100 km altitude. Short-lived trails of ionisation are produced by each meteor, but the ionisation is sufficiently intense to allow VHF radio waves to propagate beyond the horizon. The ionisation from each meteor typically lasts a few seconds but will support relatively high data rates while it lasts.

Meteor burst communications (MBC) systems use a regular probing transmission to look for channel openings, and then switch to data mode as soon as they get a reply from the other end of the link. MBC uses reasonably high power outputs – military systems use 1kW or more.

A joint Chinese-Japanese project (Mukumoto et al. 2005) operated an MBC system at 43MHz over a 1400km link between Zhongshan and Syowa stations in Antarctica. The link used 150W transmitters although the actual output power was less due to the loss in the long antenna feeders. At high latitudes, VHF propagation can often be due to sporadic-E formation (an explanation of sporadic-E can be found in Section 3.1.1) as

well as meteor burst, and the results of this study show a marked increase in throughput at night, which is consistent with this. Their best performance in terms of daily data throughput was around 30 kilobytes per day (≡10MB/yr).

2.2.5. Geostationary satellite systems

A satellite in geostationary orbit always appears to be at the same point in the sky from the point of view of a ground station, meaning that no tracking mechanism is required. The orbit is above the equator at an altitude of around 36,000km, and this produces a geometric limit on their coverage area – there is no coverage poleward of 81 degrees, and if the satellite and earth station are at significantly different longitudes then the polar coverage will be even less. This geometric limit rules out the use of geostationary satellite for communications at very high latitudes.

2.2.6. Low Earth orbit satellite systems

Satellites in low Earth orbit (LEO) – at altitudes of around 300km – appear to move across the sky and are in view for around ten minutes on each pass. In the 1990s, several companies attempted to develop telephone systems using constellations of LEO satellites, and two were successful – Iridium and Globalstar. The Globalstar satellites need to be in range of a ground station to operate, so their coverage in the polar regions is limited. Iridium offers coverage of the whole planet including both poles using a constellation of 66 satellites.

Iridium offers three data services:

- Short burst data (SBD), a message-based service typically carrying 340 bytes per message and billed by the byte
- Dial-up data, offering a two-way dial-up connection at 2400bits/s, billed by the minute

- OpenPort, an always-on streamed connection at speeds of up to 128kbit/s, billed by the megabyte.

Another LEO system, ARGOS, is popular where a miniature terminal is needed (e.g. animal tracking). ARGOS terminals send 32 byte messages, which are then stored on board the satellite and forwarded on when next passing a ground station. ARGOS terminals are transmit-only, although bidirectional communications will be possible once the ARGOS-3 system goes into operation.

2.2.7. HF radio

HF radio signals can propagate beyond line of sight, as will be described in detail in Chapter 3. This allows HF networks to operate over long ranges with modest power outputs, making HF attractive for use in the polar wilderness. HF equipment is relatively inexpensive and, unlike satellite, there are no airtime charges.

A typical polar HF communications system consists of a base station making regular scheduled contacts with several field stations. Base stations are equipped with large antennas and powerful radios (at least 100W) and manned by a dedicated radio operator. Field stations generally have portable radios with simple antennas and are operated by non-specialist personnel. A typical field-portable radio produces around 25W PEP (Peak Envelope Power) and runs from batteries, usually recharged from a solar panel.

Primarily HF is used with single sideband modulation to provide voice communications, but it has also been used for data, albeit at low data rates. Various commercial systems have been used – the British Antarctic Survey (BAS) used PACTOR modems in the past, and the Australian Antarctic Division currently use them for a short link (65km) between Wilkins and Casey stations (Yates 2008). The Italian Antarctic programme used a Rohde & Schwarz ALIS system for communications

between Rome and Terra Nova Bay in the early 1990s (Blasi and de Simone 1992). Newer HF modem technologies (see Section 4.4) have the potential to offer data rates of up to 2400 bits/s (comparable with dial-up Iridium) without the high airtime charges.

2.3. Satellite airtime costs

Tariffs of airtime charges vary between satellite systems, but often consist of a monthly standing charge and then a usage charge on top. Some example costs are given in Table 1. To give a fair comparison, these show the annual total cost.

Typical application	Annual data volume	Equivalent monthly data volume, MB	Satellite system	Total annual cost, US dollars
Weather station	3MB	0.25	Iridium SBD	$4,695
			ARGOS	$1,812
			Iridium dialup	$339
			Iridium OpenPort	$21
Magnetometer	300MB	25	Iridium dialup	$17,268
			Iridium OpenPort	$1,950
High resolution GPS	3GB	256	Iridium OpenPort	$16,404

Table 1 - example costs of satellite airtime

Iridium dialup has been used for high-latitude data communications since its launch in the mid-1990s. Its $1/min charge for 2400bit/s is equivalent to $57 per megabyte, making it prohibitively expensive for applications requiring large volumes of data. OpenPort, with its lower per-megabyte charges and zero standing charge, is now the most cost-effective satellite solution, although the terminals are bulky and not suitable for all applications.

2.4. Concluding remarks

For this project it was decided to concentrate on the feasibility of using HF radio for high-latitude data communications. HF avoids the high airtime charges of satellite and potentially offers a better total daily data throughput than meteor burst. Troposcatter and ionoscatter were considered too bulky and power-hungry.

HF radio is already widely used in the polar regions for voice communications, but rarely for data. HF data modems have a reputation for being slow, which led to them being disregarded by polar scientists in favour of satellite systems. However, dial-up Iridium is commonly used, and only offers speeds of 2400 bit/s (full duplex), so any HF modem approaching this speed could potentially be a competitor.

Table 2 - existing HF modems

Modem	Date introduced	Notes
Clover-2000	1995	"up to 3000bits/s", Reed-Solomon forward error correction (FEC)
PACTOR-III	2002	Up to 2700bits/s, FEC not published
MIL-STD-188-110B	2000	Up to 9600 bits/s, convolutional FEC

Table 2 shows the existing modem standards on the market. The two commercial standards, Clover-2000 and Pactor-III, both have their top end speeds listed as around 3000bits/s. This will be their best performance under optimum conditions, so their throughput in real polar HF channels is likely to be much less. MIL-STD-188-110B represents the state-of-the-art in HF modems, but communications technology has

advanced considerably since 2000 – more effective coding schemes (such as Turbo-codes, LDPC and Raptor) are available and modulation and equalisation techniques have also been refined. There is clearly scope for developing a faster and/or more robust HF modem for the polar regions and attempts to move towards this aim will be described in subsequent chapters.

3. Physics of ionospheric radio

HF radio depends upon the ionosphere in order to propagate beyond the horizon. This chapter introduces the physics of the ionosphere and considers how the particular environment of the high-latitude ionosphere affects HF communications in the polar regions.

3.1. The ionosphere at high latitudes

Air in the Earth's upper atmosphere is exposed to solar radiation (particularly ultraviolet and soft X-rays) and energetic charged particles, and these have sufficient energy to ionise the gas molecules. The result is a plasma known as the ionosphere, although since the ions and electrons are constantly recombining, less than 1% of the air is actually ionised (Rishbeth 1988). The level of ionisation of the plasma is expressed as the number of electrons per unit volume, which is usually referred to as *electron density* or *electron number density* (although more strictly it should be *electron concentration* or *electron number concentration*), and which is typically between 10^8 and 10^{12} electrons per cubic metre (Hunsucker and Hargreaves 2003, pp 13-14.).

3.1.1. Ionisation mechanisms

The ionosphere ranges from 60 – 800km above the Earth, and observations of electron density (such as ionograms, discussed in section 3.2.1) show that it forms three layers at different altitudes, known as the D region (60-90km), E region (90-150km) and F region (150-800km). These layers are produced by different wavelengths of solar radiation – the F region is formed by 'soft' (i.e. long wavelength) ultraviolet radiation, whereas the E and D regions are produced by shorter wavelength UV and X-rays. (Hunsucker and Hargreaves 2007, 26, 31)

However, at high geomagnetic latitude (i.e. close to the magnetic poles), the Earth's magnetic field lines make connections with the interplanetary magnetic field (IMF). This provides a path for energetic charged particles from the Sun to be drawn into the Earth's atmosphere along the magnetic field lines and cause ionisation. These same energetic particles are also responsible for forming the visual and sub-visual[1] aurora, and they produce localised enhancements of the E-region, known as auroral sporadic-E (E_s). Sporadic-E can form by other mechanisms – it can be produced by wind shear, and at low latitudes by the equatorial electrojet. (Hunsucker and Hargreaves 2007, 28–29)

3.1.2. The auroral oval

Auroras form in an annular region known as the auroral oval. The annulus is centred close to the geomagnetic pole, and is narrowest on the side facing the Sun (i.e. local noon) and widest on the opposite side – at local midnight. Under quiet geomagnetic conditions, the aurora reaches to around 67 degrees geomagnetic at midnight, but only to 77 degrees geomagnetic at noon (Hunsucker and Hargreaves 2003, 286-288). Geomagnetic storms (see section 3.1.3) will cause the auroral oval to enlarge, reaching further towards the equator. Images of the auroral oval taken from the NOAA POES satellite are shown in Figure 1. The red arrow indicates the position of the Sun, showing clearly how the oval remains in a fixed position in the Sun-Earth frame of reference and does not co-rotate with the Earth. Because of this, and because the oval is not centred on the geographic or geomagnetic pole, observations of phenomena affected by the aurora made at one location do not translate easily to another location at the same latitude but a different longitude (Cannon 1989).

[1] "sub-visual aurora" means that an aurora that is not visible to the human eye, but may be detected by other means.

Radio waves propagating through the auroral oval can suffer significant attenuation, known as *auroral absorption (*see section 3.2.7). For the propagation study described in chapter 6, the path between Halley and Rothera is sub-auroral under quiet geomagnetic conditions, but a modest enhancement to the auroral zone will bring the Halley end of the circuit into the auroral zone.

The high-latitude ionosphere is commonly divided into three regions: the auroral oval itself, the area within the centre of the annulus (known as the polar cap) and the area immediately outside the oval. This last area often has an exceptionally low electron density and is known as the *main trough*[2]. The trough varies considerably in width (Hunsucker and Hargreaves (2003) go so far as to say that there is "no general agreement" as to its width and depth, though 500-1000km is not uncommon) and is most commonly seen on the night-side, although it has been observed at all local times. Equatorward of the trough is the "normal" mid-latitude ionosphere.

HF radio circuits in the polar regions are classified geographically based on their position relative to the auroral oval: polar cap circuits lie within the polar cap; transauroral circuits cross the auroral oval and sub-auroral circuits remain outside the oval.

[2] The main trough is often called the mid-latitude trough

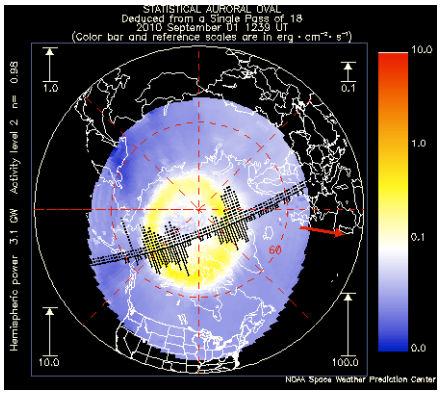

1239UT

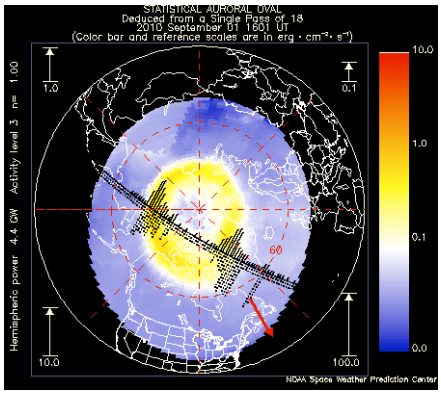

1601UT

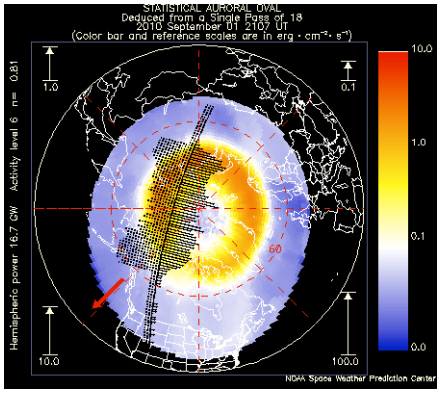

2107UT

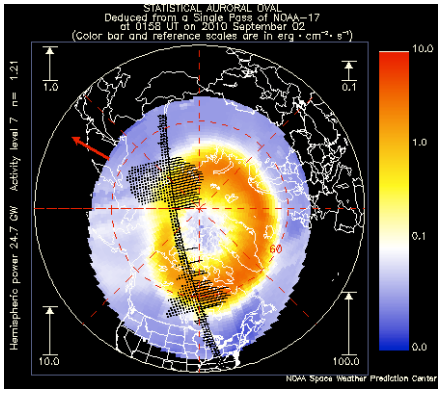

0158UT

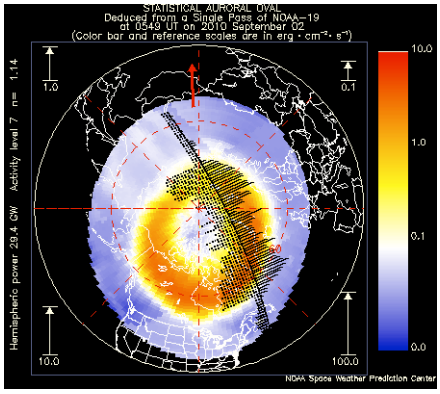

0549UT

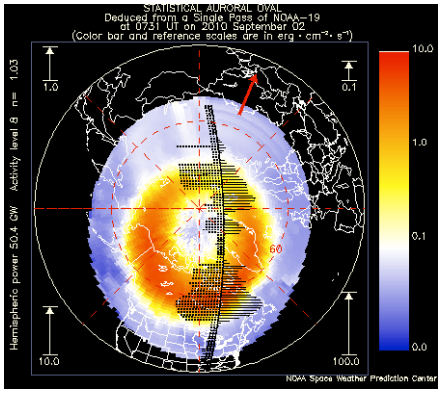

0731UT

Figure 1 – the northern auroral oval (in yellow/orange) at various points over the night of 1st/2nd September 2010. The images are from the NOAA POES satellite. The northern auroral oval was chosen for this example as it was expected that the reader was more likely to be familiar with the geography of the Arctic than the Antarctic. The colour scale is in ergs per square centimetre per second (1 erg/cm^2/s

≡ 1mJ / m^2/s ≡ 1mW/m^2). Black areas were excluded from the data processing. The red arrow points towards the noon meridian. The black solid line shows the track of the satellite, with plots each side of it representing the energy flux observed. The solid-line bars (to the right of the satellite track in the 0731 plot) show the total energy flux at that point in the satellite's orbit. The dotted-line bars (to the left of the satellite track in the 0731 plot) show the energy flux responsible for the auroral at that point in the orbit. The bars are plotted every 16 seconds, roughly 100km apart. The scales (in erg/cm^2/s) for these energy flux bars are in the corners of the plots. Images by permission of NOAA/US Department of Commerce.

3.1.3. Solar-terrestrial interactions

Changes in solar activity have a strong influence on the high-latitude ionosphere. Solar activity may be quantified by the observation of sunspots or the Sun's radio emissions at a frequency of 2.8GHz, and is generally seen to follow an 11-year cycle (Hargreaves 1995, 137). Enhanced solar activity produces increases in EM radiation, solar cosmic rays and solar wind, and all of these have an impact on the ionosphere when they reach the Earth.

In particular, the solar wind (a stream of plasma escaping from the Sun's corona) carries within it the interplanetary magnetic field (IMF), and changes in this field's interaction with the Earth's own magnetic field lead to movement of the auroral oval. These events are called *geomagnetic storms*, as the readings of magnetometers can be seen to fluctuate wildly under the Sun's influence. Strong geomagnetic storms lead to the enlargement of the auroral oval, bringing it closer to the equator (Hunsucker and Hargreaves 2007, 101). The solar wind travels relatively slowly and there may be up to 60 hours delay before a storm hits the Earth. However, the storm is preceded by a burst of faster-moving solar cosmic rays, typically protons and alpha-particles, which are drawn towards the polar cap region by the Earth's magnetic field and cause enhanced ionisation in the polar D-region. This is known as a polar cap absorbtion (PCA) event – see section 3.2.7.

3.1.4. Ionospheric irregularities

The simple description of the ionosphere in Section 3.1.1 suggests that it forms uniform layers, whereas in fact it is full of irregularities at scales from centimetres to hundreds of kilometres. One example is *polar patches*, described here.

During the polar winter, the ionosphere is observed to have a diurnal variation in electron density despite the fact that it receives no direct solar radiation. In fact, the interaction between the IMF and the Earth's magnetic field produce electric fields and currents that draw plasma from the dayside ionosphere across the polar cap and into the night-side (Rishbeth 1988). This drift across the polar cap is part of a broader circulation pattern, as plasma circulates back from night-side to day-side at lower latitudes. This is called *high-latitude convection* since the patterns resemble the convection patterns seem in fluids. The combination of this convection pattern and the rotation of the Earth is partly responsible for the formation of the main trough. Because the convection pattern is influenced by the orientation of the IMF, it changes its shape and velocity as the IMF changes. With the Bz component of the IMF pointing southward, this produces a simple two-cell convection pattern. If the Bz component of the IMF points northward, a more complex multicell pattern may form. A significant By component in the IMF will produce asymmetries in the pattern (Tsunoda 1988) This can lead to areas of highly ionised plasma building up in the dayside F-region and then being suddenly ripped across the polar cap as the convection pattern changes. These highly ionised areas are called *polar patches* and are typically observed in the polar winter night when solar activity is high. They are generally between 200km and 1000km in diameter and can have electron densities of up to ten times the normal background level for that region (Hunsucker and Hargreaves 2007, 245). Polar patches move rapidly (at up to 1000m/s) and will permit HF propagation at higher frequencies than normal for periods of tens of minutes until they move away from the circuit reflection point.

3.1.5. Sun-aligned arcs

The interaction of the Earth's magnetic field and the IMF can also produce a belt of visible aurora across the centre of the auroral oval, giving it the appearance of a Greek letter theta (θ). This is called *polar cap aurora*, *theta-aurora* or a *sun-aligned arc*, because the belt of aurora lies across the polar cap between noon and midnight. This effect is almost always present when the IMF is northward (Hunsucker and Hargreaves 2007, 302). Sun-aligned arcs are also associated with enhanced electron density in the polar cap E and F regions, producing electron densities 2-3 times greater than background (Zaalov, Warrington, and Stocker 2003).

3.2. Ionospheric radio propagation

This section takes a practical approach to describing HF radio propagation in the ionosphere, using the minimum of mathematics.

3.2.1. Ionosondes and vertically incident waves

An *ionosonde* is a form of radar used to study the ionosphere. In its simplest form, it sends a short pulse of radio waves at a given frequency vertically into the ionosphere and times how long it takes for the pulse to be reflected back. It repeats this process over a range of frequencies. The result of this process is an *ionogram*, a plot of round-trip-time (usually converted to an approximate range using the speed of light in a vacuum) against frequency. An example ionogram is given in Figure 2. What can be clearly seen is that there is a minimum frequency required in order to get a return (about 1.5MHz in this case) and a maximum frequency beyond which there is no return (just short of 6MHz).

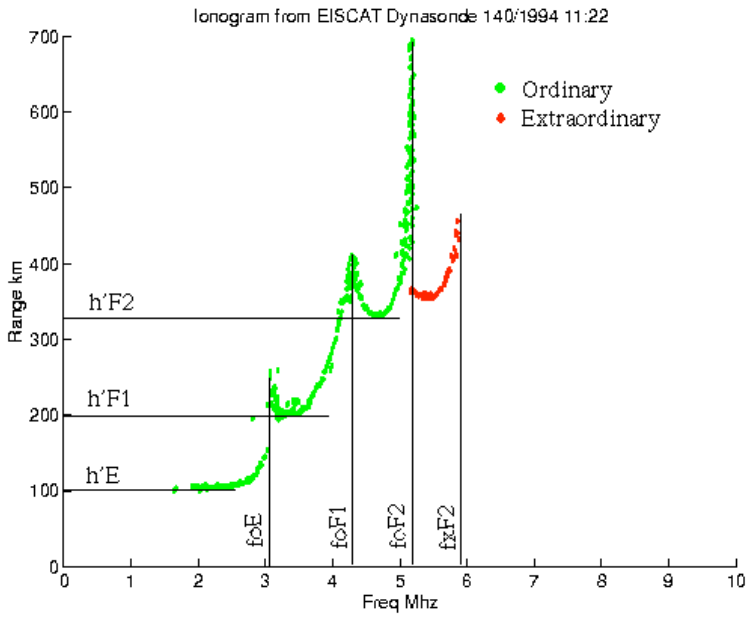

Figure 2 - an example ionogram, from

http://www.ukssdc.ac.uk/ionosondes/ionogram_interpretation.html[3]

The ionosphere does not behave like free space – as an ionised medium it has a group velocity that is inversely related to the electron density at any given height. As electron density increases with height, the pulse from the ionosonde will travel progressively more and more slowly until it is reflected and returns to the ionosonde. The frequency at which this reflection happens is called the *plasma frequency* and relates to the electron density, as seen in Equation 1.

Equation 1 - plasma frequency

(K. Davies 1990, 21; Hunsucker and Hargreaves 2007, 140)

$$F_N = \frac{1}{2\pi}\sqrt{\frac{Ne^2}{\varepsilon_0 m_e}}$$

In this equation F_N is the plasma frequency, N is the electron concentration per cubic metre, e is the charge on an electron, m_e is the mass of an electron and ε_0 is the permittivity of free space. A convenient approximation is given in Equation 2.

[3] Reproduced by kind permission of Rutherford Appleton Laboratory

Equation 2

$$F_N \approx 9\sqrt{N}$$

Since the ionosphere is made up of multiple layers, each layer produces a reflection at the frequency which corresponds to its maximum electron density. This is known as the *critical frequency of the layer*.

The minimum frequency observed on the ionogram is caused by the ionosphere's D-region, which absorbs radio waves. The absorption is inversely proportional to frequency squared (Hunsucker and Hargreaves 2007, 151), hence higher frequencies pass through with little or no attenuation. The D-region is normally only present in direct sunlight and disappears rapidly in darkness. D-region absorption is discussed in more depth in section 3.2.7.

On the ionogram of Figure 2, three layers are picked out – the E, F1 and F2 layers (the F region often divides into two layers from the perspective of an ionosonde) and the critical frequencies are labelled as FoE, FoF1 and FoF2. There is also an FxF2 frequency, which requires further explanation (see section 3.2.2).

The approximate height of each layer is shown on the y-axis – the E layer at 100km, the F1 at 200km and the F2 layer at 330km. These heights are called *virtual heights* (symbol *h'*) because they are calculated from round-trip time on the assumption that the wave travels at the speed of light in a vacuum. In fact, the wave travels more slowly when passing through the ionosphere, so the true heights are lower than the virtual ones.

3.2.2. Magnetoionic effects

The presence of the Earth's magnetic field within the ionosphere also affects the properties of radio waves passing through it. If the wave is transmitted along the magnetic field lines, it becomes divided into two waves with opposite circular polarisations. If the direction of propagation is not parallel to the magnetic field, the

circular polarisations become elliptical. These waves are called *characteristic waves* and termed *ordinary* and *extraordinary* (K. Davies 1990, 74). These two waves reflect at different heights in the ionosphere – the critical frequency for the ordinary wave depends solely on the electron concentration, whereas the critical frequency for the extraordinary wave is dependent on both the electron concentration and the magnetic flux density at the point of reflection (Hunsucker and Hargreaves 2007, 145). Hence the ionogram in Figure 2 is labelled with FoF2 (critical **F**requency, **o**rdinary wave, **F2** layer) and FxF2 (critical **F**requency, e**x**traordinary wave, **F2** layer).

3.2.3. Oblique propagation

The increasing electron density of the ionosphere with height can be thought of as giving a structure consisting of thin uniform slabs, each of slightly increasing electron density. The refractive index of each slab will decrease with electron density, and hence we can apply Snell's law from optics – the incoming wave will be refracted at each change in refractive index. The effect of this is that incoming waves bend around a curved path before leaving the ionosphere at the same angle to the vertical. Assuming that the range between the transmitter and receiver is large, the signal appears to reflect off the ionosphere as if it were a mirror, whereas in fact it is being refracted.

A convenient relationship exists between the frequency required for reflection of a vertically incident ionosonde pulse and the frequency required for oblique propagation between two stations at a distance. This is derived from Breit & Tuve's theorem, Martin's theorem and the Secant Law, all of which are described in detail in Hunsucker and Hargreaves (2003, 145-147).

Equation 3 - oblique incidence frequency

$$f_{ob} = f_v \sqrt{\left(1 + \left(\frac{D}{2h}\right)^2\right)}$$

In Equation 3, f_{ob} is the maximum frequency that will support oblique propagation, f_v is the vertical frequency reflected from the same height (as measured by an ionosonde), D is the distance between the oblique transmitter and receiver (assuming a flat earth and a plane ionosphere) and h is the height of the ionospheric layer being used to reflect the signal (as measured by the ionosonde's time of flight). The optimum working frequency will be around 0.85 x the maximum usable frequency, f_{ob} (K. Davies 1990, 180).

The relationship described in Equation 3 is an approximation based on the assumption of a flat Earth and a plane ionosphere. Davies (1990, 169) suggests that the approximation is valid for paths of up to 500km, and beyond this a small correction factor (see section 3.2.4) needs to be added to account for the curvature of the Earth.

3.2.4. Oblique propagation – a practical example

This section illustrates how vertical and oblique propagation relate to each other by considering a practical example kindly supplied by Dr Janusz Mlynarczyk of AGH Technical University in Krakow, Poland. This example is taken from experiments on HF propagation across Europe.

The transmitter is a broadcast station in Ismaning, near Munich in Germany, and the receiver is in Krakow, 625km away. Roughly mid-way between them, at Pruhonice (near Prague) in the Czech Republic, is an ionosonde.

Figure 3 shows an ionogram from Pruhonice recorded at 1700UTC on the 18th April 2010. The pink traces are the ordinary wave and the green ones are the extraordinary. The slightly fainter top traces may be ignored as they are caused by a double-hop – the ionosonde pulse has been reflected from the ionosphere, the ground and then from the ionosphere again. The E-region traces are shown at the bottom left of the ionogram.

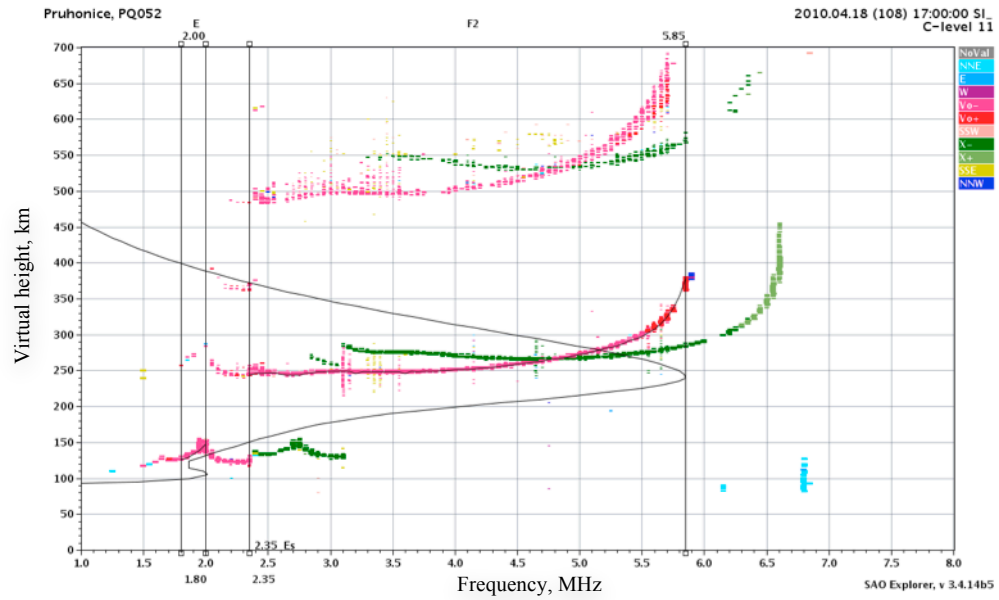

Figure 3 - ionogram from Pruhonice, 18th April 2010 at 1700UTC[4]

There is a main peak at 2MHz, but the region extends beyond this to 2.35MHz – this "extension" is sporadic-E. Looking at the F-region trace above it, there is an FoF2 of 5.85MHz. The black curve is the approximate electron density profile, derived by an inversion technique (Titheridge 1985) from the ionogram itself. The traditional approach to forecasting propagation is to use a transmission curve (Smith 1939). These are pre-calculated curves, which may be superimposed on an ionogram to provide a graphical solution to the problem of which frequency is best to use for a given range. The transmission curve is calculated by rearranging Equation 3 to solve for h and then plotting h against f_v for given values of path length (D) and oblique transmission frequency (f_{ob}). This is shown as Equation 4.

[4] Ionogram by kind permission of Dr Josef Boska, Institute of Atmospheric Physics, Pruhonice

Equation 4 - equation for Smith's transmission curves. h' is plotted against f_v for defined values of D and f_{ob}

$$h' = \frac{D}{2\sqrt{\left(\frac{f_{ob}}{f_v}\right)^2 - 1}}$$

Smith introduces a correction factor (the symbol k is used here) to compensate for the curvature of the Earth and the ionosphere. This has a value between 1.0 and 1.2 depending on the path length. The correction is introduced by substituting f_v with kf_v in Equation 4 (and hence also in Equation 3).

Figure 4 shows the appropriate transmission curve superimposed on the ionogram at the same scale. The value of k was chosen as 1.1 for this example.

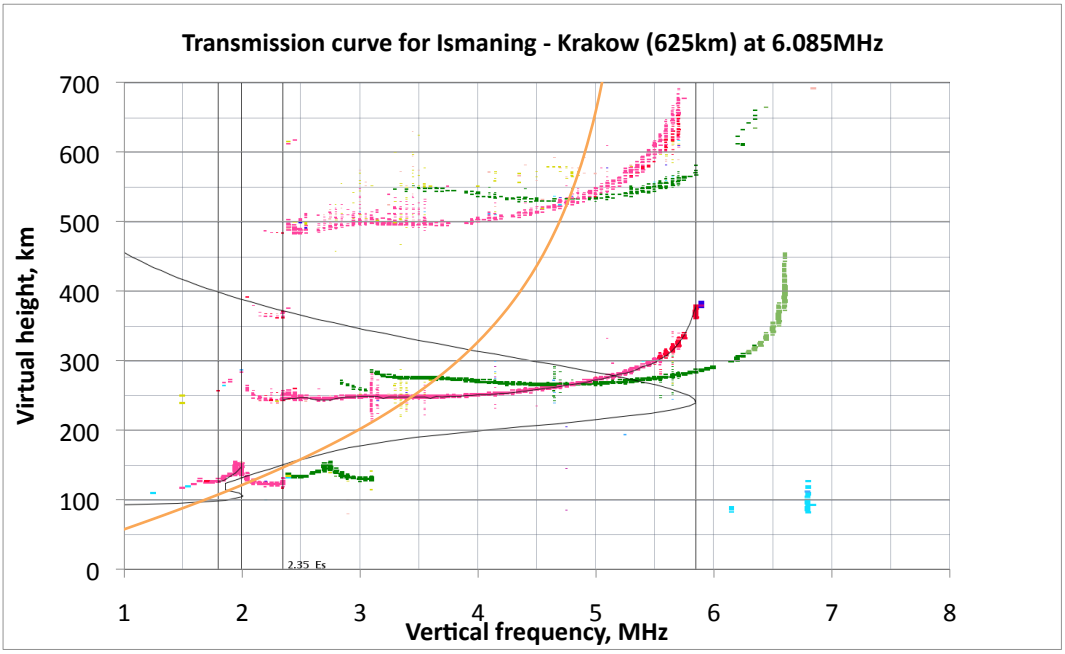

Figure 4 - transmission curve (orange) superimposed on the ionogram[5]

It can clearly be seen that the transmission curve intersects with the F layer at about 3.4MHz, showing that the signal will propagate via the F layer. But it also intersects with the area of sporadic-E just above 2MHz – so the wave will also propagate via the E

[5] Ionogram by kind permission of Dr Josef Boska, Institute of Atmospheric Physics, Pruhonice

layer for as long as the sporadic-E exists. Because the path via the E-layer is shorter than via the F-layer, the receiver should see multipath interference. The transmission curve also passes through the extraordinary wave plot for the F-layer, so the receiver should be receiving this as well, and it would be expected that this would arrive slightly after the ordinary F-layer wave since it is reflected at a higher altitude.

The use of transmission curves has now largely been eclipsed by more sophisticated ray-tracing techniques using numerical models of the ionosphere. Figure 5 is the output of a ray-tracing algorithm for this path (Mlynarczyk 2010). The particular method used is unpublished (Mlynarczyk 2011), but derives from the use of Haselgrove's equations (Haselgrove 1955), solved numerically using the Adams-Bashforth-Moulton method (H. Jeffreys and B. Jeffreys 2000). The Earth's magnetic field is modelled as a magnetic dipole, using parameters from the first-degree coefficients of the IGRF model (International Association of Geomagnetism and Aeronomy and Working Group V-MOD, 2010). The ionosphere used in these simulations uses four Chapman layers (Chapman 1931), adjusted so that the model's electron density profile matches the electron density profile from the ionogram of Figure 3. The method of ray tracing calculates the trajectories of individual rays leaving the transmitter at a particular azimuth and elevation – so in this case, where we are interested in finding the trajectories of rays between two fixed points, a search method is required to find all the rays that will arrive at the receive point. The particular search method used here was a manual search, where a large number of trajectories were calculated in two dimensions only (distance and height) to identify which elevation angles will reach the receive site. Once identified, the trajectories are recalculated in three dimensions to check for any lateral deviation of the ray due to the Earth's magnetic field. Small corrections can then be made to the transmit azimuth to ensure that the calculated ray is definitely arriving at

the correct co-ordinates for the receive site. In this case, the maximum azimuth correction required was 0.04 degrees (Mlynarczyk 2011). For paths with significant lateral deviation, or ionospheric models with significant irregularities, the use of a more sophisticated automatic "homing-in" algorithm, such as the work of Strangeways (2000), may be appropriate.

Considering Figure 5, the F-region and sporadic-E paths can be seen, and it is clear that the vertical radiation pattern of the antennas would affect the received signal strength – as the two paths are at significantly different elevations.

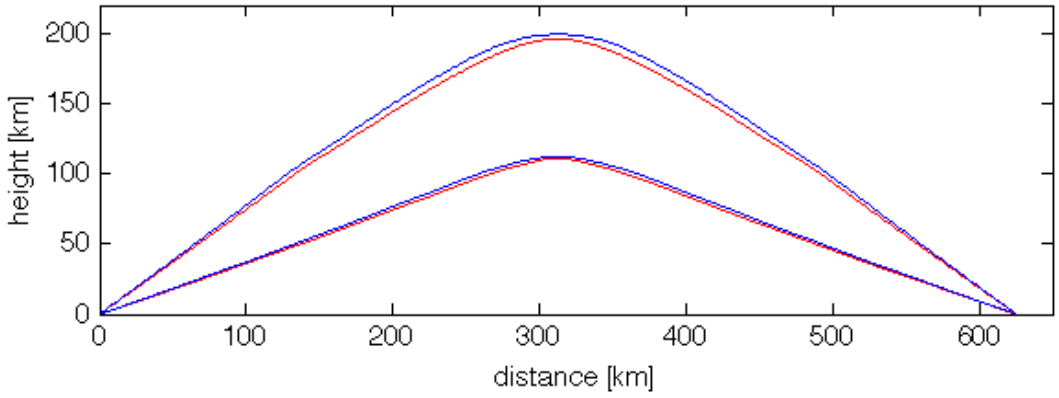

Figure 5 – Ismaning – Krakow propagation at 6.085 MHz modelled by ray tracing. Red is the ordinary wave and blue the extraordinary wave.[6]

If the path is shown in three dimensions (Figure 6), it can be seen that the ordinary and extraordinary F-layer paths take different routes through the ionosphere as a result of the influence of the Earth's magnetic field.

[6] Figures 5-8 are reproduced by kind permission of Dr Janusz Mlynarczyk

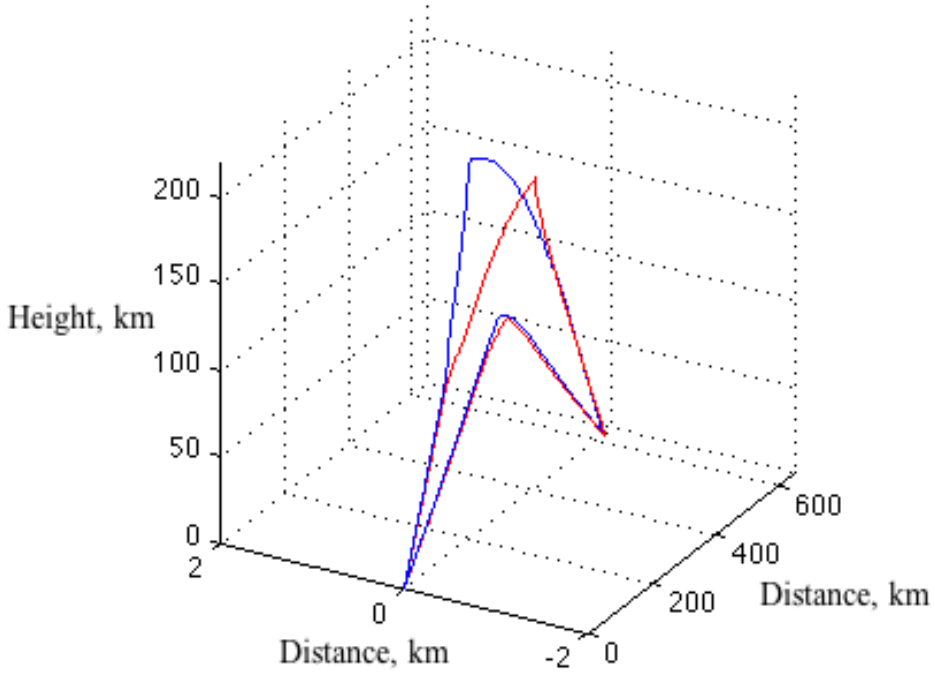

Figure 6 - 3D plot showing the effect of the Earth's magnetic field on the F-layer paths. Red is the ordinary wave and blue the extraordinary wave.

Because the transmitter at Ismaning radiates a Digital Radio Mondiale broadcast, the receiver calculates an impulse response for the channel as part of the process of decoding the signal. An impulse response from the receiver is shown in Figure 7, and two large peaks can clearly be seen.

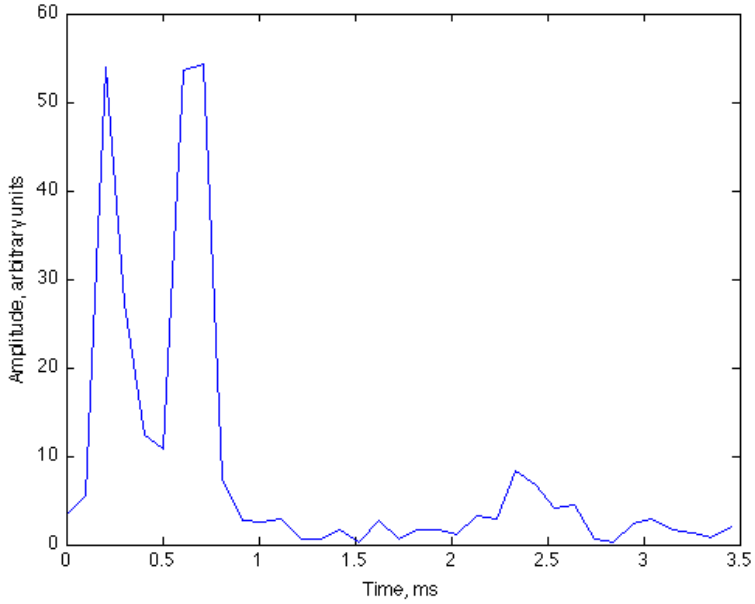

Figure 7 - impulse response seen at the receiver in Krakow on 18th April 2010 at 1700UTC. Time axis here is relative time-of-flight – this time-domain response is derived form the receiver's equaliser's measurements of the amplitude of known "pilot tones" in the DRM transmission.

The first peak (at 0.25ms) corresponds to the E-layer path and the second (at 0.75ms) to the F-layer path. The delay between them is roughly 0.5ms - the impulse response is only accurate to within 0.1ms. The ray-tracing algorithm can calculate the time-of-flight for each path and gives 2.24ms for the E-layer path and 2.7ms for the F-layer paths. The difference in propagation time between the two predicted paths is also roughly 0.5ms, confirming that the prediction matches the observed result.

Close inspection of the plot shows a smaller peak at about 2.4ms. This is a two-hop mode from the F-layer: the signal reflects from the F-layer, the ground, and then the F-layer again before arriving at the receiver. The ray-tracing algorithm showed that this was possible and confirmed that the relative delay was correct. Figure 8 shows all three paths.

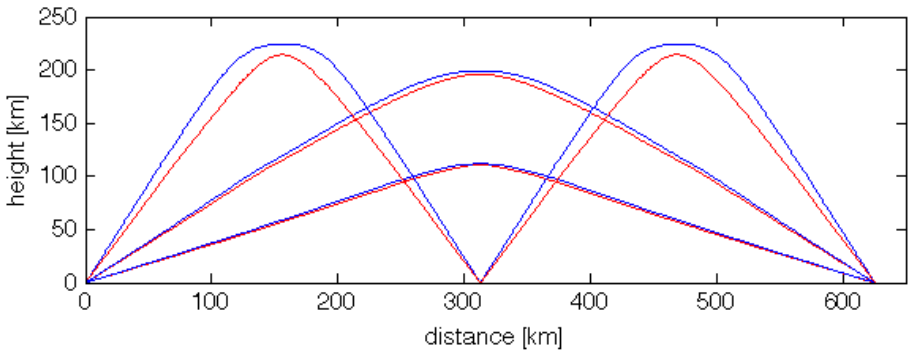

Figure 8 - showing the 2-hop mode. Red is the ordinary wave and blue the extraordinary wave.

Because the impulse response of the receiver can only be calculated to within 0.1ms, it cannot discriminate between the ordinary and extraordinary waves. However, since they arrive with different polarisations, the peaks are seen to fade up and down as the resultant polarisation rotates with respect to the antenna's polarisation response.

3.2.5. Spread-F

The ionogram shown in Figure 3 is a simple mid-latitude one, chosen for its clarity. Since the polar ionosphere is a highly irregular medium in constant motion, high-latitude ionograms are often much more "cluttered", exhibiting phenomena known as *range spread* (on the y-axis) and *spread-F* or *frequency spread* (on the x-axis). Figure 9 shows an example. Range spread is the vertical spread of the E and F region curves, indicating that the ionosonde pulse is travelling along several different-length paths (a form of multipath interference). Spread-F is the frequency spread in the F-region trace, making it hard to estimate the critical frequency. Irregularities ranging in scale size from the Fresnel scale (a few km at HF) and above, with variations in electron density of a few percent compared to the ambient density, have been shown to be the cause of spread-F (Wright, Argo, and Pitteway 1996).

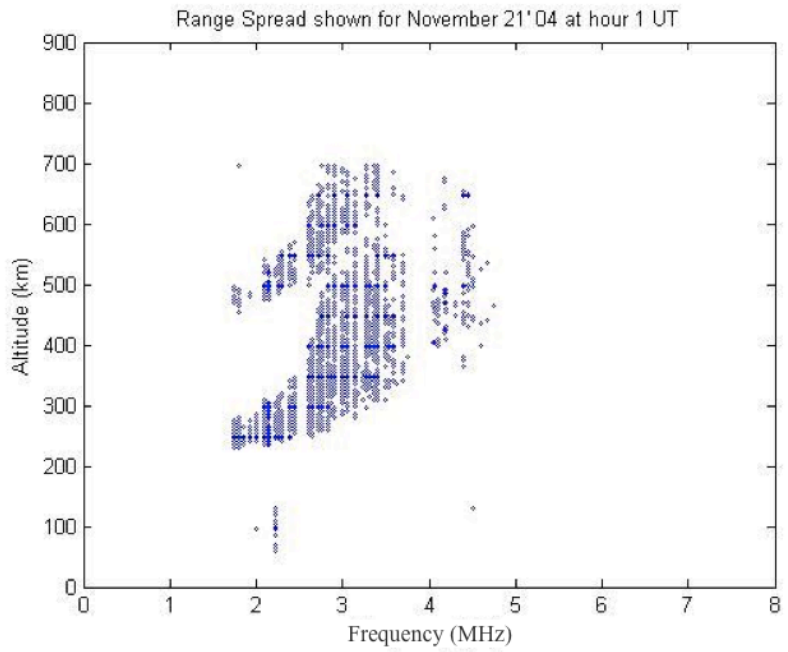

Figure 9 - ionogram showing range spread and spread-F observed at mid-latitude, from http://www.utdallas.edu/~pxb049000/ionosphere.html

3.2.6. Fading

Fading is variations in amplitude of the signal with time caused by constructive and destructive interference of signals travelling along more than one path between transmitter and receiver. Fading is classified on its effects both on the frequency and time domain of the signal.

In the time domain, fading may be *fast* or *slow*. A fast fading channel "flutters" rapidly, whereas a slow fading channel will simply fade in and out over a much longer period. What constitutes "fast" fading depends upon the application – fast fading conditions occur if the channel's *coherence time* (the period over which the channel impulse response may be considered as constant) is short compared to the maximum delay tolerance of the end user. Fast fading is easily mitigated using error-corrective coding but slow fading needs both a powerful error-corrective code and a long interleaver (see section 4.3.3) in order to overcome it.

In the frequency domain, fading is described as *flat* or *frequency-selective*. Flat fading means that the whole channel fades together, whereas frequency-selective fading introduces one or more notches into the spectrum. Frequency-selective fading may be mitigated by equalisation or OFDM techniques (see Section 4.4).

Two numerical parameters are used to help describe fading. *Delay spread* or *multipath spread* is the time-domain measurement - the time delay between the arrival times of signals following different paths. Long delay spreads lead to frequency-selective fades – the longer the delay spread, the narrower the gap between the spectral notches.

Signals also experience frequency or phase shifts as a result of the Doppler effect – particularly at HF since the ionospheric plasma at high latitudes is often irregular and moving – and each path will experience a different Doppler shift at any given instant. At the receiver, these phase shifts will also sum together constructively and destructively to cause fading. *Doppler spread* is the measurement of the maximum range of Doppler shifts between each path. A high Doppler spread will produce fast fading, whereas low Doppler spread produces slow fading. Doppler spread can be calculated for the overall received signal, or for each multipath component.

In HF communications, long multipath comes about from reflections from multiple layers. However, short multipath is also produced by the separation of ordinary and extraordinary waves, and by the "roughness" of the ionosphere causing multiple reflections from the same layer. Motion of the layers and irregularities in the ionosphere produces Doppler spread in the multipath components. Since all these waves arrive at the receiving antenna with different elevation angles and polarisations, experiments have shown (Peco et al. 2009) that diversity reception techniques using multiple receiving antennas of different patterns and polarisations can at least partly mitigate these fading effects. The same study also showed that fading effects may also be partly

overcome by using multiple receiving antennas separated from each other by more than two wavelengths.

3.2.7. Absorption

Absorption (or attenuation) of radio waves by the ionosphere, particularly by the D region, is a limiting factor in high-latitude communications, particularly if the transmitting station is power-constrained. D-region absorption is proportional to electron density and inversely proportional to the square of the radio frequency (K. Davies 1990, 215), so working at as high a frequency as possible is desirable when operating HF links. Any phenomena that enhance electron density in the D-region will also increase absorption and be detrimental to wave propagation.

At high latitudes, two principal phenomena are responsible for enhancing D-region absorption: *auroral radio absorption (AA)* and *polar-cap absorption (PCA)*. Auroral absorption occurs when circuits pass through the auroral zone. Higher levels of geomagnetic activity will expand the auroral zone to lower geomagnetic latitudes, affecting circuits that would not normally experience AA under undisturbed conditions. A typical AA event will attenuate an HF signal by at least 20dB (Hunsucker and Hargreaves 2007, 367).

Polar-cap absorption events are produced by energetic protons emitted from the Sun, and are usually the product of solar flares. PCAs produce large-scale enhancement of the polar D-region and can totally black out HF communications circuits for hours or even days. They are a relatively infrequent phenomenon, with only around 10 events per year at solar maximum, and typically fewer than three per year at solar minimum (Hunsucker and Hargreaves 2007, 384). The protons that cause PCAs travel relatively slowly and thus the events can be forecast by observations of solar flares and solar X-ray emissions.

3.2.8. High-latitude propagation experiments

HF propagation experiments have been conducted in both the polar regions since the 1950s. Work at the University of Alaska (Owren et al. 1959) showed that propagation experiments between Alaska and Scandinavia were most effective when pulsed transmissions were used rather than CW beacons.

More recent work has attempted to characterise the channel by measuring multipath and Doppler spread in order to provide requirements for the design of robust HF modems. In particular, the DAMSON sounding network in Scandinavia (P. S. Cannon et al. 2000) was used to inform the development of the most recent military modem standards. Four paths were used, ranging from ~200km to ~2000km. All of the paths were wholly or partially within the auroral zone, and consequently some very large Doppler spreads were recorded – up to 73Hz. The experiment ran between 1995 and 1999, starting during a period of low solar activity and ending close to solar maximum. The result was a characterisation of the delay and Doppler properties of the paths, and this was used both to evaluate existing modem technologies and to provide design criteria for new ones (Matthew J. Angling et al. 1998).

More recent work in Scandinavia (Warrington, Stocker, and Siddle 2006) has used a similar sounding system, although over slightly different paths, and leads to the channel model described in Section 5.2.

Propagation studies in Antarctica are hard to find in the open literature – for example, Hunsucker and Hargreaves (2007) devotes two chapters to reviews of HF propagation studies at high latitudes, and yet contains no Antarctic results.

3.3. Summary

The ionosphere allows HF radio signals to propagate beyond line-of-sight, but introduces significant impairments that must be overcome. These are summarised in Table 3.

Table 3 - impairments caused by the ionosphere, and ways to mitigate them

Impairment	**Mitigations**
Absorption[7]	Increase transmit power Increase coding gain
Variations in electron density profile	Frequency selection, automatic link management
Fading – multipath and Doppler	Modulation and equalisation techniques, interleaving, forward error correction

Subsequent chapters will discuss these mitigation techniques in detail and show how they may be used to engineer a polar HF communications system.

[7] Even with very high transmit powers and highly effective coding it may not be possible to mitigate against very severe absorption events, such as PCAs. Fortunately, these events are relatively infrequent.

4. HF radio system design

4.1. Autonomous instruments in the polar regions

Scientific study in the polar regions often involves the collection of time-series measurements. Historically, these were collected manually by scientists on research stations, but increasing numbers of instruments can now log their own data automatically. This has made possible the development of fully autonomous instrument platforms, which are deployed in the wilderness away from the manned research stations. Early systems, such as the Automated Geophysical Observatories (Dudeney, Kressman, and Rodger 1998), were small buildings with generators providing heat and electrical power to the instruments. Later designs (Kadokura et al. 2008) have used much smaller, unheated, housings and been powered by wind turbines or solar panels. Some are fitted with Iridium or ARGOS satellite communications links, but many rely instead on an annual visit by an aircraft to retrieve their stored data. Using HF to retrieve data from these instruments would potentially be cheaper than satellite and save on valuable aircraft time.

4.2. Requirements analysis

This section considers the requirements for an HF communications system for autonomous instrument platforms.

4.2.1. Autonomous operation

The system needs to be capable of operating entirely autonomously, with no intervention at the remote sites, and with only limited and occasional intervention at the manned stations.

4.2.2. Power consumption

The system needs to have sufficiently low power consumption that the whole instrument platform may be powered from a small number of solar panels and wind turbines. Lead-acid or lithium-ion batteries are used for energy storage, so quite large amounts of instantaneous power are available provided that the overall average power consumption is low.

Table 4 shows the results of some simple calculations showing how the power consumption of the transmitter and the duration of the transmission affects the average daily power consumption of the communications system. For a system with a 100W power consumption on transmit (which is realistic – suggesting an RF output power of around 50W PEP), two hours of daily communications would produce a continuous daily power requirement of just over eight watts. This could be fulfilled by a solar panel in summer and a single wind turbine in winter. Renewable power systems capable of supplying instrumentation requiring up to 30W continuously have been successfully deployed at field sites in Antarctica (M.C. Rose, Maxfield, and Junyent 2009), so this is well within the capabilities of existing technologies.

Table 4 - average daily power supply (W) required from renewables, as a function of transmitter power consumption and communications time

Sched length, minutes per day	10	30	60	120
Daily data transferred at 1200bits/s, kB	88	264	527	1055
Volume of data transmitted per year, MB	31	94	188	376
Transmit DC power consumption, W				
5	0.03	0.10	0.21	0.42
10	0.07	0.21	0.42	0.83
20	0.14	0.42	0.83	1.67
50	0.35	1.04	2.08	4.17
100	0.69	2.08	4.17	8.33

4.2.3. Frequency use

The system needs to be able to select the best frequency to use, given the time of day, time of year and station to be contacted. In Antarctica, the sparse population and lack of a radio licensing authority means that large numbers of frequencies are available. Remote sites may be located at a variety of ranges from the base station – from 200 to 2000km, and so different frequencies will be required in order to reach different sites. Each site will need alternate frequencies to deal with variations in propagation. Assuming at least three different sites at significantly different ranges and three frequencies per site, the system needs to be able to work with at least nine frequencies.

4.2.4. Timing

All stations in the system need a source of accurate time (such as may be obtained from a GPS receiver) so that scheduled contacts may be made exactly on time. Remote stations that go into hibernation mode to save power may need to be woken ahead of their scheduled contact time in order to resynchronise their internal clock with the GPS.

4.2.5. Environmental factors

The polar regions are a demanding environment – cold, dry and windy – and any such system must withstand the polar weather. This may place particular demands on the robustness of any antenna design.

4.3. HF radio technology

Having identified the requirements for the proposed system, this section serves to provide an overview of the various HF radio concepts and technologies that may be needed to fulfil them.

4.3.1. Network architecture

The expected use case is retrieving data from autonomous instrument platforms in Antarctica. This could be done entirely by HF, with the signals received by a station outside Antarctica, but for reasons of power consumption it makes more sense to use the HF link to connect the instrument platforms (hereafter referred to as *remote sites*) to one of the manned research stations (*base stations*) which are equipped with a satellite link to the outside world. These manned stations have reliable supplies of electricity, so low power consumption is not as important for them as for the remote sites.

Consequently, a network architecture akin to a cellular phone system seems logical: one or more base stations communicating with multiple low-power remote sites. This also mirrors the arrangements made for HF voice communications with aircraft and field parties.

The following alternative topologies (Meyers 2010) have also been considered:

- Partially-connected mesh. This is a popular technique for sensor networks in environmental science, based on short-range radio links. Nodes relay messages over multiple hops, allowing the network to be bigger than the range of the radio links. Range is rarely a problem for HF networks (assuming that suitable frequencies are available), and the network nodes forming part of the mesh would need to keep their radios powered up at all times in order to relay messages from other stations, increasing their power consumption.
- Fully-connected mesh. This is used by military HF systems (e.g. STANAG 5066 (NATO 2000)), usually on a single frequency. Such networks use a controlling node to regulate access to the channel, although in the event of the controlling node being destroyed, another node may take over. This topology requires every node needs to be in contact with every other node at all times. Consequently,

this type of topology operates best over a relatively small geographical area and would not be suitable for the long ranges required in the polar regions.

- Token ring. This technique has been considered for use on HF (Gillespie and Trinder 2006) as it avoids the need for a controlling node. Each node talks only to the two nodes adjacent in the ring. Nodes regulate access to the channel by circulating a "token" packet around the ring – any node having data to send will "capture" the token when it arrives and then send its data. When it has finished, it "releases" the token so that other nodes may use the channel. Token ring requires all the nodes in the ring to be powered up and passing the token, which wastes power at nodes that are not actively communicating.

Most network designs work on the assumption that a single channel (a cable or a radio channel) must be shared between all the nodes. HF networks often have access to a number of possible frequencies, and so it is not necessary to share a single channel between all the nodes on the network. As a result, many of the complexities introduced by topologies like token ring and fully-connected meshes provide no benefit. In fact, a multi-frequency HF network where nodes communicate directly with one another using the most suitable frequency has been shown to provide better performance than token ring (Gillespie and Trinder 2006).

4.3.2. Link establishment and management

The choice of frequency is crucial when communicating using HF. The frequency to use will depend on, amongst other things, the length of the link; the time of day; the time of year and the state of the sunspot cycle. Traditionally this was the skill of the radio operator, but Automatic Link Establishment (ALE) systems are now capable of choosing frequencies and establishing communications. The most widely used ALE standard is MIL-STD-188-141A, usually referred to as "2G ALE". It has now been

superseded by -141B, known as “3G ALE”, which is backwards-compatible with the 2G system. These ALE systems are designed for use in military networks with large numbers of permanently operating nodes. Idle nodes scan through all their available frequencies and monitor network traffic in order to establish which frequencies are currently best for contacting other nodes. They may also send out sounding signals to assist with this. When a node wishes to call another, it tries the frequencies in the order of likelihood of a connection based on the information it has gathered.

The military ALE schemes are not ideal for a power-constrained application, as nodes not undertaking data transmission need to stay powered up in order to monitor the present state of the network. This is not a drawback in a military application, as communications nodes are usually operated continuously in order to pass on commands and reports with the minimum of delay. For scientific telemetry in the polar regions, much of the communications is not time-critical, and keeping power consumption down is more important than being in continuous communications contact with a base station. A system of scheduled communications is more appropriate in this case: the base station makes a call to a specific remote site on a pre-agreed frequency at a precise time. If it does not get a reply, it moves to a secondary frequency after a fixed delay – and then on to further frequencies if necessary. Once contact is established, a mechanism can be provided for changing the primary frequency at the next contact time if this is necessary. This system has the advantage of much lower complexity than military ALE, and the remote site can go into sleep mode between scheduled contacts to save power.

4.3.3. Error corrective coding and ARQ

Knowing that a message has been received correctly is an important part of any communications system. There are two general approaches to this, which are known as Forward Error Correction (FEC) and Automatic Repeat Request (ARQ).

ARQ is the simpler approach. The incoming datastream is broken into short units, and each data unit is then transmitted along with an error-detection code. The receiver compares the received data with the error-detection code – if an error is detected, the data unit is discarded and a retransmission is requested.

ARQ works well on channels where error rates are low, and the error-detection codes are simple and impose a small overhead.

FEC may be used with or without ARQ, and encodes data units using an error-*corrective* code. These codes add extra bits to the data unit such that if any of the bits in the data unit are in error, the error may be corrected. The penalty paid is the overhead for the FEC bits – the more FEC bits are used, the more resistant the code is to errors, but the lower the usable data rate. FEC codes are quoted in terms of a "code rate" - a code of rate 7/8 means that for every 8 bits transmitted, 7 are data.

Both WinDRM (see Section 5.4) and the NATO modems (see Sections 4.4.2 and 5.5) use *convolutional codes*. These were first proposed by Elias (1955) although the most widely-used decoder was invented by Viterbi (1967). A convolutional encoder consists of a shift register into which data bits are fed, and a number of linear operations that perform modulo-2 addition of the values of certain bits in the shift register in order to produce output bits. The *constraint length* of the code is the number of bits in the shift register which are involved in the calculation of the output bits. The most widely-used convolutional code has a constraint length of 7 – and this is the code that is used in WinDRM and the NATO modems. Increasing the constraint length will improve the code's performance, but at the expense of increasing the computational complexity of the decoder and also increasing the latency of the coding and decoding process.

More recent developments in forward error correction techniques include Turbo codes, low-density parity check (LDPC) codes and digital fountain codes (MacKay 2003).

These all offer benefits in terms of code performance – greater resilience to errors for a given code rate – than convolutional codes, but have yet to be implemented in any HF systems.

Convolutional codes have good error-correction performance where the errors are evenly distributed over time, but in reality most channels produce errors in bursts. This issue can be mitigated by the use of *interleaving*. An interleaver is simply a memory buffer installed at both ends of the link. At the transmitter, the interleaver buffer is filled by data coming from the FEC encoder and then the data bits are read out from the buffer in a different order and transmitted over the channel. At the receiver, the datastream is reconstructed by reading data into the buffer and reassembling the bits into the correct sequence – the receiver must know *a priori* which interleaving pattern has been used and how long the buffer is. The effect of interleaving is that a burst of errors that occurs on the channel will be scattered across the received datastream by the de-interleaving process. In a fading channel, the length of the interleaver can make a significant difference to the performance of the link: too short and the interleaving will fail to break up the bursts of errors. In a channel experiencing periodic fades, choosing an interleaver that is slightly too long will start to incorporate more than one fade into the interleaver period and can actually worsen the peformance.

4.4. Physical layer techniques for HF

The high-latitude HF channel places many demands on the physical layer of any HF communication system – it must cope with multipath, slow fading, noise, interferers and Doppler effects. For this reason, modulation techniques for HF channels have been a major part of the research leading to this thesis.

4.4.1. Basic approaches

In simple terms, digital modulation operates by altering the amplitude, frequency or phase of a radio signal so as to convey the binary data that are to be transmitted. A receiver can then identify these changes and demodulate the signal back into digital data again.

Amplitude modulation (AM) is used for analogue broadcast stations on HF, but its digital equivalent, Amplitude Shift Keying (ASK) is rarely used – the variations in amplitude produced by noise and fading make this too unreliable for use on the HF channel.

Frequency modulation is used by many slow data modems on HF. The simplest form, known as Frequency Shift Keying (FSK), uses two frequencies to represent 0 and 1. The modulator shifts the carrier frequency back and forth between these frequencies to send data. This principle may be extended to any number of frequencies. The MIL-STD-188-141B standard for ALE uses 8-FSK, with eight frequencies: each frequency tone represents three bits.

Phase modulation, referred to as Phase Shift Keying (PSK), is now used in many digital modulation schemes. The simplest form, Bipolar PSK (BPSK), uses two phase states 180° apart, each representing one bit. Quadrature PSK uses four phase states 90° apart, each representing two bits.

Where a system has a high signal-to-noise ratio it is possible to use higher order modulation schemes, where each modulated symbol carries a large number of bits. A popular scheme for this is Quadrature Amplitude Modulation (QAM), where both amplitude and phase are used together. 16-QAM carries 4 bits per symbol, and 64-QAM and even 256-QAM can be used on UHF and microwave links where high SNRs and low distortion are guaranteed.

4.4.2. Serial-tone

The current state-of-the-art for military HF modems is US MIL-STD-188-110B, which uses "serial-tone" technology. These modems use a single phase-modulated carrier and overcome impairments in the channel through the use of a sophisticated equaliser. To do this, the transmitter sends predetermined sounding sequences interspersed with the data. Because the receiver knows what these sequences should be, it can calculate the channel impulse response and hence correct much of the distortion in the signal when it receives the wanted data. This process of equalisation can be computationally very complex, and assumes that the channel is largely time-invariant between soundings. These sounding sequences (also known as *training sequences* or *probes*) are an overhead and reduce spectral efficiency. The sounding sequence needs to be at least as long as the maximum multipath delay spread in order for the equaliser to be able to overcome the multipath (Jorgenson and Moreland 1999). In fact, the same paper recommends that for high-order modulation schemes (i.e. 16QAM or higher) the sounding sequence must be at least double the maximum multipath delay spread. Long sounding sequences help the equaliser to overcome multipath, but to overcome significant Doppler spread the sequences must be sent frequently. For a given waveform efficiency (i.e. for a fixed user data rate), doubling the length of the sounding sequence doubles the resistance to multipath, but requires a halving of the frequency with which sounding sequences are sent, and hence halves the resistance to Doppler spread (Otnes and V. Jodalen 2001). Otnes and Jodalen show in the same paper that resistance to both high Doppler and high multipath are rarely required simultaneously, and that using a family of three waveforms – a "Doppler optimised" waveform, a "multipath optimised" waveform and a "compromise" waveform – allows a modem to achieve higher link availability on representative high-latitude HF channels.

Table 5 - probe transmissions in the MIL-STD-188-110B family of waveforms

Waveform	Length of probe sequence (ms)	Frequency of probe transmissions (Hz)	Waveform efficiency
110B at less than 2400bits/s	8.33	60	50%
110B at 2400bits/s	6.67	50	67%
110B at more than 2400bits/s	12	8	89%

As an example, Table 5 shows the different waveform probe sequence characteristics in the MIL-STD-188-110B family of waveforms. The waveforms with the data rates of less than 2400bits/s have a 50% waveform efficiency – half the transmission time is used in sending data and half for probe sequences. This allows them to provide a high tolerance to multipath and Doppler with long, frequent probe sequences. In the other waveforms resistance to impairments is sacrificed for higher data rates – the 2400bits/s waveform has a shorter probe sequence, giving less resistance to multipath, and also sends probes less frequently, giving less resistance to Doppler spread. For the high data rate waveforms the waveform efficiency is raised to 89%, predominantly at the expense of resistance to Doppler spread. The probe length (12ms) is much longer than for the other waveforms, but this reflects the situation identified earlier: high order modulation schemes need sounding sequences at least double the length of the maximum multipath

spread (Jorgenson and Moreland 1999), so the multipath resistance is comparable to the 2400bits/s waveform which only has a 6ms probe sequence length.

4.4.3. OFDM

OFDM stands for Orthogonal Frequency Division Multiplex. The FDM part indicates that it uses multiple parallel sub-carriers to carry the data. The term orthogonal is used to indicate that the individual carriers are spaced at an interval equal to the inverse of the symbol period (Stott 1998). This condition can be shown to produce frequency spectra for each carrier that do not overlap, allowing the carriers to be spaced closely together without introducing intercarrier interference.

The individual carriers are modulated (usually with PSK or QAM) and then grouped together and passed through an inverse Fast Fourier Transform (FFT), to produce an OFDM waveform. At the receiver, a forward FFT is used to separate the carriers before they are demodulated.

Each OFDM carrier has a long symbol period to help resist fading. Most implementations include a *guard interval* (or *cyclic prefix)* to improve resistance to multipath. The cyclic prefix is generated in the time domain by repeating part of the OFDM waveform for each symbol, and thus reduces spectral efficiency. The waveform can resist multipath delays that fall within the period of the cyclic prefix.

Convolutional FEC is often used with OFDM as the Viterbi decoder can take into account the SNR of each individual OFDM carrier when calculating the output – trusting the results given by those carriers with high SNR and ignoring those where the SNR is low. This is extremely effective within an environment where multipath gives rise to frequency-selective fading.

OFDM may be used in conjunction with an equaliser. Pilot tones (carriers with known values) are inserted regularly in between the data carriers. At the receiver, the equaliser

interpolates between them to give an approximate channel frequency response, and then applies the inverse of it to the data carriers. This is very effective and adds little complexity to the receiver, although adding the pilot tones reduces the spectral efficiency.

OFDM is used by Digital Radio Mondiale, the standard for digital HF audio broadcasts (ETSI 2009), and by Globe Wireless's proprietary HF data service for merchant ships (Kierans and Hanson 2004).

4.4.4. PCC-OFDM

Polynomial Cancellation Coding OFDM (PCC-OFDM) (J. Armstrong 1999; Seaton and J. Armstrong 2000; J. Armstrong, Grant, and Povey 1998) is claimed by its proponents to be a variant of OFDM that is particularly resistant to frequency offsets and Doppler spread. It works by modulating multiple adjacent carriers in the OFDM set with identical data. Each carrier is then weighted according to the binomial coefficients of the polynomial expansion of Equation 5, where k is the number of adjacent carriers being given the same data.

Equation 5

$$(1-x)^{k-1}$$

For the simplest case, two adjacent carriers are used, so the coefficients are 1 and -1. At the receiver, the two carriers are weighted again and then summed together before being demodulated.

Previous work on PCC-OFDM (Panta, Suraweera, and J. Armstrong 2004) highlights its benefits when operating in a multipath fading channel. The principal mechanism is that because the amplitude of each modulated symbol is not constant over the symbol period, multipath components are much less likely to have identical amplitudes when

they arrive 180 degrees out of phase from the directly-received signal component. This means that total cancellation is much less likely - resulting in fewer frequency-selective fades.

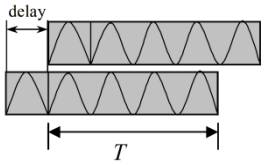

Figure 10 - OFDM symbols in a two-path channel[8]

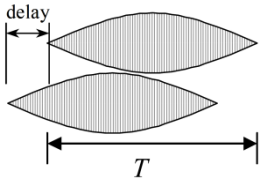

Figure 11 - PCC-OFDM symbols in a two-path channel

The figures above show the difference between OFDM (Figure 10) and PCC-OFDM (Figure 11) in a two-path channel. In the OFDM case (Figure 10), we can see that the two components have equal amplitude over the symbol period, so if the delay was such that they arrived 180 degrees out of phase, they would cancel and produce a notch in the spectrum at this frequency. By contrast, the PCC-OFDM case in Figure 11 shows how the variation of amplitude over the symbol period means that even if the two components are 180 degrees out of phase, their amplitudes will not be identical and the result will not be a complete cancellation, merely a reduction in received amplitude. This enhanced resistance to frequency-selective fading allows PCC-OFDM to dispense with a cyclic prefix, allowing it to regain some of the spectral efficiency lost by the PCC process.

All the literature on the subject of PCC-OFDM approaches it from a theoretical standpoint, using channel models that are easy to analyse algebraically. In particular,

[8] These figures are reproduced from Panta, Suraweera, and J. Armstrong 2004 by kind permission of the authors.

comparisons are made between PCC-OFDM and classical cyclic-prefix OFDM but which do not take into account the fact that any real OFDM system implementation would include frequency synchronisation techniques such as the use of some carriers as constantly-transmitted “pilot tones” for the receiver to use as a frequency reference. Details of more practical experiments with PCC-OFDM are given in Chapter 5.

4.5. Outline system design

The system has been broken down into a series of “layers”, although the specific nature of HF networks means that these layers do not correspond to the ISO-OSI seven-layer model (ITU-T 1994). The layers are shown in Figure 12.

The system is designed to operate in two modes – scheduled and contended. In scheduled mode, the base station calls the specific remote site which is expecting a call at that time (the *sched time*). At the sched time, the base station puts out a beacon call on the primary frequency and the remote site powers up its receiver and listens for it. If the remote site considers that it has enough power to communicate and that the SNR on the beacon call is acceptable, it makes a reply. If not, it waits until the base station tries other frequencies – the frequency list has been agreed between the two stations at the previous sched. If no frequency is suitable, the remote site remains quiet and powers down its radio until the next sched time.

To allow for communications outside the schedule – say for a new remote site joining the network – there is a contended mode where any remote site may hail the base station. The base station will automatically switch to contended mode when it is not making scheduled contacts.

In contended mode, the base station cycles through a standard set of frequencies, putting out a short broadcast and listening for responses on each one in turn. The listening time after the broadcast is divided into slots, and stations wishing to reply pick a slot at

random and transmit a short burst in reply, requesting a contact. This slotted approach reduces the chance of a collision. The base station can then broadcast a longer message, telling the stations requesting contacts when and on which frequencies their requested contacts will be made.

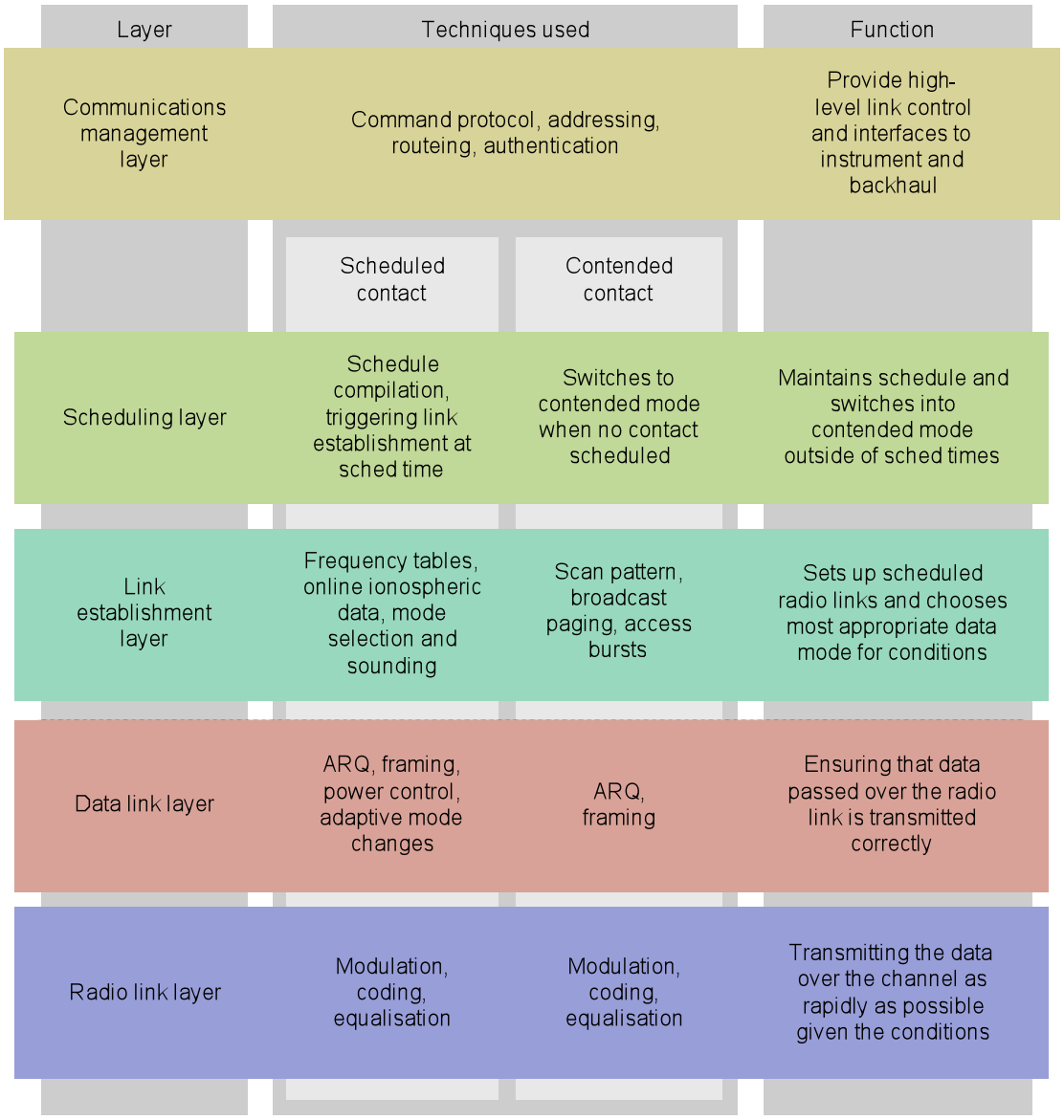

Figure 12 - outline system design

Starting from the top of Figure 12, the communications management layer is responsible for interfacing the HF network to the outside world. This includes routeing and data format conversion. This layer is also responsible for allowing new stations to

join the network, including provision for an authentication protocol so that the radio network is not hijacked by unauthorised users.

Below the management layer is a scheduling layer – which keeps the master schedule of contact times and frequencies, and which switches the base station between scheduled and contended modes.

The link establishment layer is a simple ALE protocol designed to try and find the best frequency to use for any given contact. It may also break off a contact if the propagation worsens and try to re-establish the link on a different frequency.

The data link layer is responsible for getting the data over the radio link correctly, using ARQ to request retransmissions of packets corrupted in transit. It also undertakes *power control* (adjusting the transmit power at the remote site so as to avoid wasting power when propagation is good) and adjusts the modulation and FEC coding scheme (collectively known as the *robustness mode*) to get the fastest reliable data transfer that the channel will support.

The radio link layer comprises the modulation and FEC coding required to send the data bits over the HF channel. It may also involve some equalisation to improve the receive performance.

This project has focussed on the radio link layer, being the most fundamental part of the system, and that which is most strongly affected by the unique properties of the polar ionosphere. Subsequent chapters present research into channel modelling, modulation and propagation conditions. For a full practical implementation, the remaining layers of the system would need to be developed.

5. Channel modelling

The variability of the ionosphere, which is most pronounced at high latitudes, makes it difficult to make meaningful comparisons between on-air tests of HF communications systems. Accordingly, simulators have been developed which reproduce the propagation-related effects of the HF channel in a repeatable fashion. This chapter describes a new HF channel simulator that we have developed and gives details of the performance of several HF modem waveforms in the simulated environment.

5.1. Previous work

The most widely-used approach to HF channel simulation (Watterson, Juroshek, and Bensema 1970) uses a tapped delay line with each tap subjected to independent random fading before being summed. Although Watterson's model supports any number of paths, several standard channels are described in ITU-R Recommendation F.1487 (ITU 2000) that use two paths of equal mean amplitude and Doppler spread, fading independently.

A number of more sophisticated simulators have been developed in recent years, notably the system developed by Mastrangelo *et al.* (1997) based on the wideband model of Vogler and Hoffmeyer (1993). This is a more complex statistical model, implemented in specialist hardware. Angling and Davies (1997) used real high-latitude ionospheric propagation data collected from the DAMSON propagation experiment (Cannon et al. 2000, see section 3.2.8) to drive an implementation of Vogler and Hoffmeyer's model; they later also implemented a replay simulator using the same dataset (M.J. Angling and N.C. Davies 1999). With increased understanding of propagation mechanisms and increased computer power, rigorous physical models have become possible, such as the work of Gherm (2005) and Strangeways *et al.* (2002).

None of these simulation techniques is available as a ready-to-use software package, so significant work would have been required to implement one of them based on the published literature. Consequently, it was decided to adapt existing work by the Radio Systems research group at the University of Leicester in order to produce a new high-latitude channel simulator.

5.2. The Warrington/Siddle/Stocker model

Research at the University of Leicester into off-great-circle propagation led to the development of an advanced channel model (Warrington, Stocker, and Siddle 2006) that can simulate high-latitude propagation. The model is implemented in MATLAB. Each propagation mode is simulated as a grid of point sources distributed in both azimuth and elevation. Frequency shifts may be applied to the point sources to simulate Doppler shift and spread. Multiple grids are then used to represent each propagation mode, and each may have a different mean amplitude. Finally, band-limited Gaussian noise is added to the combined signals to produce a realistic signal-to-noise ratio.

The simulation parameters are drawn from oblique sounding measurements in Scandinavia, and the original version mimicked the action of the sounder by driving the modes with a Barker-13 sequence modulated onto a carrier as BPSK.

To develop it into a more general channel model, the Barker sequence was replaced with a modem signal input as baseband audio from a WAV file.

Calculating the channel behaviour is computationally intensive, so this is performed first and the data saved. A range of different signals can then be played through the pre-calculated channel and a resultant WAV file saved.

The current implementation of the simulator is simplex, and so it is not suitable for any protocol relying on ARQ (such as SITOR).

The original paper includes eleven different test cases, identified with the letters A to K, which are representative of different channels observed in the polar ionosphere above Scandinavia, although the behaviour of the ionosphere is likely to be similar in Antarctica at comparable geomagnetic latitudes. The channels observed were on auroral and trans-auroral paths and are therefore likely to suffer higher levels of impairments than the sub-auroral Halley-Rothera path described in Chapter 6. A 90-second sequence of each channel was modelled in the simulator, and then "sounded" using a Barker sequence to determine the multipath spread, Doppler spread and Doppler shift present in the simulation (Table 6).

Table 6 - measured properties of the standard simulator channels

Channel	Number of modes	Effective multipath spread (ms)	Multipath spread (ms)	Doppler spread (Hz)	Doppler shift (Hz)
A	1	0	0	0.5 - 1.5	-0.25 - +0.75
B	1	0	0	0.5 – 2	-0.25 - +0.75
C	2 (equal delay)	0	0	0.24 – 3.5	-1.25 - +1.25
D	3	0.1	0.1	0.5	0.25
E	2	0.1	0.1	3 – 40	17 – 22
F	3	0.3 – 0.5	0.3 - 1	0.5 - 18	-0.75 – 4.75
G	4	0.3 – 0.6	1.1 – 1.2	0.5 – 1	0.25
H	4	0 – 0.2	0 – 1.5	1.5 – 3	-0.75 - +1.25
I	4	0 – 0.2	0 – 0.7	0.5 – 11	-4.25 - +6.75
J	4	1 – 9	3 – 12	0.8 – 13	-5.75 - +1.75
K	6	0.6 – 0.8	0.6 – 1.3	0.8 – 15	-2.25 – 3.25

The channels in Table 6 fall into several groups, shown in Table 7.

Table 7 - the channels grouped by difficulty

Classification	Channels included	Notes
Very easy	D	Time invariant, mild multipath spread and Doppler spread.
Easy	A, B and C	No multipath, varying Doppler shift and fading.
Moderate	G and I	G has mild Doppler spread and moderate multipath spread, I is vice versa.
Hard	H, J and K	Many modes, moderate multipath and Doppler spreads.
Very hard	E and F	Very severe Doppler spread despite short multipath spread.

5.3. Evaluation of the performance of PCC-OFDM

PCC-OFDM was introduced in Section 4.4.4, and is claimed by its proponents to offer greater resistance to multipath interference at the expense of spectral efficiency. In order to test the validity of these claims, a simple PCC-OFDM system was compared with a classic OFDM system in the high-latitude simulator described in Section 5.2. A random sequence of data was transmitted through each of the sample channels using DQPSK modulated OFDM. Once demodulated, the received sequence was compared to the original in order to calculate a bit error rate (BER). A variety of FFT and cyclic prefix sizes were tried and the best performing combination for each channel found. This combination was then run at a range of SNR values to determine its noise performance. The same process was then repeated for *k=2* PCC-OFDM, again using DQPSK and a range of FFT sizes. Noise performance tests were again conducted on the best performing FFT size.

5.3.1. Results

Table 8 - results of the PCC-OFDM simulation trials. Rows shaded in grey indicate where PCC-OFDM performed better than conventional OFDM.

Channel	Best conventional scheme			Best PCC scheme	
	FFT size	Cyclic prefix	Lowest BER	FFT	Lowest BER
A	128	1/32	4.86e-3	128	2.44e-3
B	256	1/8	3.34e-3	256	1.07e-4
C	128	1/64	7.18e-3	128	1.32e-2
D	256	1/4	0.00	128	6.68e-4
E	32	1/8	1.06e-1	32	2.03e-1
F	64	1/8	9.58e-2	64	7.92e-2
G	128	1/2	2.00e-2	256	5.79e-3
H	64	1/8	4.00e-2	128	2.29e-2
I	64	1/8	1.53e-2	64	6.33e-2
J	128	1/4	1.40e-1	128	1.69e-1
K	64	1/8	5.50e-2	64	9.01e-2

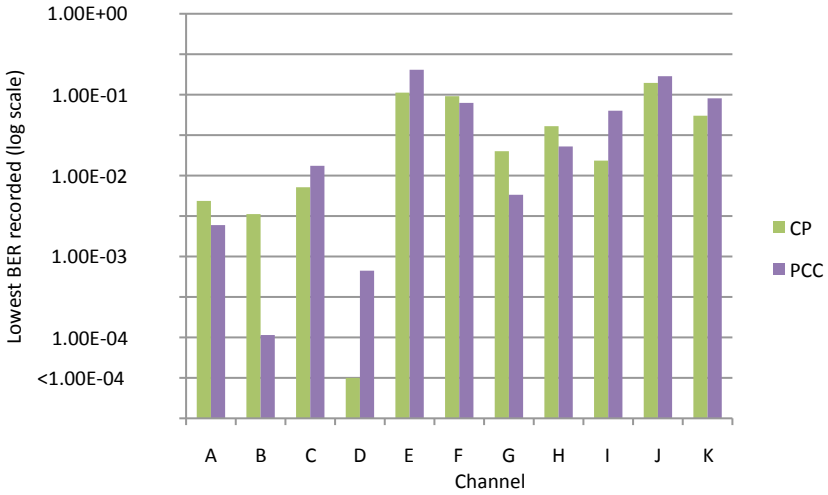

Figure 13 - comparing ordinary (CP) OFDM with PCC-OFDM. Shorter bars indicate better performance.

The results shown in Table 8 and Figure 13 indicate that PCC performs better than the conventional technique in five out of the eleven test channels. PCC has a spectral efficiency equivalent to using a cyclic prefix of ½, so in all but channel G the conventional technique was operating at a higher data rate. The only channel in which PCC makes a really significant reduction in BER is channel B.

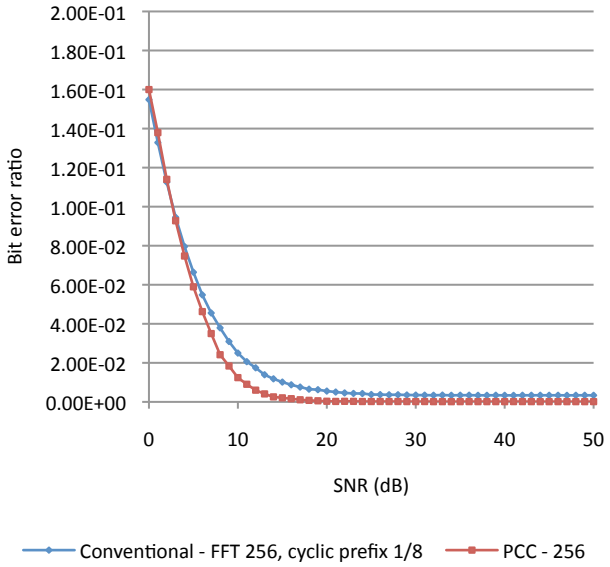

Figure 14- SNR Performance in channel B

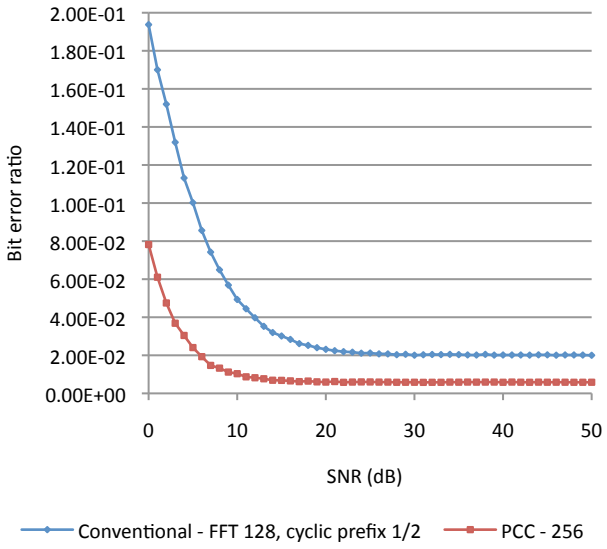

Figure 15 - SNR performance in channel G

Figure 14 shows the relative noise performance in Channel B. It's clear that PCC produces lower BERs (i.e. better performance) for the same SNR than the conventional technique. This is even more marked in channel G (Figure 15). Figure 16 shows performance in channel C, where PCC performed worse than the conventional technique.

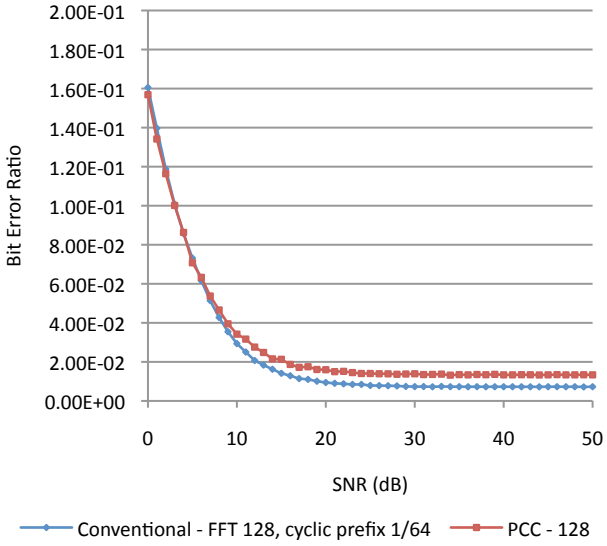

Figure 16- SNR performance in channel C

In both the conventional and PCC experiments, no carrier recovery ("automatic frequency control") was used, and the timing recovery was very rudimentary. PCC is more resistant to carrier and timing offsets, but in a real-world system the carrier and timing recovery systems customarily used with OFDM may well negate this benefit. For example, Fischer and Kurpiers (2002) show that the carrier recovery (aka frequency synchronisation) algorithm used by WinDRM can track a frequency shift between each OFDM symbol of up to 25% of the carrier spacing.

These results indicate that PCC did not exhibit sufficient improvement in performance over conventional OFDM to merit further consideration.

5.4. Evaluation of the performance of WinDRM

"WinDRM" is an open-source software HF modem aimed at radio amateurs (Lanza 2004)[9]. It is derived from the Digital Radio Mondiale (DRM) standard for digital audio broadcasting on HF (ETSI 2009), and the software itself has been developed from the open-source DRM receiver known as DREAM (Fischer 2001).

The modem's source code was made available by the author, and so it has been possible to modify it - longer interleavers were implemented for one particular experiment.

5.4.1. Digital Radio Mondiale

DRM uses an OFDM-based approach to combat the effects of the HF channel. The broadcasts are radiated at high output powers, so high order modulation schemes (16QAM and 64QAM) are used in order to give sufficient data rate for the audio codecs. The DRM standard (ETSI 2009) describes four robustness modes for MF and

[9] The WinDRM source code is available from the author by request, but an executable may be obtained from http://n1su.com/windrm/

HF channels – A to D – for specific applications. In addition to robustness mode, the broadcaster may choose the modulation order and interleaver length.

The robustness modes specify the number of carriers, the cyclic prefix length and the positioning of the pilot tones used for synchronisation and equalisation.

DRM also includes metadata in the transmitted datastream to enable the receiver to identify and decode the incoming signal. The Fast Access Channel (FAC) is used for acquisition, and is repeated within each 400ms DRM frame. FAC cells are always encoded with the same robust modulation and coding scheme, so a receiver may pick up the FAC at lower SNRs than the Main Service Channel (MSC), which carries the main audio or data service.

5.4.2. Description of the waveform

The WinDRM waveform is broadly similar to DRM, but modified to work in a narrower channel bandwidth. DRM is based around the 9 or 10kHz channels used in audio broadcasting, whereas WinDRM needs to fit into the 3kHz channel bandwidth used for SSB communications. To allow for the filters on HF transceivers, WinDRM offers the choice of a 2.3kHz or a 2.5kHz bandwidth. In all the experiments described here the 2.5kHz mode has been used.

Like DRM, WinDRM offers a choice of robustness mode: there are three modes, called A, B and E[10] (see Table 9). Mode A is the fastest and least robust, while mode E is the slowest and most robust. A choice of interleaver length is provided: 400ms or 2s in the original version of WinDRM. There is also a choice of modulation order: QPSK, 16QAM or 64QAM. WinDRM's noise performance is determined by the modulation

[10] WinDRM's mode A and B use the same OFDM parameters as DRM's mode A and B. WinDRM's mode E is not based on a mode in the DRM standard, and was named mode E to avoid confusion with DRM's modes C and D. To further complicate matters, the latest version of the DRM standard now includes a completely different Mode E intended for use on frequencies from 50 to 150MHz.

order chosen. Tests were conducted on the AWGN performance of WinDRM, and these show that QPSK modulation requires 6dB SNR for error-free reception whilst 16QAM requires 9dB (see Figure 17). The majority of the experiments have been carried out using QPSK.

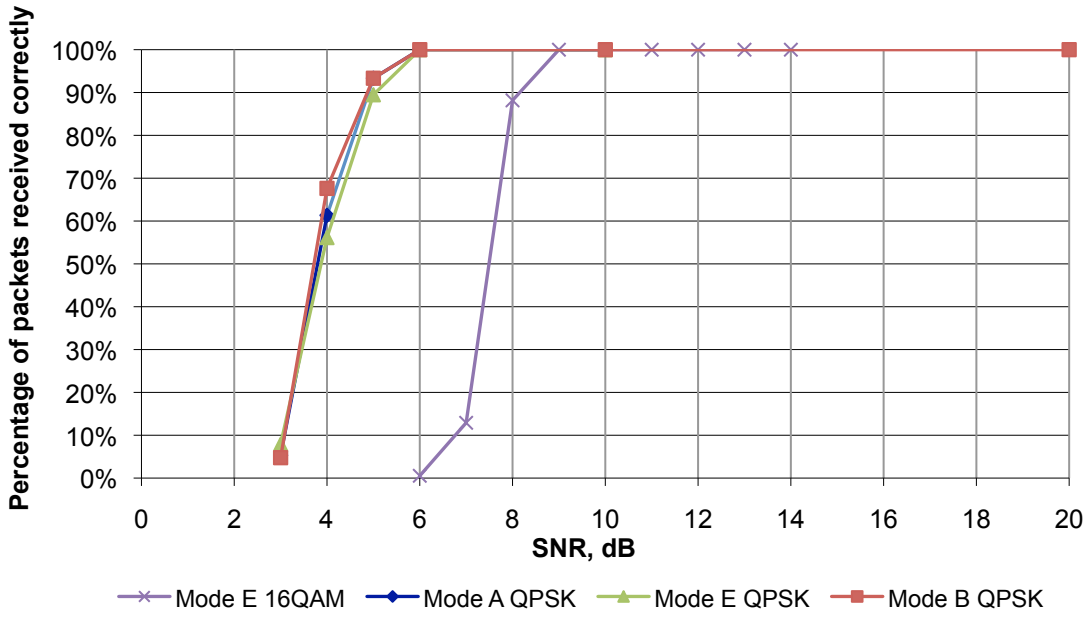

Figure 17 - noise performance of WinDRM modes A, B and E with QPSK modulation and for mode E with 16QAM modulation.

Table 9 - the WinDRM robustness modes

Mode	Number of carriers	Carrier spacing (Hz)	Guard interval fraction	Guard interval duration (ms)	Symbols per frame	Usable MSC data rate, QPSK (kbit/s)	Packet size (bytes)
A	57	41.67	1/9	2.67	15	2.092	104
B	51	46.875	¼	5.33	15	1.568	78
E	31	75	1/2	6.67	20	1.087	54

DRM and WinDRM both use three pilot tones, transmitted continuously, to allow the receiver to acquire frequency synchronisation (i.e. compensate for Doppler shift and local oscillator frequency offsets). In WinDRM, these three tones are at 375, 1125 and 1500Hz. These tones exist at the same frequencies in all robustness modes.

Like DRM, the waveform is divided into 400ms frames. The start of a frame contains "time pilots" which allow the receiver to synchronise to the frame structure. There are also "boosted pilots" at the edges of the channel bandwidth which exist to give a phase and amplitude reference for coherent demodulation.

Finally, there are "scattered pilots" providing amplitude and phase references right across the channel bandwidth to help with equalisation at the receiver.

The frequency, time and boosted pilots exist in all robustness modes, but the density of the scattered pilots changes: mode A uses 3 scattered pilots in each OFDM symbol whereas mode E uses 7.

5.4.3. Experimental method

WinDRM was tested in the high-latitude HF channel simulator, as described in Section 5.2. Because the primary interest was how the high-latitude impairments affected the performance, the experiments were conducted with 15dB SNR, a figure considerably in excess of the minimum required for QPSK or 16QAM. Relatively short simulation periods (90s) were used since longer channel sequences placed a high demand on the computing power available.

Performance was measured by counting the number of packets successfully transmitted through the test channel. WinDRM implements a packet layer internally and the packet size for each robustness mode is shown in Table 9. The packets include a cyclic redundancy check so that it can be determined that they have been received correctly. A more classical approach would have been to examine the BER, but this would have required considerable modifications to WinDRM's internal architecture. A packet-based approach to performance is also appropriate since any real system would incorporate an ARQ protocol, which would request retransmissions of any packets in error. Since the process of requesting and receiving retransmissions is very time-consuming on a

simplex link, there is some value in using packet error rate as a metric: the fine detail provided by a BER study is not needed, since packets containing errors will be retransmitted regardless of exactly how many errors they contain.

5.4.4. Results

The first experiments were conducted using all three robustness modes with the short (400ms) interleaver and QPSK modulation.

Table 10 - performance of the three robustness modes in the channel simulator using QPSK and 400ms interleaver. Results are accurate to one percentage point.

Mode / Modulation	A / QPSK	B / QPSK	E / QPSK
Data rate (bit/s)	2400	1667	1200
Interleaver length (s)	0.4	0.4	0.4
SNR	15dB	15dB	15dB
Channel	Percentage of packets received correctly		
A	80%	81%	83%
B	89%	84%	91%
C	85%	86%	85%
D	100%	100%	100%
E	0%	0%	0%
F	0%	0%	0%
G	69%	89%	89%
H	0%	5%	53%
I	52%	77%	84%
J	10%	22%	34%
K	0%	0%	1%

Table 10 shows how the three robustness modes perform differently in the eleven test channels. The results are accurate to one percentage point. As expected, mode A is generally the least robust and mode E the most. The “hard” channels (H, J and K) prove very difficult for all three modes, and the “very hard” ones (E and F) defeat them altogether. In channel C all three robustness modes give very similar performance,

showing that none of them are especially well suited to the low-multipath, moderate Doppler channel conditions.

Using higher order modulation (16QAM vs QPSK) gives increased speed but reduced robustness, as Table 11 shows.

Table 11 - performance of 16QAM vs QPSK in mode E. Results are accurate to one percentage point.

Mode / Modulation	E / QPSK	E / QPSK	E / 16QAM	E / 16QAM
Data rate (bit/s)	1200	1200	2005	2005
Interleaver length (s)	0.4	2	0.4	2
SNR	15dB	15dB	15dB	15dB
Channel				
A	83%	88%	76%	83%
B	91%	98%	78%	91%
C	85%	90%	84%	89%
D	100%	100%	100%	100%
E	0%	0%	0%	0%
F	0%	0%	0%	0%
G	89%	98%	75%	96%
H	53%	19%	3%	2%
I	84%	77%	62%	87%
J	34%	19%	19%	3%
K	1%	0%	0%	0%

It is also clear from the results in Table 11 that interleaver length can also have a very significant impact on the performance of the modem. Big enhancements in performance come from having the correct interleaver length for the channel - and longer is not necessarily better. For instance, in channel I, increasing the interleaver length for the QPSK mode produces a reduction in successful transmission, whereas in 16QAM mode it produces an improvement. The 16QAM mode tested here incorporates stronger FEC than the QPSK mode, which accounts for this apparent discrepancy. To further explore the relationship between interleaver length and channel conditions, a series of

experiments were undertaken using Mode E with QPSK and progressively longer interleavers. The results are shown in Table 12.

Table 12 - effect of interleaver length on mode E / QPSK performance

Mode / Modulation	E / QPSK				
Data rate (bit/s)	1200				
Interleaver length (s)	0.4	2	4.8	6.4	9.6
SNR	15dB				
Channel	Percentage of packets received correctly				
A	83%	88%	93%	95%	97%
B	91%	98%	100%	100%	99%
C	85%	90%	95%	96%	98%
D	100%	100%	94%	98%	100%
E	0%	0%	0%	0%	0%
F	0%	0%	0%	0%	0%
G	89%	98%	94%	97%	92%
H	53%	19%	40%	29%	3%
I	84%	77%	97%	97%	81%
J	34%	19%	0%	1%	0%
K	1%	0%	0%	0%	0%

Channels A and C, with their slow fading, clearly benefit from long interleavers, with the performance becoming significantly better as the interleaver size increases. Conversely, channel J has a high Doppler spread (meaning fast fading) and performs best with a short interleaver. For the other channels the relationship between interleaver size and Doppler spread is less clear, but the importance of choosing the correct length for the channel remains. From a systems engineering perspective, the option to vary interleaver length adaptively depending on channel conditions is likely to be very valuable.

5.5. Evaluation of the performance of NATO standard modems

Two military HF modems were tested in the high-latitude simulator. Initially, tests were performed using a General Atronics GA-122 modem. This modem supports the STANAG 4285 standard (NATO 1989). The modem was tested using the same methodology as was used for the evaluation of WinDRM (see Section 5.4.3), using the same packet layer to measure performance. Packets were generated and checked by a PC, which communicated with the modem using a serial interface. Table 13 shows the performance in terms of the percentage of packets received correctly.

Table 13 - performance of the GA-122 modem using STANAG 4285 at 15dB SNR. Results are accurate to one percentage point.

Channel	2400bit/s coded, 853ms interleaver, 127 packets	1200bit/s coded, 853ms interleaver, 91 packets
A	39%	68%
B	38%	82%
C	16%	69%
D	100%	100%
E	0%	0%
F	0%	0%
G	2%	35%
H	0%	0%
I	4%	29%
J	0%	4%
K	0%	0%

The performance is not good. Even in the “easy” channels A-C the modem only produces a barely acceptable performance at 1200bit/s – the 30% packet loss in channels A and C would result in a maximum throughput of 800bit/s assuming ideal ARQ.

Subsequently, a more recent military modem, a Harris RF5710A supporting STANAG 4539 and MIL-STD-188-110B, was tested. This modem required a different approach, as it was not suitable for operation with a PC serial port. Consequently, a Fireberd serial test set was used to provide a synchronous serial datastream to the modem, whose output could then be recorded on the PC as a WAV file. After passing through the high-latitude simulator, the resultant WAV file was played back to the modem, and the block error rates calculated by the test set. The test set's block size was chosen to match the WinDRM packet size in order that the results would be comparable. As with the WinDRM tests in Section 5.4, tests were run at 15dB SNR.

Table 14 - performance of the RF5710A modem, percentage of packets received correctly. Results are accurate to one percentage point.

Channel		Mode	110B, 1200bit/s	110B, 1200bit/s	110B, 2400bit/s
Name	Doppler spread (Hz)	Interleaver length (s)	4.8	0.6	0.6
A	0.5 - 1.5		99%	87%	72%
B	0.5 – 2		100%	93%	76%
C	0.24 – 3.5		100%	93%	80%
D	0.5		100%	100%	100%
E	3 – 40		0%	0%	0%
F	0.5 - 18		0%	40%	0%
G	0.5 – 1		100%	96%	67%
H	1.5 – 3		29%	83%	0%
I	0.5 – 11		99%	90%	39%
J	0.8 – 13		98%	73%	12%
K	0.8 – 15		32%	26%	0%

The results in Table 14 show that the modem performs well in all channels except E, F and K. Once again (see Section 5.4.4) choosing the correct interleaver for the environment can make a very significant difference to the performance. Where the interleaver is long enough to overcome the fading of the channel, performance improves noticeably. For example, consider 110B in channel J – with the 0.6s interleaver it achieves 73% successful transmission, but a longer interleaver boosts this to 98%.

There is a secondary effect though – that if a long interleaver is not long enough to overcome the fading, a shorter interleaver will perform better. Channel H shows how 110B's 4.8s interleaver is not long enough to overcome the channel fading, with the shorter interleaver giving superior performance. The relationship between Doppler spread (and hence fading rates) and the required interleaver length is not always clear-cut because other channel conditions (multipath, for example) have also changed between channels, but the essential point remains that an HF communications system may enhance its performance considerably by being able to adapt its interleaver length to the channel conditions.

5.6. Comparison of WinDRM and MIL-STD-188-110B

MIL-STD-188-110B, as implemented by the Harris RF5710A modem, performs well at 1200bit/s in the high-latitude simulator – particularly when the most suitable interleaver size is chosen for the channel. However, the performance of the 2400bit/s waveform at 15dB SNR is reasonable but not excellent.

WinDRM does not achieve the same performance at 1200bit/s as 110B, and it is noticeable that while 110B makes a little headway into the very hard channel F, WinDRM fails completely. However, using WinDRM's mode E with 16QAM modulation produces quite a respectable performance at 2000bit/s, in fact rather better than 110B at 2400bit/s.

A further experiment showed that 110B's ultra-rugged 75bps mode (equivalent to STANAG 4415) was capable of handling channels E and F with 100% successful transmission at 15dB SNR, thus showing that a 110B modem is capable of operating in all of the test-case channels. Although it provides a very low data rate, this may still be of use in providing small amounts of information (such as "instrument OK", battery

voltages and data summaries) during periods of poor propagation such as the polar winter.

However, there is a further issue to consider – that of peak-to-average-power ratio (PAPR). A waveform with a high PAPR requires amplifier headroom in order to be transmitted without distortion, and hence requires a more powerful amplifier for the same average output power than one with a low PAPR. OFDM signals have long been criticised for their high PAPR, and WinDRM is no different: measurements made of WinDRM mode E show that it has a PAPR of 13dB, regardless of whether QPSK or 16QAM are used. By contrast, a 110B waveform (the 2400 baud 0.6s interleaver variant was measured) has a PAPR of 4dB. These measurements were made by importing the waveform samples used for the simulations into MATLAB and calculating the PAPR by dividing the peak sample value by the RMS value of the whole sequence of samples. Backing off a power amplifier to accommodate the PAPR of a signal generally results in a dramatic reduction in power efficiency. Many researchers have therefore worked on reducing the PAPR of OFDM waveforms, and whilst many techniques have been identified, there is no single solution for all circumstances (Han and Lee 2005).

To conclude this section, it is clear that the 110B modem is a very capable product and suitable for polar region operation despite the fact that the waveforms are optimised for mid-latitude conditions. WinDRM is also shown to perform respectably, but there is certainly room for improvement in both its performance in the more demanding channels and in reducing its PAPR.

6. On-air tests in Antarctica

Practical experiments in Antarctica were seen as a valuable part of this project, although the high cost of travel to the region precluded hands-on fieldwork. However, using the British Antarctic Survey's logistics and communications infrastructure, and with thanks to the kind assistance of colleagues, it has been possible to install equipment at two research stations. This chapter describes the studies undertaken in Antarctica and presents their results.

6.1. Geophysical conditions

The path chosen was between Halley and Rothera stations (see Figure 18) and was chosen simply for practical reasons: both stations are manned year-round, and both have free-to-use satellite data links to the UK, allowing equipment to be controlled remotely. Halley is at 75°35'S, 26°34'W and Rothera is at 67°34'S, 68°08'W. This puts the path midpoint at 72°39'S, 51°55'W, over the Weddell Sea. The great-circle distance between the transmitter and receiver is 1665km.

The path itself is sub-auroral, although Halley station is on the edge of the auroral zone, and moves into it with any mild enhancements in auroral activity. The solar minimum had occurred in January 2009, shortly before the experiment began, and activity picked up during 2009 and 2010 whilst the experiment was in progress. See Figure 19 for a plot of the variations in sunspot number.

Figure 18 - map showing the position of Rothera and Halley and the great-circle path between them. The map projection (south pole stereographic with a 71°S latitude of true scale and a central meridian of longitude 50°W) has been chosen so that the great circle path appears to be almost a straight line. See Figure 38 for a smaller-scale map that includes all of the southern continents. (Cartography by Peter Fretwell, reproduced by kind permission of the British Antarctic Survey)

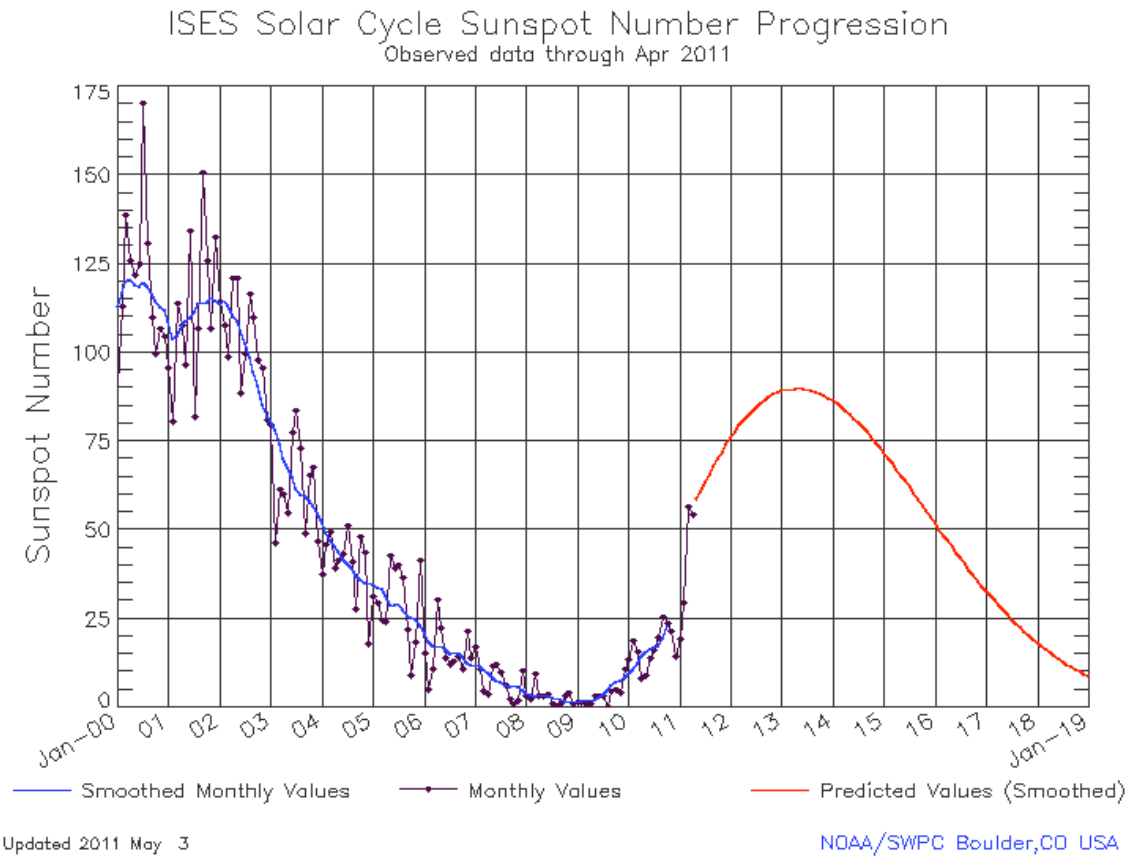

Figure 19 - sunspot number observations and predictions for the period 2000 - 2019. Note the solar minimum in January 2009 and the rise in activity during 2009 and 2010. Image reproduced by permission of NOAA/US Department of Commerce from http://www.swpc.noaa.gov/SolarCycle/index.html

6.1.1. Direct solar influence

Both stations are within the Antarctic Circle and so experience continuous daylight in summer and continuous darkness in winter. The path midpoint (72°39'S, 51°55'W) is in darkness *at ground level* between the 12th May and 1st August each year, according to the NOAA Solar Calculator (http://www.esrl.noaa.gov/gmd/grad/solcalc/).

However, at significant altitudes above the Earth's surface sunrise occurs earlier than at ground level, and sunset occurs later. In Figure 20 the line T is a tangent to the Earth's

surface. An observer on the ground, *O*, will see the Sun rise as it crosses the tangent *T*. However, an observer at a height *h* above the ground will see the Sun rise earlier, when it crosses the tangent *U*. To find out how much earlier, the angle *b* must be found. *T* and *T'* are parallel lines, so the angle *b* is the (negative) solar elevation for the elevated observer. Angles *b* and *a* form a right angle, so *b* can be found if *a* is known. The angle *a* is part of a right-angled triangle where two of the sides are known. Equation 6 shows how *b* may be found.

Since the distance from the Earth to the Sun is very much larger than the distance *h* we can consider the angle *b* to be equal to the solar elevation observed from the ground.

$$\sin a = \frac{R}{R+h}$$
$$b = 90° - a$$

Equation 6 - finding the solar elevation angle

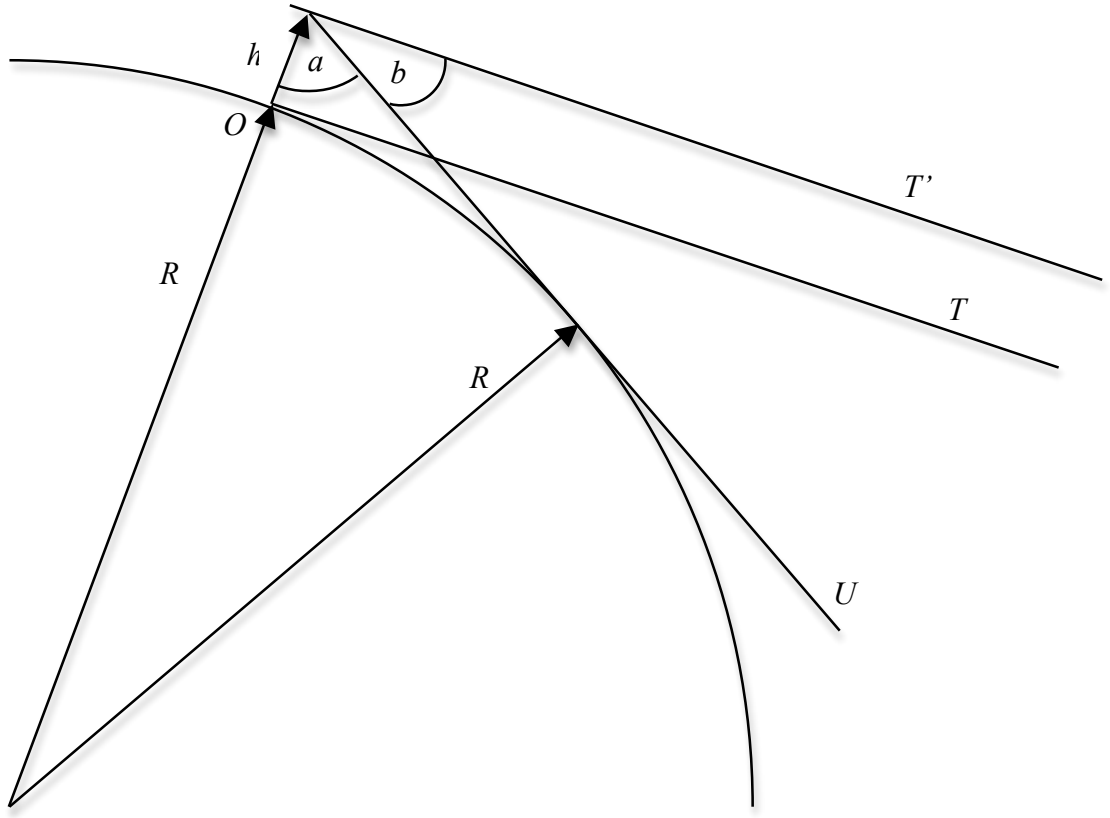

Figure 20 - showing how an observer high in the atmosphere will see the Sun rise earlier than an observer at ground level

Table 15 shows the elevation angles at which the Sun becomes visible for a number of different heights above the ground.

Table 15 - elevation angle at which the Sun becomes visible at different altitudes

Height above ground, km	Elevation angle at which the Sun becomes visible, degrees
500	-22.0
400	-19.8
300	-17.2
200	-14.2
100	-10.1

So, for the F-layer of the ionosphere at roughly 300km, the sun becomes visible when it is still 17 degrees below the horizon at ground level. Similarly, the E-layer at roughly 100km will be in daylight if the sun is less than 10 degrees below the horizon at ground level. What this means in practice is that for latitudes equatorward of 84 degrees, the F-layer is still weakly illuminated for a period each day even in midwinter. For example, Figure 21 shows the diurnal variation in solar elevation angle for 21st June 2009 – midwinter's day – at the midpoint of the Halley-Rothera circuit. The calculations are from NOAA (http://www.esrl.noaa.gov/gmd/grad/solcalc/calcdetails.html).

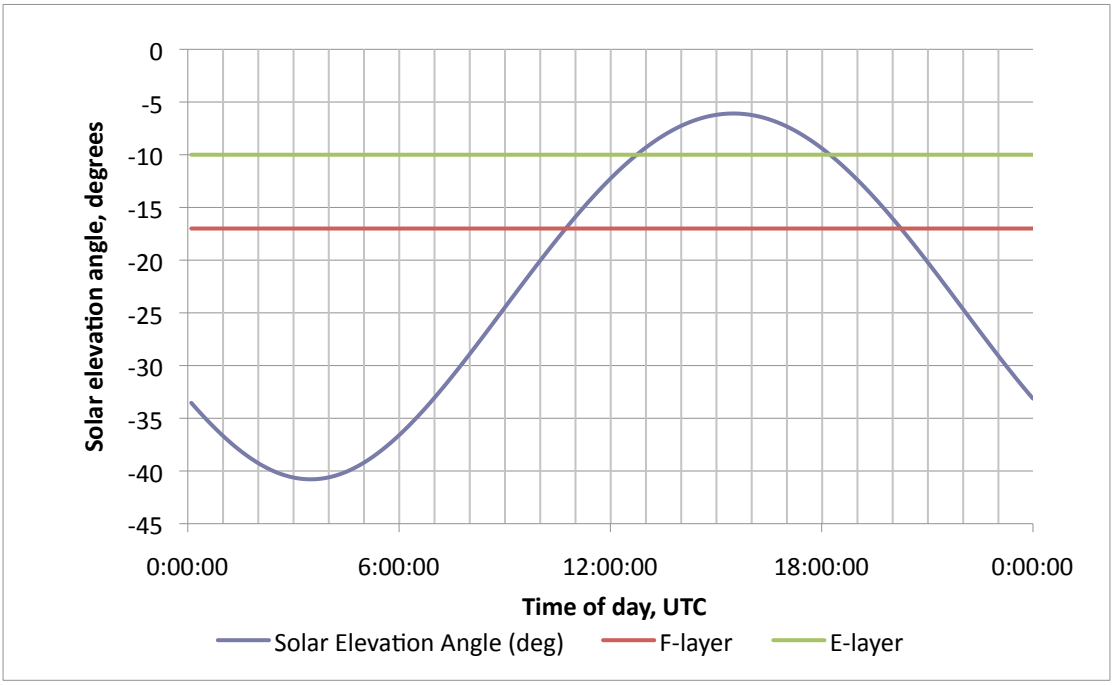

Figure 21 - diurnal variation in solar elevation angle for the Halley-Rothera circuit midpoint on 21st June 2009 (Midwinter's Day)

As can be seen here, the F-layer comes into daylight at around 1045 UTC and goes into darkness again at 2015 UTC. The E-layer (-10 degrees) is in daylight between 1300 and 1800 UTC.

The angle of the Sun has a direct impact on the level of ionisation produced in the ionosphere, which may be described using Chapman's model of ion production (Chapman 1931). For the purpose of this description, we may further approximate the Chapman model by saying that the maximum level of ion production is proportional to the cosine of the solar zenith angle (Hargreaves 1995, 213). Solar zenith angle is the complement of the solar elevation angle, so ion production is maximum with a zenith angle of 0° (elevation 90°, i.e overhead) and drops to zero with a zenith angle of 90° (i.e. at sunset). The approximation becomes less valid as the sun gets closer to the horizon, but it suffices to say that at low angles of the Sun (such as in the polar winter) the ion production is very significantly lower than when the Sun is at its zenith. Table

16 shows how the noon solar zenith angle at the path midpoint changes over the first year of the experiment, and shows the approximate ionisation level for each month as a percentage, taking the maximum in December (midsummer) as 100%. The negative numbers for May, June and July indicate that the sun is illuminating the ionosphere from below rather than from above – so June (midwinter) actually has a higher level of relative ionisation than April, May, July and August.

Table 16 - variation in solar zenith angle and relative ionisation over the period May 2009 - April 2010

Date	Solar zenith angle at noon	Cosine of solar zenith angle at noon	Relative ionisation with respect to Midsummer
21st May 2009	92.9	-0.05	-8%
21st June 2009	96.1	-0.11	-16%
21st July 2009	93.0	-0.05	-8%
21st August 2009	84.6	0.09	14%
21st September 2009	73.1	0.29	44%
21st October 2009	61.8	0.47	72%
21st November 2009	52.6	0.61	93%
21st December 2009	49.2	0.65	100%
21st January 2010	52.8	0.60	92%
21st February 2010	62.2	0.47	71%
21st March 2010	73.0	0.29	45%
21st April 2010	84.6	0.09	14%

6.2. Methods

6.2.1. Equipment

Because of the lead time on shipping equipment to Antarctica (typically around five months), it was decided to install equipment that offered a high degree of flexibility. A software-defined radio system was chosen since this allowed the software to be modified after the hardware had been deployed. Two Flex-5000 amateur radio transceivers were purchased, together with two standard PCs, and these were deployed to Rothera and Halley research stations in the 2008/9 Antarctic summer season. The transceivers connect to the PCs using an IEEE-1394 (aka FireWire) interface. When receiving, a broad band of received spectrum (up to 96kHz) is passed to the PC via the IEEE-1394 link, and the PC performs final demodulation in software. When transmitting, the Flex-5000 transceiver has a power output of 100W PEP[11].
FlexRadio supply a software package, called PowerSDR, to control the radio and make it function as a general-purpose voice transceiver. It runs on Microsoft Windows XP.

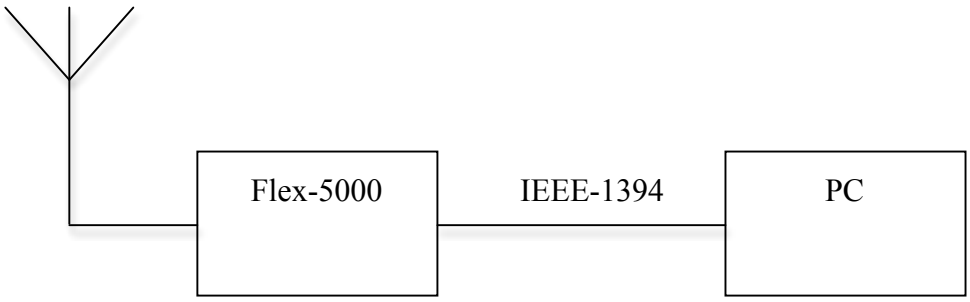

Figure 22 - block diagram of the hardware installed at Rothera and Halley

Although the PowerSDR package is open-source, it would have been extremely time-consuming to develop software to interface directly with the radios. Instead, PowerSDR was used to control the radio, and other software was then used to control PowerSDR.

[11] PEP is Peak Envelope Power output, the standard way of measuring the power of radio transmitters carrying modulated signals.

Audio signals were piped in and out of PowerSDR using a piece of software called Virtual Audio Cable (VAC), and control commands were sent via a virtual serial port system, as PowerSDR can emulate the control protocol of a Kenwood amateur radio transceiver.

6.2.2. Operation

The equipment was installed at Rothera and Halley in February 2009. Teething troubles with the software and a faulty antenna feeder at Halley prevented the experiments from working until May that year. At Rothera, the equipment was given its own antenna, an Icom AH-710 broadband folded dipole, mounted low to the ground to simulate a field deployment. At Halley, the equipment used one of the main communications antennas, a broadband dipole at a height of 15m, orientated to radiate north-south. Since this antenna was needed in the austral summer for operational communications, the equipment was often disconnected during this period (Dec 2009 – Feb 2010), limiting the opportunities for data collection at that time.

The WinDRM software was modified to operate from a pre-programmed schedule file. The usual format of the schedule was to use ten frequencies and to try both mode B and mode E on each frequency. All transmissions used QPSK. Each transmission lasted one minute, so a full cycle lasted twenty minutes. The frequencies in the set were changed in order to allow for changes in propagation between summer and winter, and Table 17 shows which frequencies were used at which times of year.

Table 17 - details of the frequency sets used at different periods during the experiment

Date of schedule change	Frequencies in use (kHz)	Modes
10th June 2009	2272, 3186, 4067, 5150, 6386, 7623, 8198, 9106, 10049, 11255	B only
21st July 2009	As above	B and E
25th September 2009	3186, 4067, 5150, 6386, 7623, 8198, 9106, 10049, 11255, 14475	B and E
30th October 2009	6386, 7623, 8198, 9115, 10049, 11255, 14475, 16315, 17975, 23250	B and E
4th June 2010	3186, 3800, 4067, 4553, 6386, 7623, 8198, 9115, 10049, 11255	B and E

6.2.3. Data quality

Various issues have caused problems with the experiment during its operation. These have ranged from operational issues, such as the antenna at Halley being needed for aircraft communications, to software bugs and hardware faults. As a consequence, a data quality assurance log has been kept, with notes recording any issues observed during daily checks, and each day graded on the quality of its data. Subsequent analysis has used this log to ensure that only days graded "OK" are considered as part of the

experiment. Table 18 shows how many valid days have been recorded in each month that the experiment has been running.

Table 18 - number of days in each month that the experiment was fully operational

Month	Year	Number of valid days
May	2009	7
June	2009	10
July	2009	21
August	2009	23
September	2009	18
October	2009	5
November	2009	4
December	2009	10
January	2010	8
February	2010	4
March	2010	23
April	2010	16
May	2010	27
June	2010	22
July	2010	31
August	2010	29

6.2.4. Analysis software

The software modem was modified to produce a log file, which shows the status of the receiver roughly twice per second. The log captures a large number of parameters measured by the receiver, including the packet number of the last packet to be successfully received. By looking for changes in this number it is possible to count the number of packets received and thus give a reasonable estimate of the channel throughput. Processing the very large Comma Separated Value (CSV) log files generated by the receiver was done using an Oracle database. The log files were imported into the database using SQL*Loader and then a series of Perl scripts were written to create monthly reports summarising the successful packet count by hour and frequency.

To obtain a figure for the data throughput on the link, it was decided to employ a simple method to simulate the effect of an automatic link establishment (ALE) system. The analysis technique identified the combination of frequency and robustness mode which received the highest throughput in any given hour. Since the cycle of measurements takes twenty minutes, this hourly figure is based on a three different one-minute measurements at twenty-minute intervals. The “extrapolated throughput” figure in the results is simply the total measured throughput in those three one-minute measurements multiplied by twenty, making the assumption that the throughput would be broadly similar to the measured results over the whole hour. A real ALE system would probably change frequency in a more intelligent manner, so although this analysis is rather simple it should give a conservative estimate of how well the link performs.

6.3. Results

6.3.1. Diurnal variation in data throughput

The propagation of HF signals is usually subject to a diurnal variation under the influence of the sun. At high latitudes the variation is more complex, and the results of the propagation study show how the diurnal variation is subject to seasonal changes. The plots of diurnal variation on the next few pages (Figure 23 through to Figure 34) show the average extrapolated throughput for each hour of the day during each month and include the data from all the valid days in the month (see Table 18 for the number of valid days in each month).

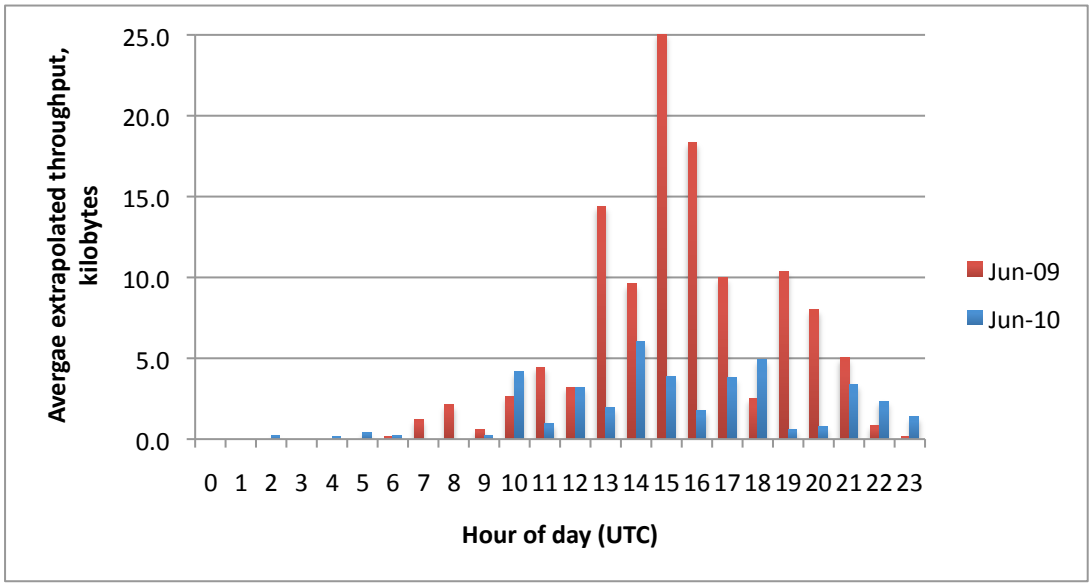

Figure 23 - diurnal variation in data throughput for June

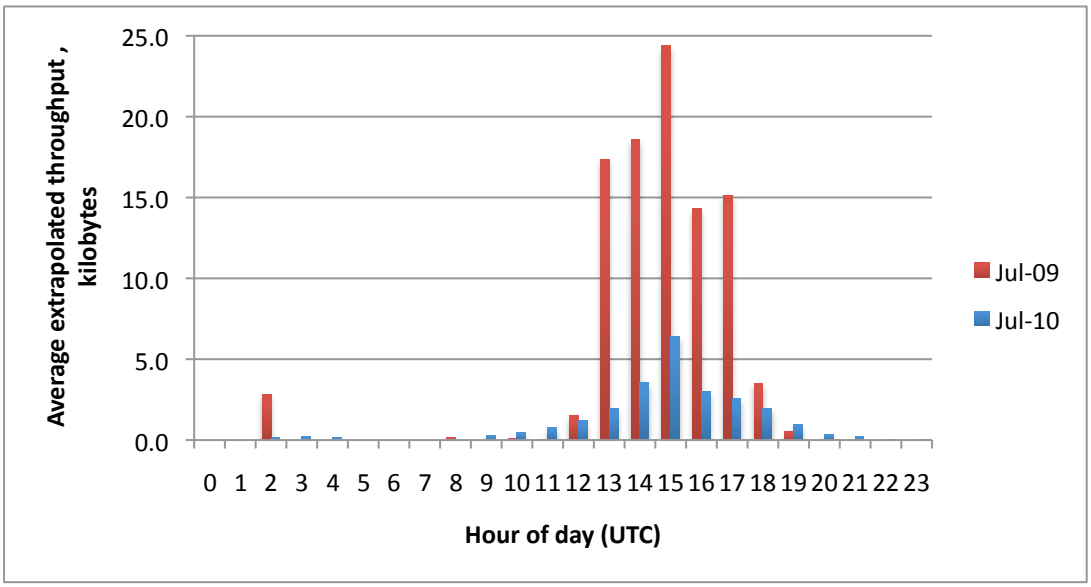

Figure 24 - diurnal variation in data throughput for July

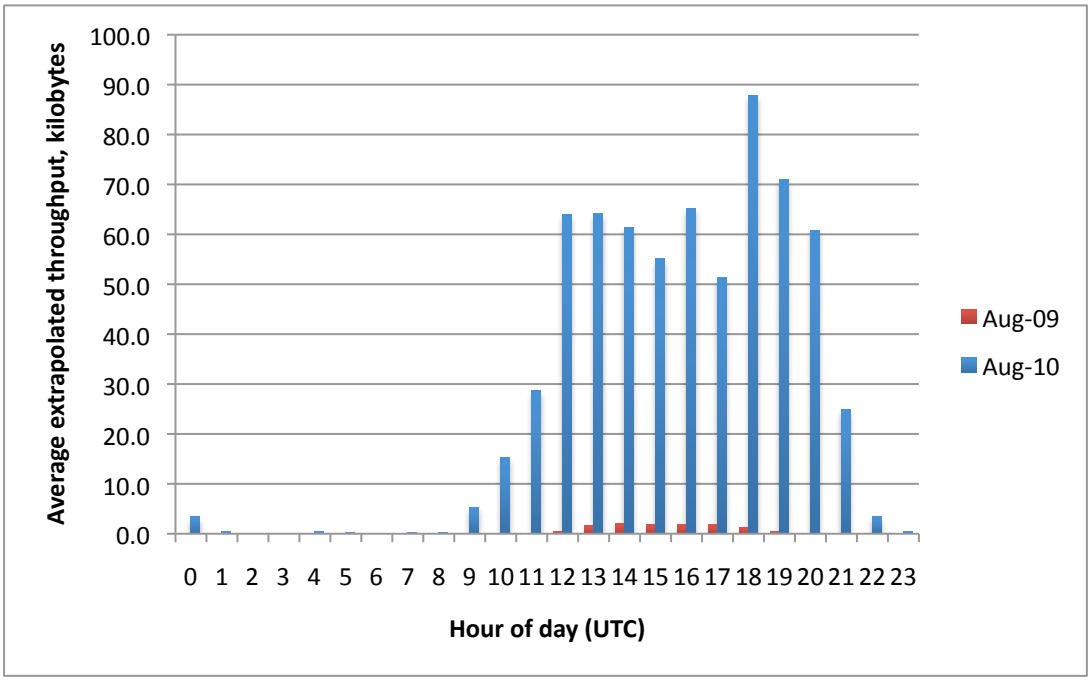

Figure 25 - diurnal variation in data throughput for August

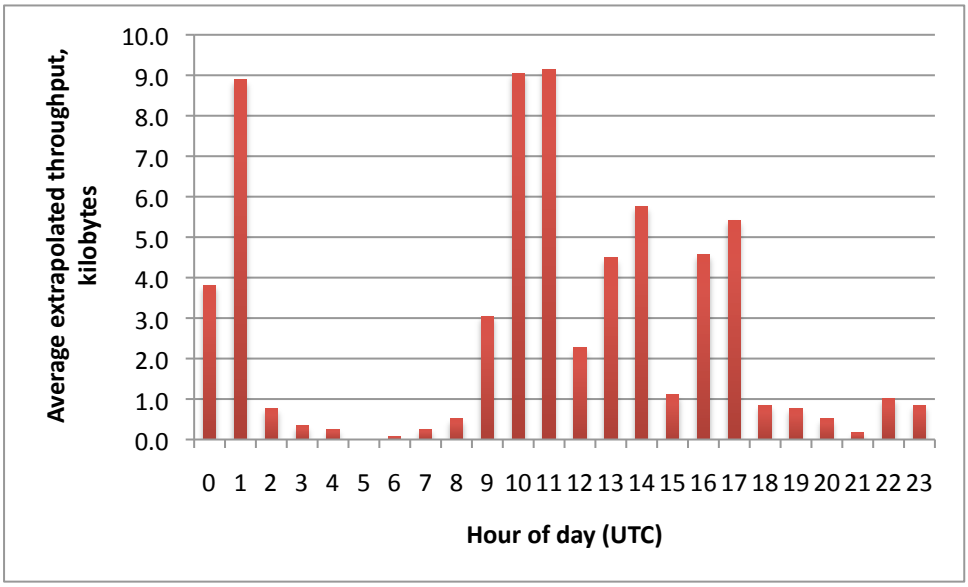

Figure 26 - diurnal variation in data throughput for September 2009

Please note that the plots on this page are not to the same scale because the dynamic range of the data varies considerably over the year.

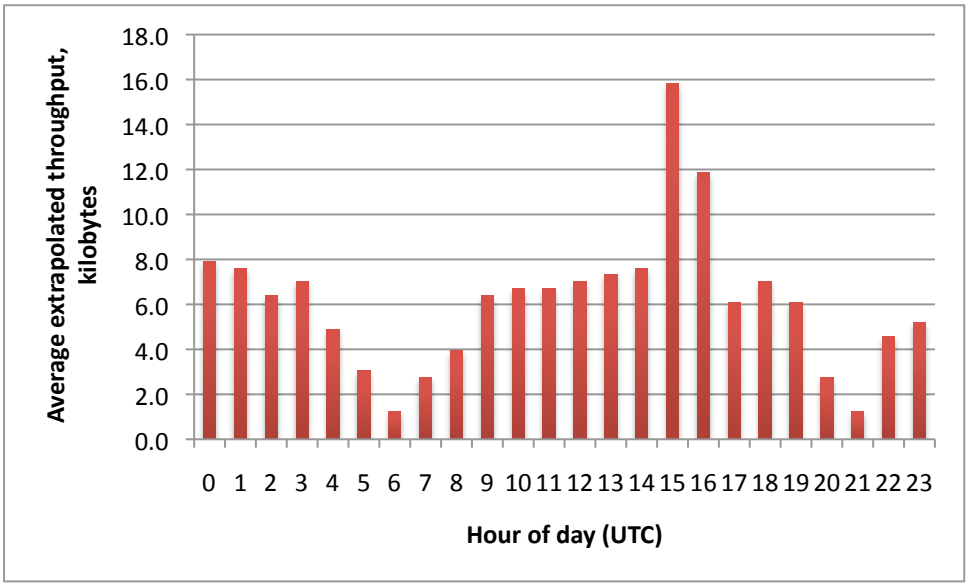

Figure 27 - diurnal variation in data throughput for October 2009

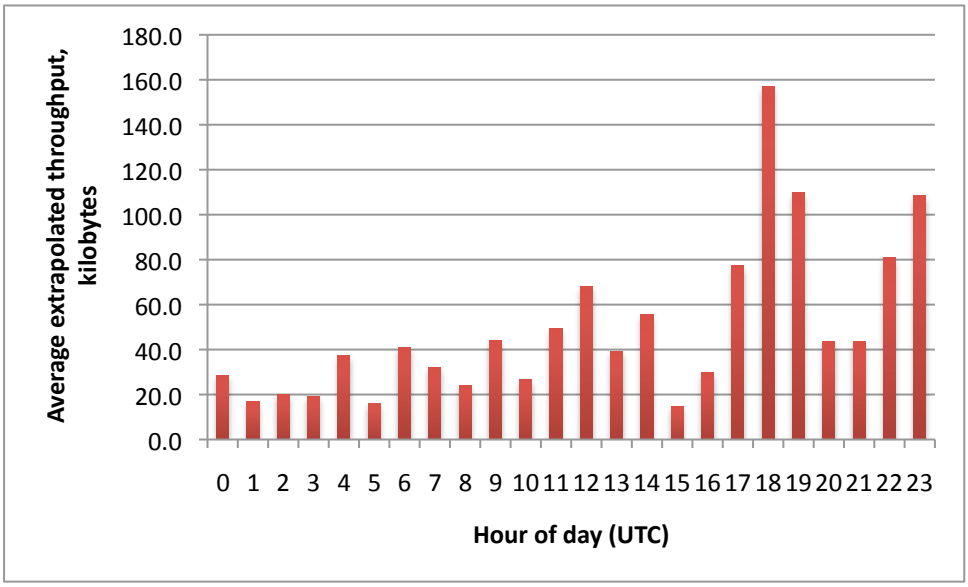

Figure 28 - diurnal variation in data throughput for November 2009

Please note that the plots on this page are not to the same scale because the dynamic range of the data varies considerably over the year.

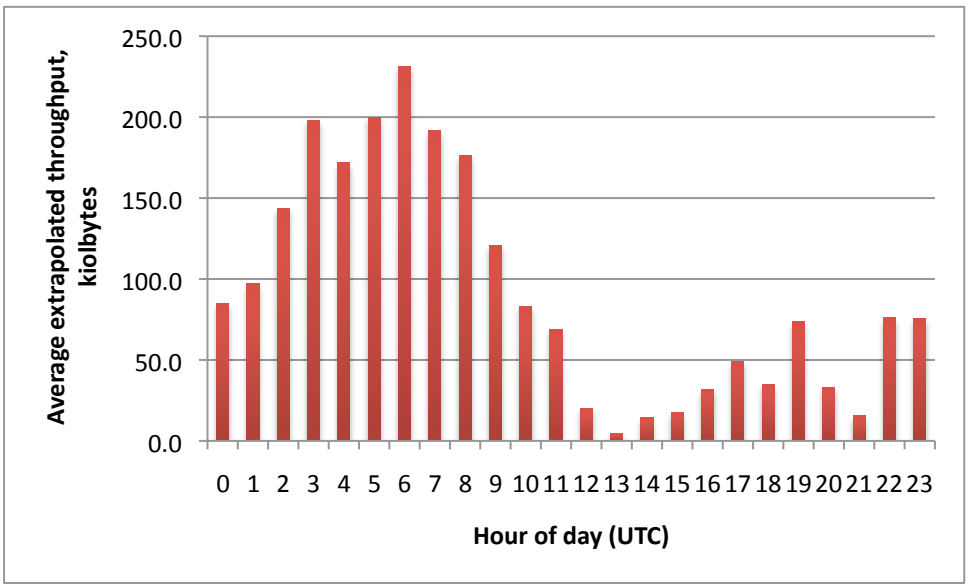

Figure 29 - diurnal variation in data throughput for December 2009

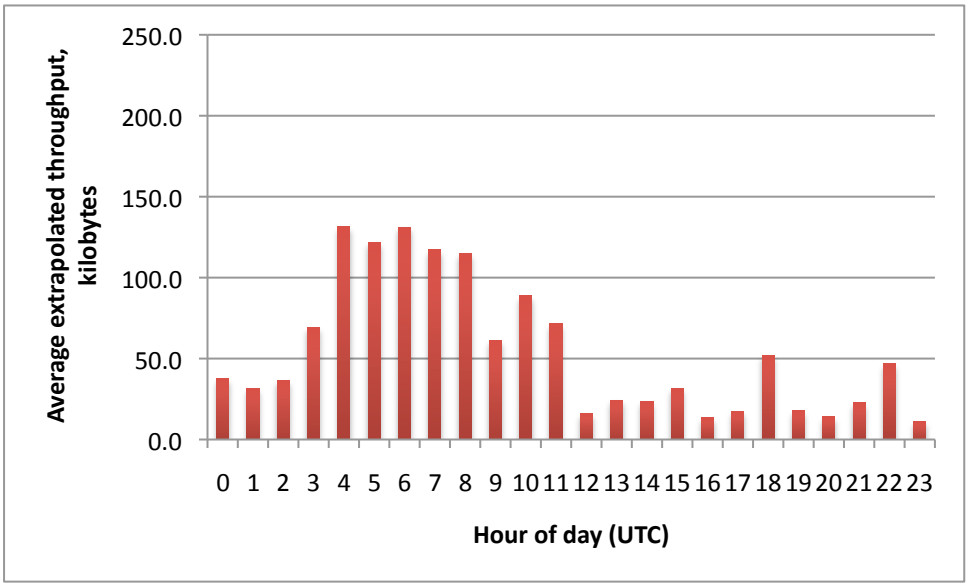

Figure 30 - diurnal variation in data throughput for January 2010

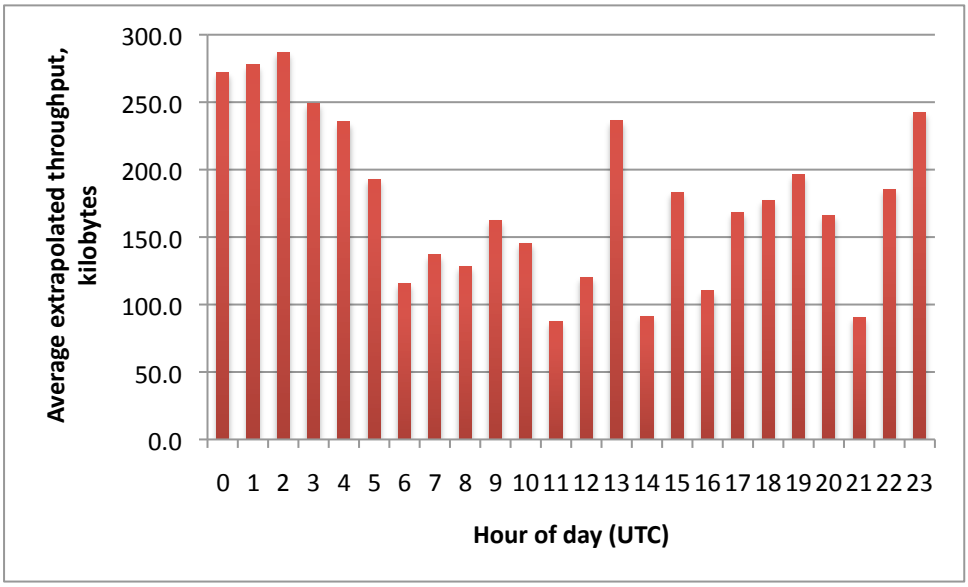

Figure 31 - diurnal variation in data throughput for February 2010

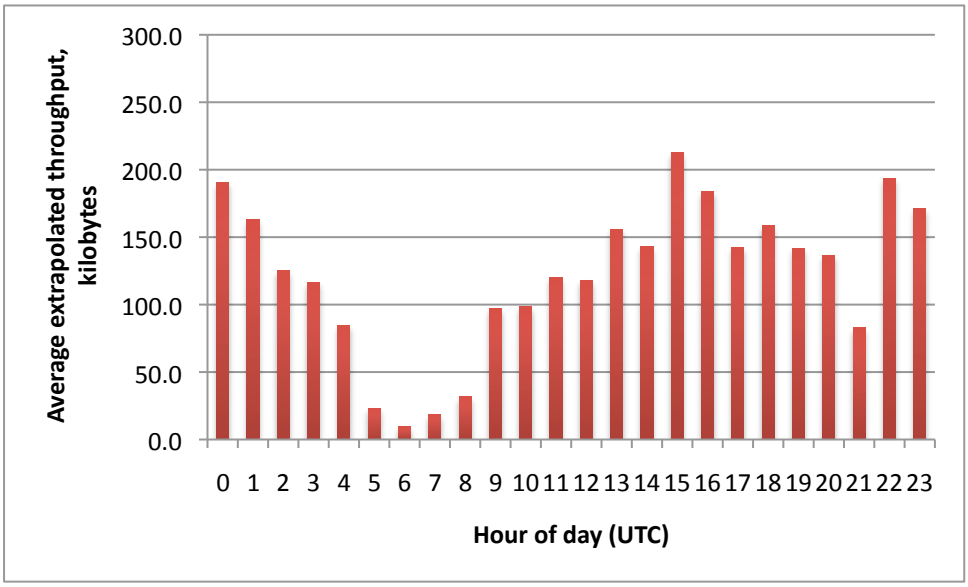

Figure 32 - diurnal variation in data throughput for March 2010

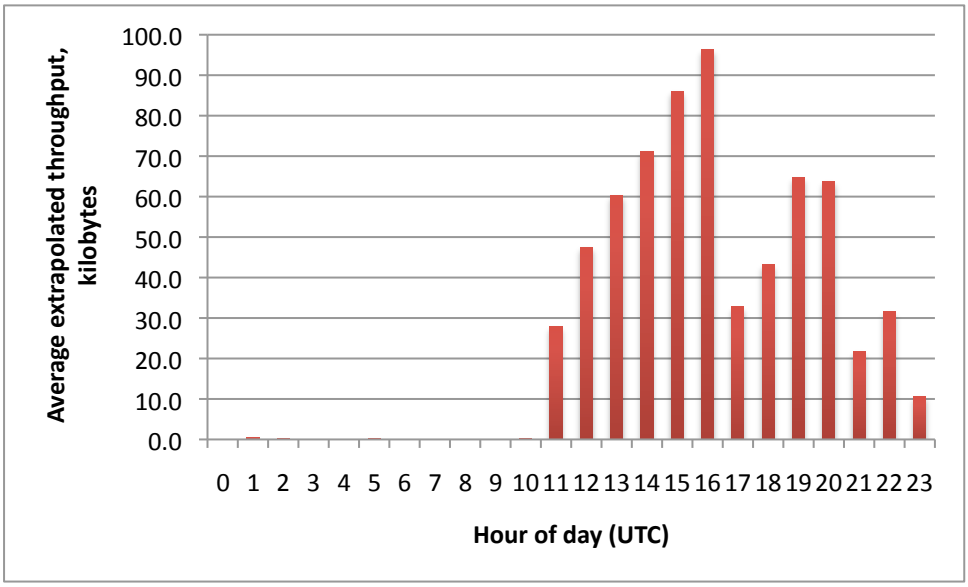

Figure 33 - diurnal variation in data throughput for April 2010

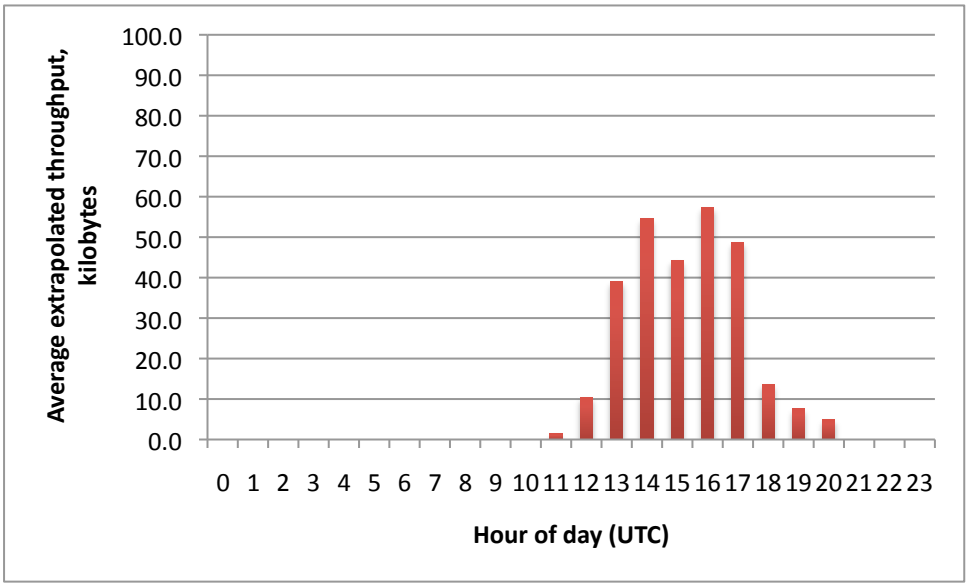

Figure 34 - diurnal variation in data throughput for May 2010

Figures 23 - 34 show average data throughput on the best performing frequency in each hour against UTC time for each month of the year. Rothera is in the UTC-3 timezone, so local noon falls at around 1500. Note that the scales of the plots vary as the volume of data changes considerably between austral summer and winter.

The austral winter months (April – August) show strong diurnal variation around local noon, which confirms that the Sun still has a direct influence on the ionosphere even though it is below the horizon at ground level (see Figure 21 and associated text). There is a distinct variation between 2009 and 2010: in June and July the data throughput was much higher in 2009, whereas for August, 2010 has the higher throughput. This is not readily explained: June-Aug 2009 have very low sunspot numbers, whereas by the following year the sunspot numbers are considerably higher. One possibility is that the higher ionisation present in 2010 creates multipath and Doppler spread in June/July, whereas in August the greater solar irradiance is permitting much higher working frequencies with lower levels of absorption. This suggestion seems to be borne out by

the median restricted MOF[12] data shown in Figures 35-37 – the data for June and July 2010 show relatively little diurnal variation in rMOF, whereas in August 2010 there is a strong rise in rMOF during the later part of the day. In fact, in August 2010 the rMOF is being limited by the frequencies being tested: 11255kHz is the highest frequency that was being tried during that month.

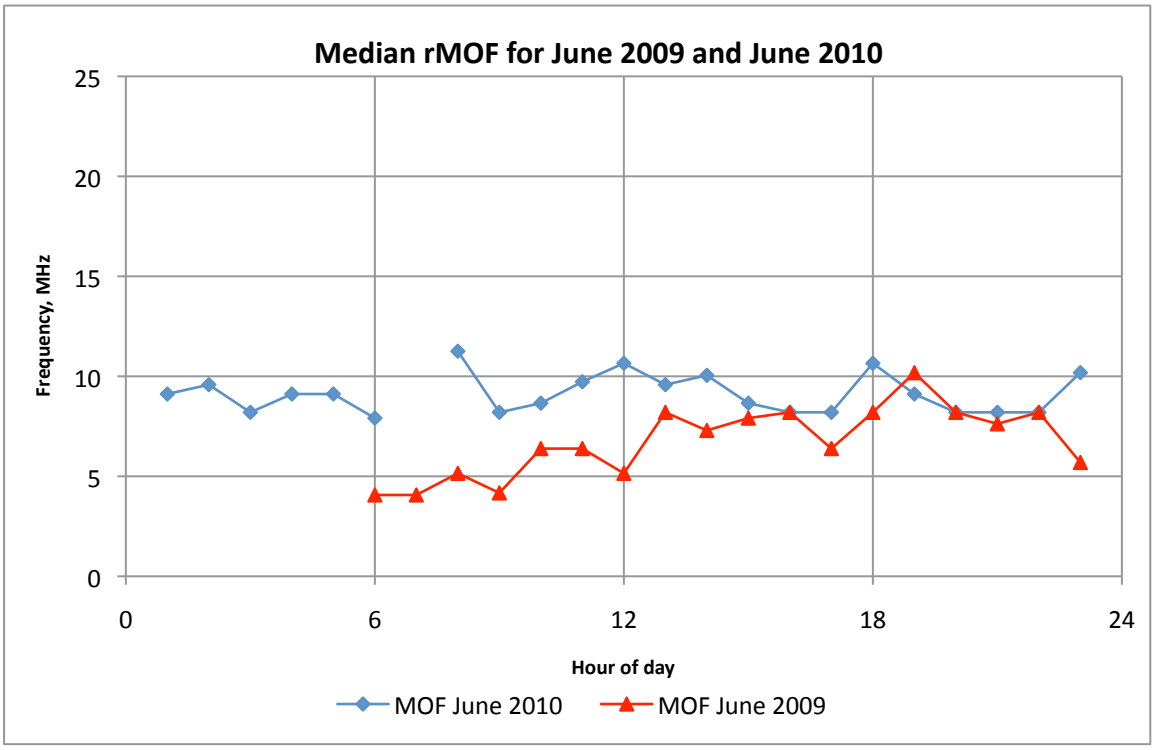

Figure 35 - Median rMOF comparison between June 2009 and June 2010

October and November show a much more even distribution of data throughput across the day, although October shows peak propagation still around local noon whereas by November it has shifted back a few hours. December and January are quite different – the peak in data throughput is now broadly in the early morning (0400-0800 UTC, i.e. 0100 – 0500 local time) with almost a minimum around local noon. February shows good data throughput at all hours, and by March the influence of local noon is

[12] MOF means Maximum Observed Frequency. In these experiments we did not have frequency coverage of the whole HF band, so the term "restricted MOF" (rMOF) is used to refer to the maximum frequency observed in this experiment.

beginning to re-emerge, although there is still a respectable volume of data throughput overnight.

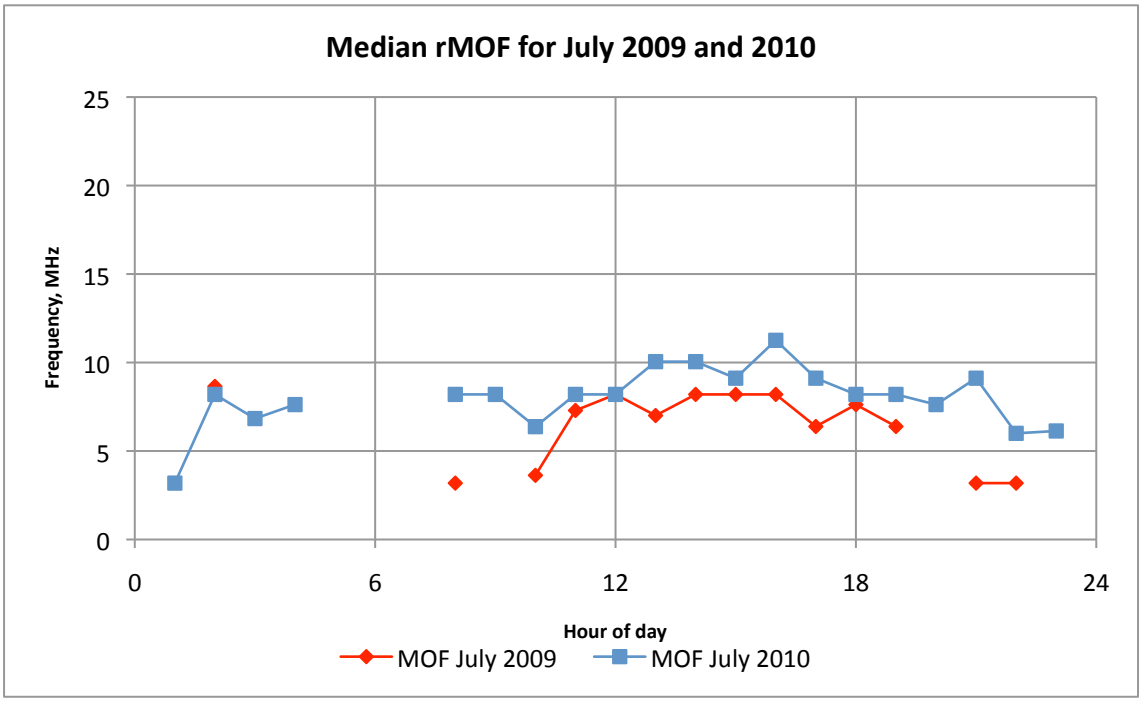

Figure 36 - Median rMOF comparison between July 2009 and July 2010

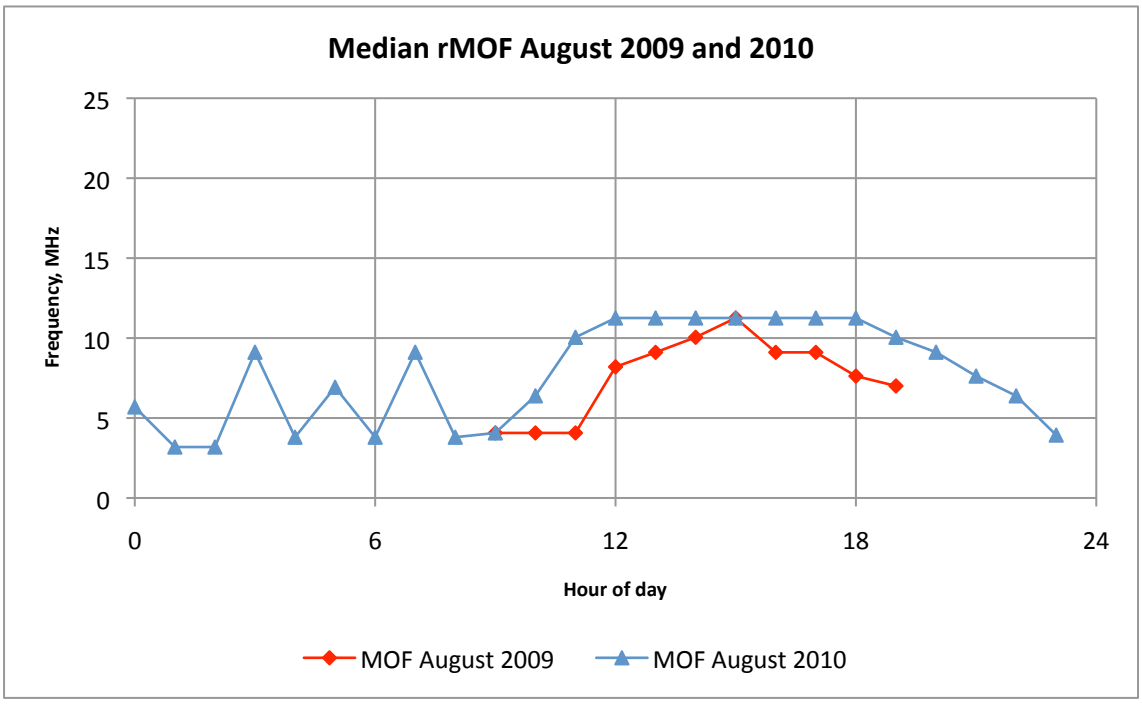

Figure 37 - Median rMOF comparison between August 2009 and August 2010

6.3.2. T-index

An oblique propagation experiment such as this would ideally be carried out in conjunction with ionosondes and riometers in order to relate the observed propagation to the state of the ionosphere. Unfortunately, the ionosonde and riometer at Halley research station are in storage whilst the station is rebuilt, and there are no other instruments close to the Halley-Rothera circuit.

As an alternative, the Antarctic region T-index has been used to give some indication of the state of the ionosphere. This index is compiled by the Ionospheric Prediction Service (IPS) in Sydney, Australia, and is based on ionosonde data from several Antarctic ionosondes in the Australian and New Zealand sectors of Antarctica. The T-index is derived from comparing historical observations of the monthly median of the daily noon value for FoF2 from a large number of ionosondes with the Zurich twelve month smoothed monthly sunspot number, known as R12 (Turner 1968). R12 is used as

the initial estimate of the T-index and then an iterative technique is used: a straight line is fitted to the data (T-index against FoF2) by the least-squares method and the residuals used to adjust the values of the T-index for the next iteration. IPS have calculated the relationship between T-index and FoF2 for all ionosondes with at least ten years of available data. A separate calibration is calculated for each hour of the day in each calendar month. Having done these calibrations, they are then used to convert the FoF2 data from each ionosonde into T-index. Multiple stations may then be combined by a process of weighted averages to give a regional or global T-index for any given hour. These T-indices are used by IPS in order to make predictions of optimum working frequencies – a higher T-index means higher frequencies may be used.

Two caveats exist with the Antarctic T-index in particular: the data availability from the ionosondes is often patchy, and the automatic FoF2 scaling algorithm used copes poorly with spread-F, which is commonly encountered in Antarctica. The ionosondes contributing to the data are at Scott Base, Mawson, Davis, Casey and Macquarie Island.

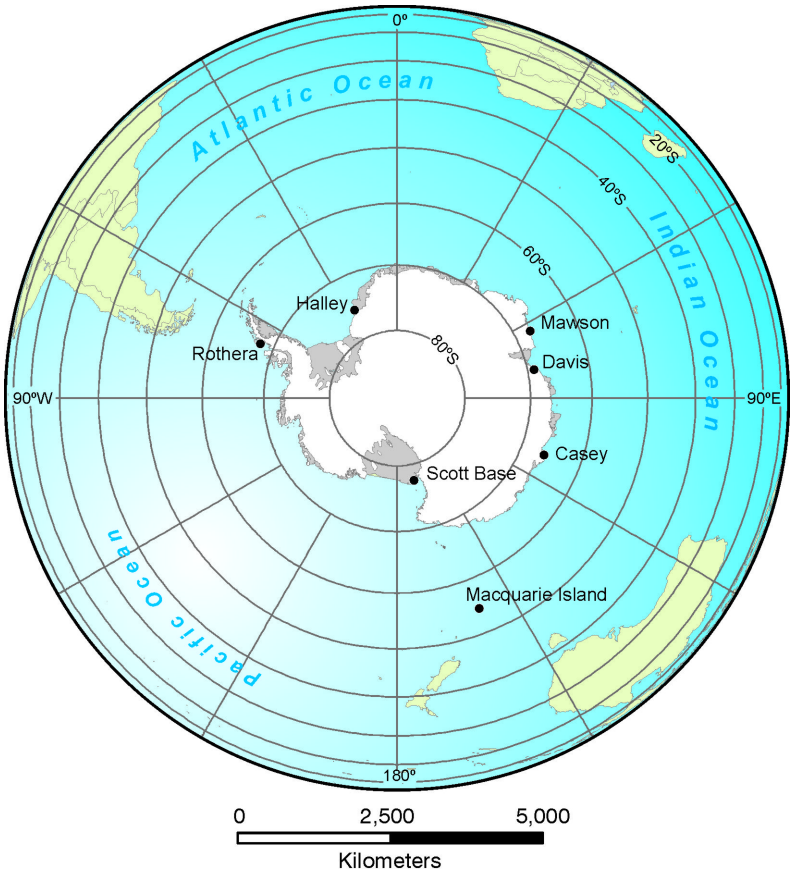

Figure 38 - Map showing the locations of the stations contributing to the T-index and their position relative to Rothera and Halley. Cartography by Peter Fretwell, reproduced by kind permission of the British Antarctic Survey.

Despite these drawbacks, plotting the daily T-index variation against the variations in Halley-Rothera throughput shows some clear correlations. The months of March and May 2010 are illustrated here as they provide the clearest examples. Higher T-index corresponds to higher values of FoF2 and hence should correspond to higher working frequencies for the circuit. Data throughput should increase with higher levels of ionisation because operating at higher frequencies reduces ionospheric absorption. It may also provide a more consistent channel with less fading.

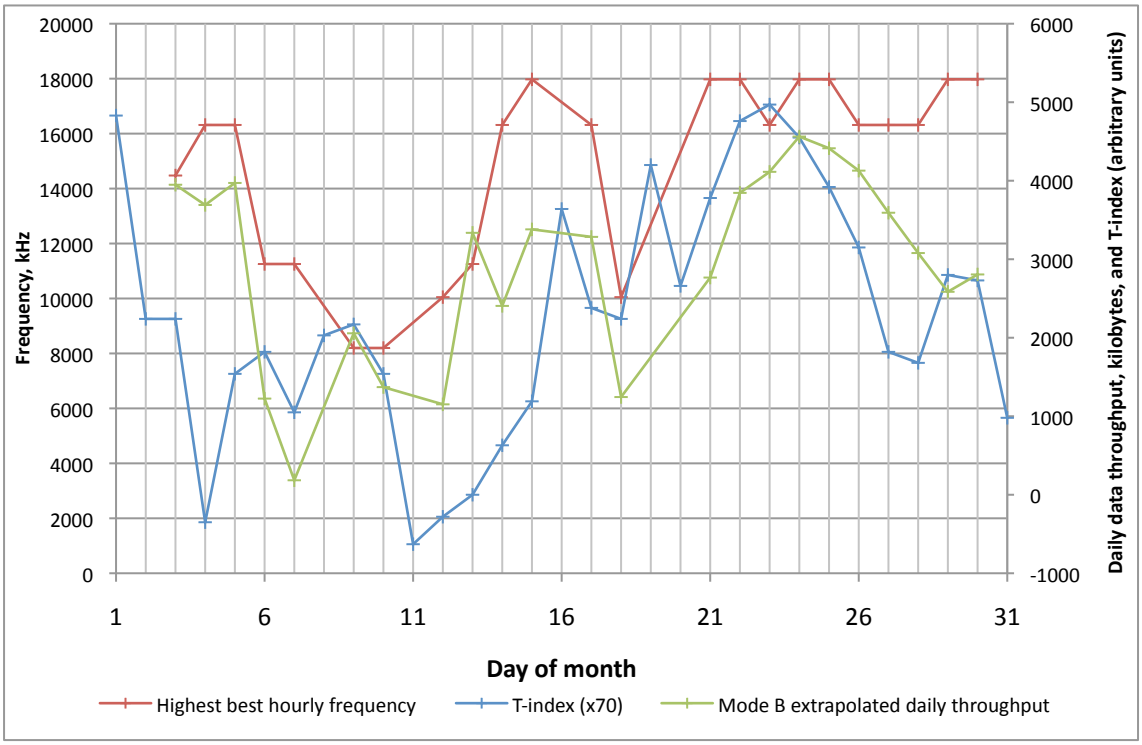

Figure 39 - variation of T-index, highest best hourly frequency and throughput for days during March 2010. Daily data throughput is calculated based on the performance of the best performing (i.e. highest throughput) frequency in each hour. The highest value of the best-performing hourly frequency each day is plotted as the red trace.

As Figure 39 shows, during the latter part of March 2010 (16th onwards), the throughput and highest best-performing hourly frequency follow the same general trend as the T-index but a day behind. This lag may be explained by the fact that the stations contributing to the T index are at UTC+8 through to UTC+12 whereas the circuit is at UTC-3. If the variations in the propagation conditions are caused by variations in solar radiation, the fact that the ionosonde stations are at least twelve hours offset from Rothera may cause them to measure the same solar influence on a different calendar day. Considering Figure 40, we again see the T-index value leading the data throughput during the period 4th – 12th May. However, the relationship is more complex than in

March: from the 1st-4th May we see the data throughput falling despite a rise in T-index and operating frequency. This may be the result of complex ionospheric phenomena, such as polar patches, causing localised variations in the ionosphere. However, given the unreliability of the Antarctic T-index data, it is only possible to draw tentative conclusions from these observations.

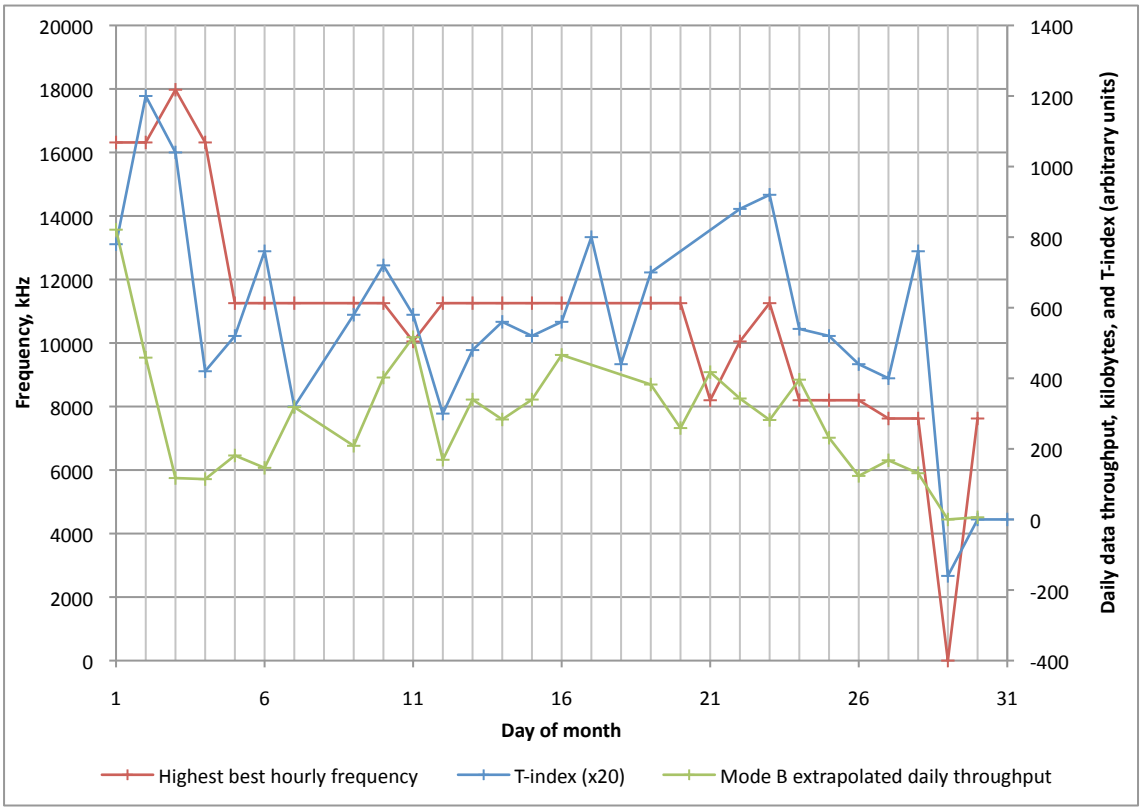

Figure 40 - variation of data throughput with T-index for May 2010

6.3.3. Best performing frequencies

Table 19 shows a monthly breakdown of the link's performance by hour and by frequency. The numbers shown in the table are the number of valid days for which that particular frequency performed best during that particular hour. The row and column totals show therefore the number of days on which communication was achieved at that particular time or the number of hours on which communication was possible on that

particular frequency. This data can be used to select primary, secondary and tertiary frequencies for future communications on this particular circuit.

Table 19 - performance of the link by hour and frequency for each month

Jul-09	2272	3186	3800	4067	4553	5150	6386	7623	8198	9106	9115	10049	11255	14475	16315	17975	23250	Total
0																		
1																		
2								1	1									2
3																		
4																		
5																		
6																		
7																		
8		1																1
9																		
10				1					1									2
11							1											1
12		1					1	1	2									5
13				2			1	1	1									5
14				2			4	1	6	1								14
15				1			7		5	1			1					15
16				1			6	3	3									13
17				2		1	8	1		1								13
18		1					2	1										4
19							2											2
20																		
21																		
22																		
23																		
Total		3		9		1	32	9	19	3			1					77
Aug-09	2272	3186	3800	4067	4553	5150	6386	7623	8198	9106	9115	10049	11255	14475	16315	17975	23250	Total
0																		
1																		
2																		
3																		
4																		
5																		
6																		
7																		
8																		
9				1														1
10																		
11		1		1														2
12							2											2
13								1	2									3
14									3									3
15							2		1	1								4
16								1	2									3
17							2			1								3
18							3											3
19							2											2
20																		
21																		
22																		
23																		
Total		1		2			11	2	8	2								26

Sep-09	2272	3186	3800	4067	4553	5150	6386	7623	8198	9106	9115	10049	11255	14475	16315	17975	23250	Total
0								1	1	1								3
1							1	1	1									3
2							2											2
3				1			1											2
4				1			1											2
5		1																1
6				1														1
7				1			1											2
8				1			1											2
9							2			1								3
10							1		1	1								3
11							2		1									3
12							2											2
13							1					1						2
14												1	1					2
15									1				1					2
16												1	1					2
17							1		1									2
18							1						1					2
19												1	1					2
20							1		1									2
21							1					1						2
22									1			1						2
23									1			1						2
Grand Total		1		5			19	2	9	3		7	5					51

Oct-09	2272	3186	3800	4067	4553	5150	6386	7623	8198	9106	9115	10049	11255	14475	16315	17975	23250	Grand Total
0				1			1		1			1	1					5
1								3	1			1						5
2							1	1	3									5
3							2		2	1								5
4				2				1	1									4
5				1			2	1										4
6						1	1											2
7							4		1									5
8							1		3									4
9								1	3	1								5
10									1	3			1					5
11							1		1			1	2					5
12							2						3					5
13							1					1	3					5
14										1			4					5
15												1	3	1				5
16							1		1				2					4
17									1			1	2					4
18									1			1	2					4
19							1						3					4
20							1	1	1				1					4
21							2	2										4
22							2					2						4
23							1	1				2						4
Grand Total				4		1	24	11	21	6		11	27	1				106

Nov-09	2272	3186	3800	4067	4553	5150	6386	7623	8198	9106	9115	10049	11255	14475	16315	17975	23250	Grand Total
0									1									1
1									1									1
2											1							1
3														1				1
4											1							1
5												1						1
6									1									1
7											1							1
8									1									1
9									1									1
10									1									1
11											1					1		2
12											1					2		3
13												1				1	1	3
14											2				1	1		4
15									1		2					1		4
16											2	1				1		4
17									1		1		1		1			4
18												1	1		1	1		4
19									1			1	1			1		4
20											1	1	1			1		4
21							1		1			2						4
22									1			2	1					4
23											2			2				4
Grand Total							1		11		15	10	5	3	3	10	1	59
Dec-09	2272	3186	3800	4067	4553	5150	6386	7623	8198	9106	9115	10049	11255	14475	16315	17975	23250	Grand Total
0									2		5	1						8
1									1		3		2	1	1			8
2								1	3		1		1	2	2			10
3									1		1	1			4	2		9
4									1			1	2		3	2		9
5									1			1	1		1	5		9
6											1		1		2	5		9
7									1			1			5	2		9
8												1	1		3	4		9
9									2		1		2		3			8
10									1		1	1	2	1	1	1		8
11							1		2		1		1	1		2		8
12									1				2	1	4			8
13								2	1			1	1			2		7
14									2		1	2	1			1		7
15									1			1	2		1	1		6
16								1				1	3			1		6
17													4			1		5
18													5		1			6
19													4		1			5
20												1	4					5
21								1	1			2	1		1			6
22								1			2	1	2	1		1		8
23								2	3		1		1					7
Grand Total							1	8	24		18	16	43	7	33	30		180

Jan-10	2272	3186	3800	4067	4553	5150	6386	7623	8198	9106	9115	10049	11255	14475	16315	17975	23250	Grand Total
0									1		1				1	1		4
1								1	1					1	2			5
2								1	1					3		1		6
3									1					1	3			5
4									1					3	3			7
5									1					3	3			7
6								1						4	2	1		8
7									2					4	2			8
8											1			2	4			7
9												1		4	3			8
10									2					1	2			5
11													1		3			4
12															3	1		4
13															3	1		4
14											1				2	1		4
15															2	2		4
16															3	1		4
17													1		2	1		4
18									1				1		2			4
19									1				1		2			4
20									1						3			4
21													1		1			2
22									1			1		2	1			5
23								1					1		1			3
Grand Total								4	14		3	2	6	28	53	10		120

Feb-10	2272	3186	3800	4067	4553	5150	6386	7623	8198	9106	9115	10049	11255	14475	16315	17975	23250	Grand Total
0											1	2			1			4
1								2	1						1			4
2								2	1			1						4
3								3	1									4
4								1	2			1						4
5									3			1						4
6									2			2						4
7								1	1		1	1						4
8								1	2				1					4
9								1	3									4
10									2			2						4
11									1		1	2						4
12									2		1	1						4
13									2				1		1			4
14								1					1		2			4
15									2					1	1			4
16									4									4
17								1	3									4
18								3	1									4
19								2	1			1						4
20									4									4
21								1	2		1							4
22								1	3									4
23								2	1		1							4
Grand Total								22	44		6	14	3	1	6			96

Mar-10	2272	3186	3800	4067	4553	5150	6386	7623	8198	9106	9115	10049	11255	14475	16315	17975	23250	Grand Total
0								9	7		1		3		1			21
1								14	3			2	1	1				21
2								11	6		1		1					19
3								11	3		1							15
4								9	5									14
5								6	2									8
6								4	2									6
7								5	1									6
8								10	3									13
9								8	10				1					19
10								1	8		4	2	5					20
11							1	1	9		2	1	4		2			20
12								1	4		2	3	4		6			20
13									8			2	2		5	3		20
14								2	2		1	4	2	1	4	4		20
15								2	4			3	1	1	9	2		22
16								2	4			2	2		10	2		22
17								4	7		3	4	2		2			22
18								5	8		1	2	3		4			23
19								6	6		1	3	3					19
20								5	5		1	3	7					21
21								9	6		1	2	3					21
22								10	7			2	3					22
23								7	7		2	1	2					19
Grand Total							1	142	127		21	36	49	3	43	11		433

Apr-10	2272	3186	3800	4067	4553	5150	6386	7623	8198	9106	9115	10049	11255	14475	16315	17975	23250	Grand Total
0																		
1									1									1
2								1										1
3									1									1
4																		
5								2										2
6																		
7																		
8																		
9																		
10								2										2
11							1	5	5			1	1					13
12									3			3	5					11
13									4			2	3		2			11
14									6				1		3	1		11
15									2			1	1		6			10
16									4			1	1		4			10
17								1	3		1		3	1	1			10
18								2	2			2	4	1				11
19								3	3		2	5						13
20								3	6		1	3						13
21							1	2	3		1	1						8
22								4	3									7
23								2										2
Grand Total							2	27	46		5	19	19	2	16	1		137

May-10	2272	3186	3800	4067	4553	5150	6386	7623	8198	9106	9115	10049	11255	14475	16315	17975	23250	Grand Total
0																		
1															1			1
2																		
3															1			1
4																		
5																		
6																		
7																		
8									1									1
9																		
10									1									1
11								1				2						3
12							1	7	4			3						15
13								5	6		3	4	4					22
14								4	3		1	6	9					23
15								4	4			6	5		4			23
16								3	5		4	2	9		2	1		26
17								10	7			4	3		1			25
18							1	9			1	2	2	2				17
19							1	3	2		2		1					9
20							1		1			1						3
21																		
22																		
23																		
Grand Total							4	46	34		11	30	33	2	9	1		170

Jun-10	2272	3186	3800	4067	4553	5150	6386	7623	8198	9106	9115	10049	11255	14475	16315	17975	23250	Grand Total
0																		
1									1									1
2									1									1
3									1									1
4												1						1
5									2			1						3
6								1	1									2
7																		
8									1									1
9								1	1									2
10					1		1		3		1							6
11							1	1	2									4
12								1	1			1						3
13								3	1			2						6
14				1			1	3	4		1				1			11
15							2	5	5			2						14
16							5	1	1			2						9
17							1	3	2			2						8
18								2	3			1	1					7
19								2	3									5
20							1	3	1									5
21									3									3
22							1		1									2
23									1			1						2
Grand Total				1	1		13	26	39		2	13	1		1			97

Because of the long range of HF signals and the lack of a coordinating authority for HF frequency use in Antarctica, interferering signals are a common problem in Antarctic HF communications. The presence of an interferer would explain the relatively poor performance of some frequencies (e.g. 7623 during September and October 2009) when compared with adjacent ones.

Table 20 summarises the dataset still further, giving recommended frequencies for each month and details of the best time of day to try and communicate. During the austral summer (November – March) communications are possible at all hours of the day, whereas during the austral winter months the circuit is only available for part of the day. Communication between Rothera and Halley by HF during the austral summer has been considered "difficult" according to anecdotal evidence from radio operators and pilots, and this table gives a partial explanation. BAS's typical working frequencies for aircraft operations are 5080, 7775 and 9106kHz, whereas the optimum frequencies for December and January identified by this study are much higher: 11255, 14475 and 16315kHz. This table has already been made available to the radio operators at Rothera and Halley and should hopefully help them to make good decisions about working frequencies in the future.

Table 20 - recommended frequencies for Halley-Rothera

Month	Time of day (**bold means best chance of communicating)**	Primary	Secondary	Others to try
January	**0000 - 1000**	16315	14475	8198
	1000 - 1700	16315	17975	8198
	1700 - 0000	16315	11255	8198
February	All hours	8198	7623	10049
March	All hours (though best **1000 - 1900**)	7623	8198	11255, 16315, 10049
April	**1100 - 2300**	8198	7623	10049, 11255
May	**1200 - 2000**	7623	8198	10049, 11255
June	All hours, though best **around 1500**	8918	7623	6386, 10049
July	**1100 - 1800**	6386	8198	7623, 4067
August	**1200 - 1900**	6386	8198	7623, 4067, 9106
September	**0900 – 2100**	6386	8198	10049
October	**1000 – 0000**	11255	6386	10049
	0000 – 1000	8198	7623	6386, 4067, 10049
November	**1100 – 0000**	9115	17975	10049
	0000 – 1100	8198	9115	10049, 14475
December	All hours	11255	16315	17975, 8198

6.3.4. Volume of data transferred

One of the key questions to be answered by this study is whether an HF link can carry sufficient data to be useful for practical applications. Table 21 shows the mean daily data throughput (using WinDRM mode B) for each month, which has then been multiplied by the number of days in each month to get an estimate of the expected total throughput for the month. The standard deviation figures reflect a large day-to-day variation in the data throughput, and some monthly figures are extrapolated from small numbers of days. The reason for not simply using the total actual data recorded is because most months have significant gaps in the data set.

As can be seen, the highest daily throughput figures are in the austral summer, as expected, and the estimated total adds up to around 400MB per year. Given that a magnetometer produces around 300MB of raw data per year, and that straightforward gzip data compression will reduce that by about 50%, it seems reasonable that the system would support at least two magnetometers from a single base station, assuming that there was sufficient power available to keep the communications link running. Automatic weather stations produce far less data – around 3MB each per year – and so this system could easily service BAS's entire network of weather stations.

Year	Month	Number of valid days	Mean daily mode B throughput, kilobytes	Standard deviation of daily mode B throughput (n-1 method), kilobytes	Mean value extrapolated up to a full month, megabytes
2009	July	21	98	125	3.0
	August	23	12	30	0.4
	September	18	64	198	1.9
	October	5	147	56	4.5
	November	4	1183	754	35.8
	December	10	2215	1279	67.0
2010	January	8	1303	1310	39.4
	February	4	4257	391	128.9
	March	23	2919	1211	88.4
	April	16	659	505	19.9
	May	27	282	175	8.5
	June	22	40	54	1.2
				Annual total	399.0

Table 21 - estimating the total annual throughput

However, the results in Table 21 are based only on the use of Mode B. If adaptive mode switching is used, it should be possible to obtain additional throughput by using Mode E during times when the conditions are not good enough for Mode B to work.

Table 22 - showing the throughput obtained by using both mode B and mode E

Year	Month	Number of valid days	Mean daily throughput, using both modes B and E, kilobytes	Standard deviation of daily throughput, (n-1) method, kilobytes	Mean extrapolated up to a full month, megabytes
2009	July	21	105	143	3.2
	August	23	12	31	0.4
	September	18	127	402	3.8
	October	5	152	55	4.6
	November	4	1310	767	39.7
	December	10	2374	1371	71.9
2010	January	8	1400	1312	42.4
	February	4	4449	282	134.7
	March	23	3016	1195	91.3
	April	16	749	539	22.7
	May	27	331	177	10.0
	June	22	53	67	1.6
				Annual total	426.1

In fact, as Table 22 shows, the gains from doing so are quite modest, and the largest relative improvements are in the spring and autumn. It may prove useful to consider adding a higher data rate mode (such as Mode B with 16QAM) to the system to get as much throughput as possible out of the austral summer period when the best propagation conditions are available.

6.3.5. Comparison of maximum observed frequencies with predictions from VOACAP

The results in this section are analysed on a different basis from those presented in previous sections: this analysis treats the data link as a crude oblique sounder rather than a communications system. The plots that follow are based on finding the maximum observed frequency (rMOF, see page 94) on which the signal could be identified (i.e. the highest frequency at which the modem would synchronise) rather than the best working frequency in terms of successful data throughput. This has been done in order

to give comparisons with numerical models of ionospheric behaviour and propagation predictions based on historical ionosonde data. The plots that follow (Figures 41-52) show (in blue) the median value of the rMOF for each hour of the day in each month. For comparison purposes, they also show (in red) the predicted Maximum Usable Frequency (MUF) produced by the numerical modelling package VOACAP (Lane 1993). If the modelling is realistic, the rMOF should be similar to (or slightly less than) the MUF. An rMOF exceeding the MUF indicates that the model has underestimated the level of ionisation at the circuit reflection point.

The analysis was run using VOACAP method 20, using CCIR coefficients and smoothed monthly sunspot numbers.

In fact, an examination of the plots reveals that only in one month does VOACAP produce predictions that match up with the observed data: in August 2009 (see Figure 42). For all the other months we see that VOACAP underestimates the level of ionisation at some times of day. Its performance is worst during the austral summer (November – February) when it predicts a lack of diurnal variation, presumably as a result of the constant solar irradiance.

Although the rMOF data is of some interest in its own right (given the paucity of published data on HF propagation in Antarctica), the main result from this section is that VOACAP does not represent a good model for forecasting predictions of propagation on this circuit.

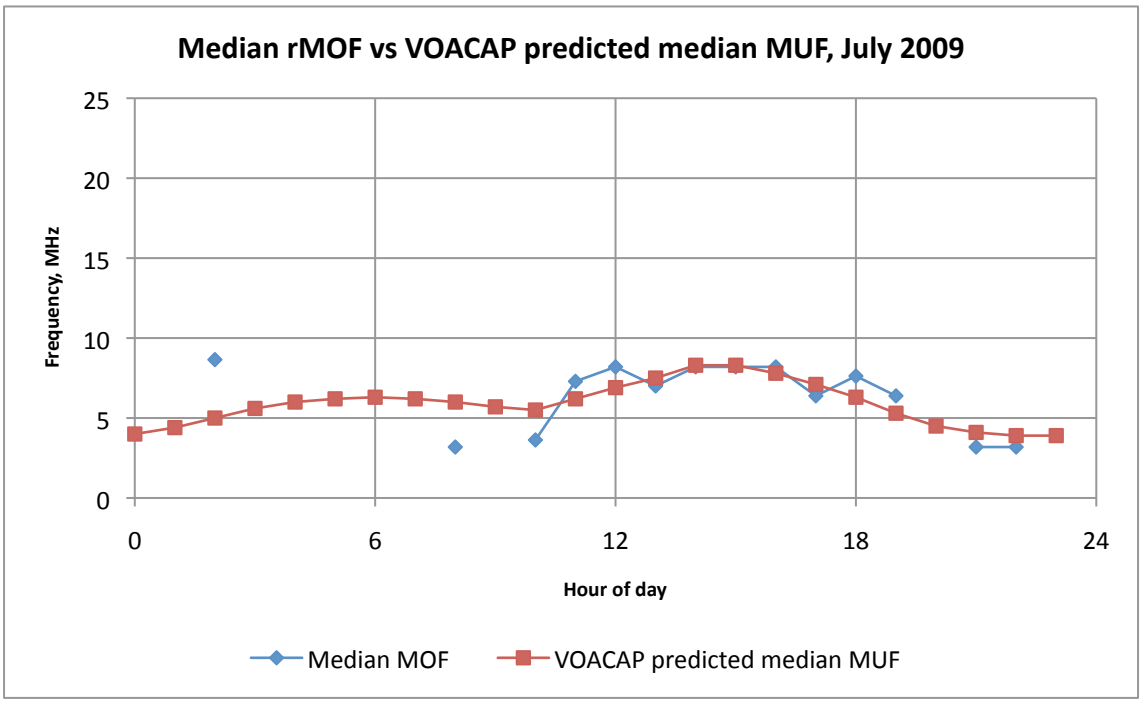

Figure 41 - Median rMOF vs VOACAP predicted median MUF for July 2009

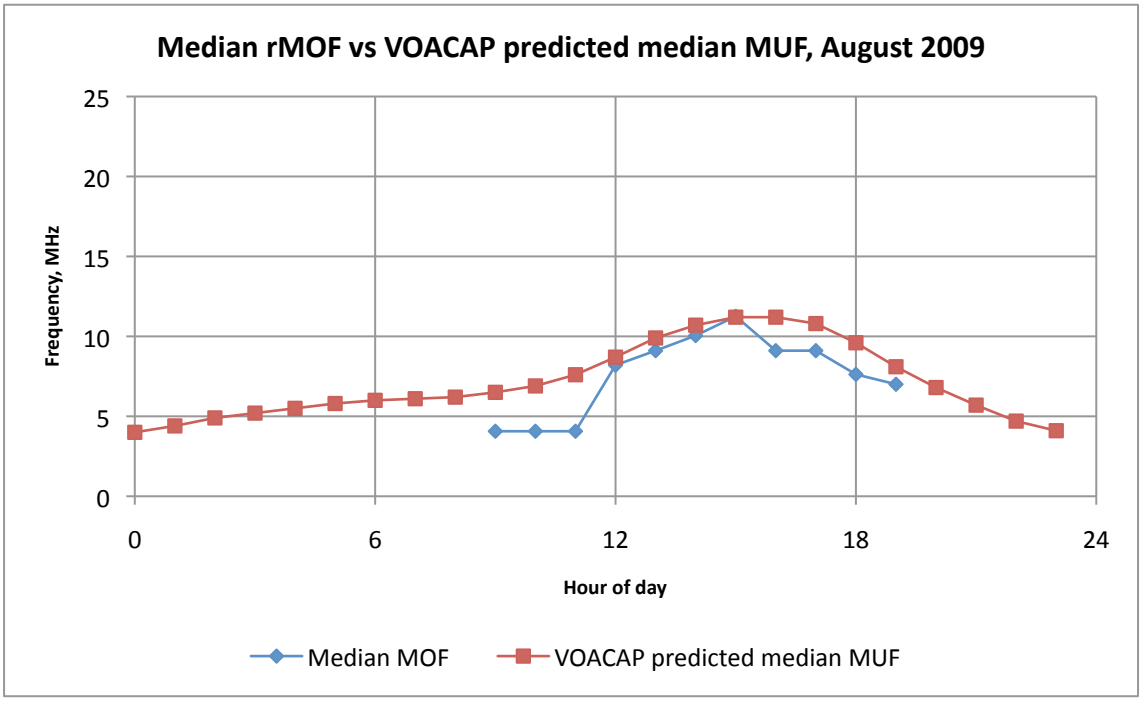

Figure 42 - Median rMOF vs VOACAP predicted median MUF for August 2009

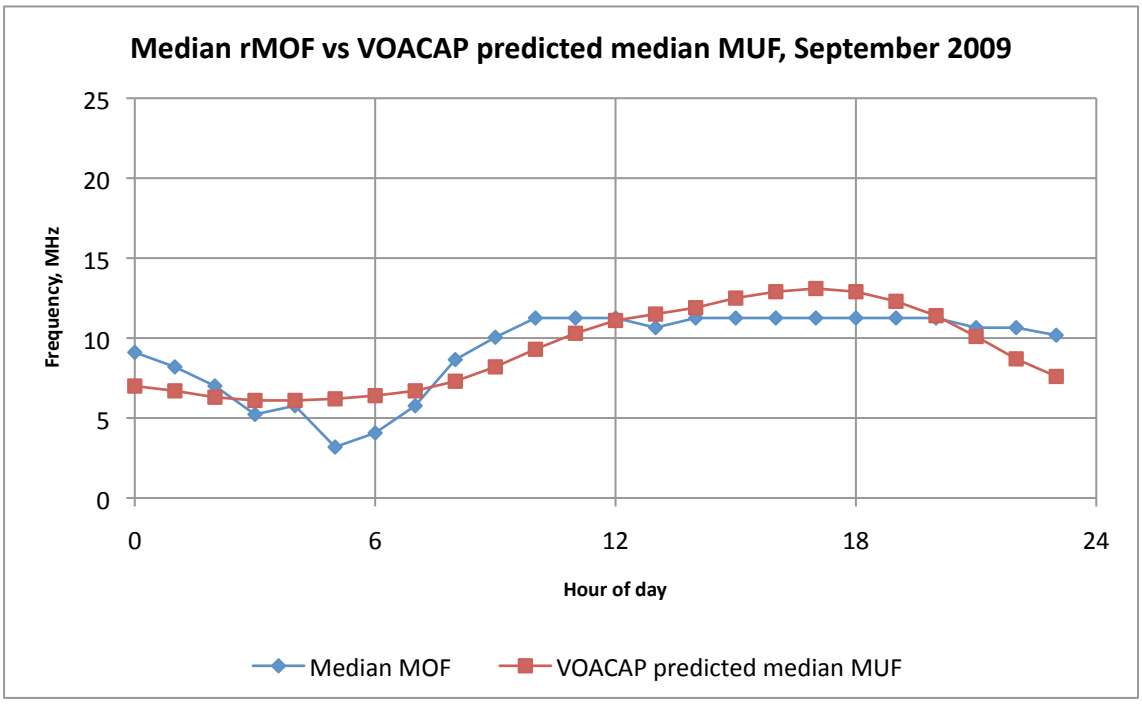

Figure 43 - Median rMOF vs VOACAP predicted median MUF for September 2009

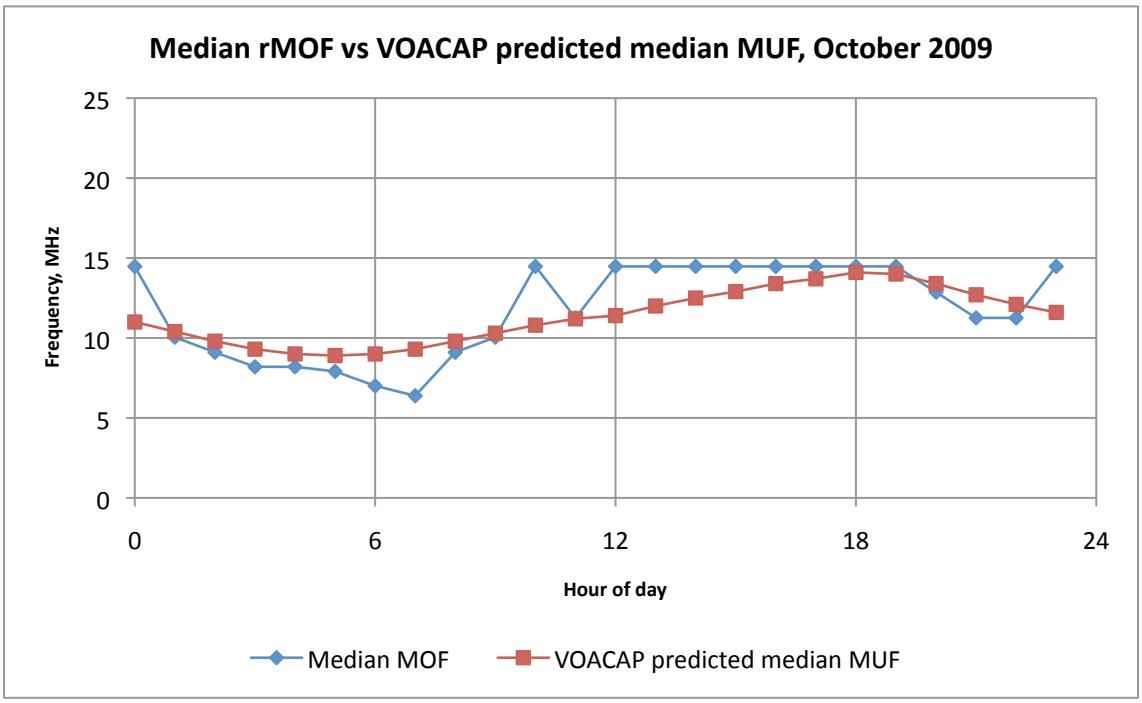

Figure 44 - Median rMOF vs VOACAP predicted median MUF for October 2009

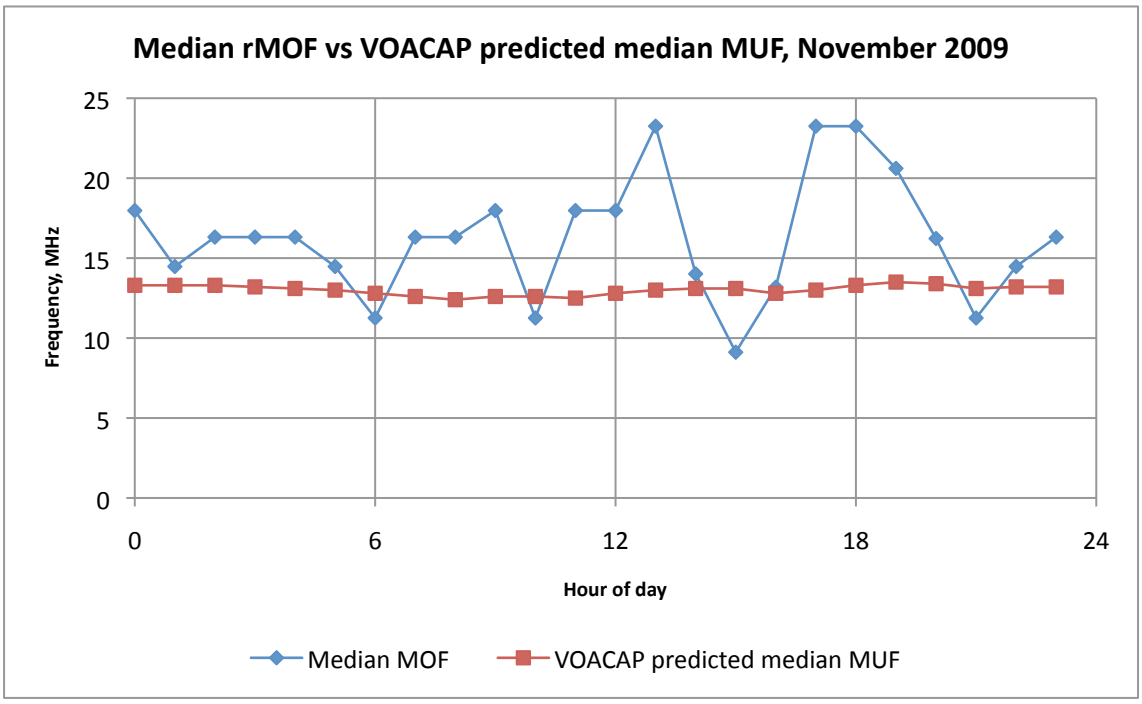

Figure 45 - Median rMOF vs VOACAP predicted median MUF for November 2009

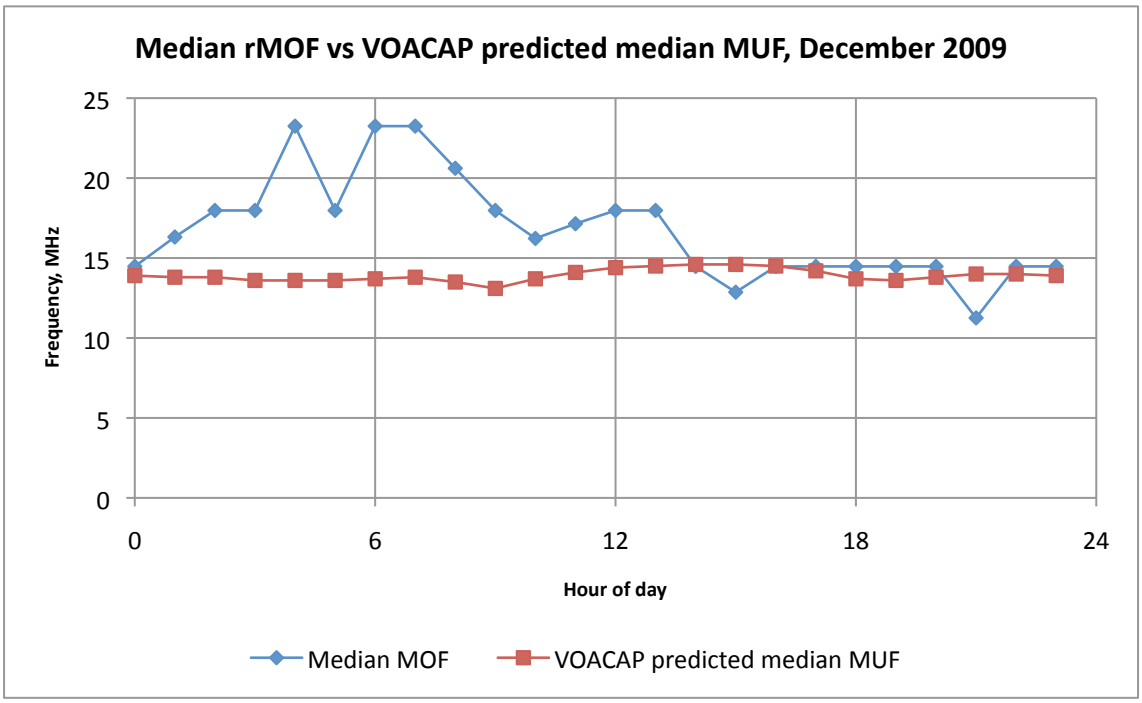

Figure 46 - Median rMOF vs VOACAP predicted median MUF for December 2009

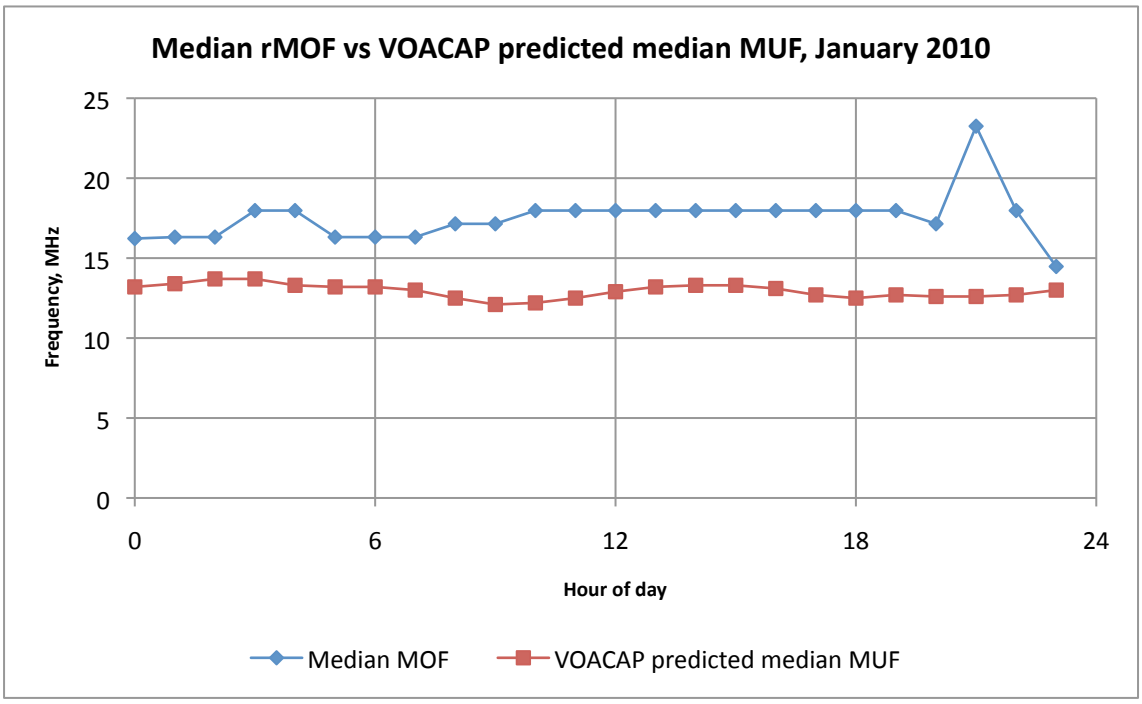

Figure 47 - Median rMOF vs VOACAP predicted median MUF for January 2010

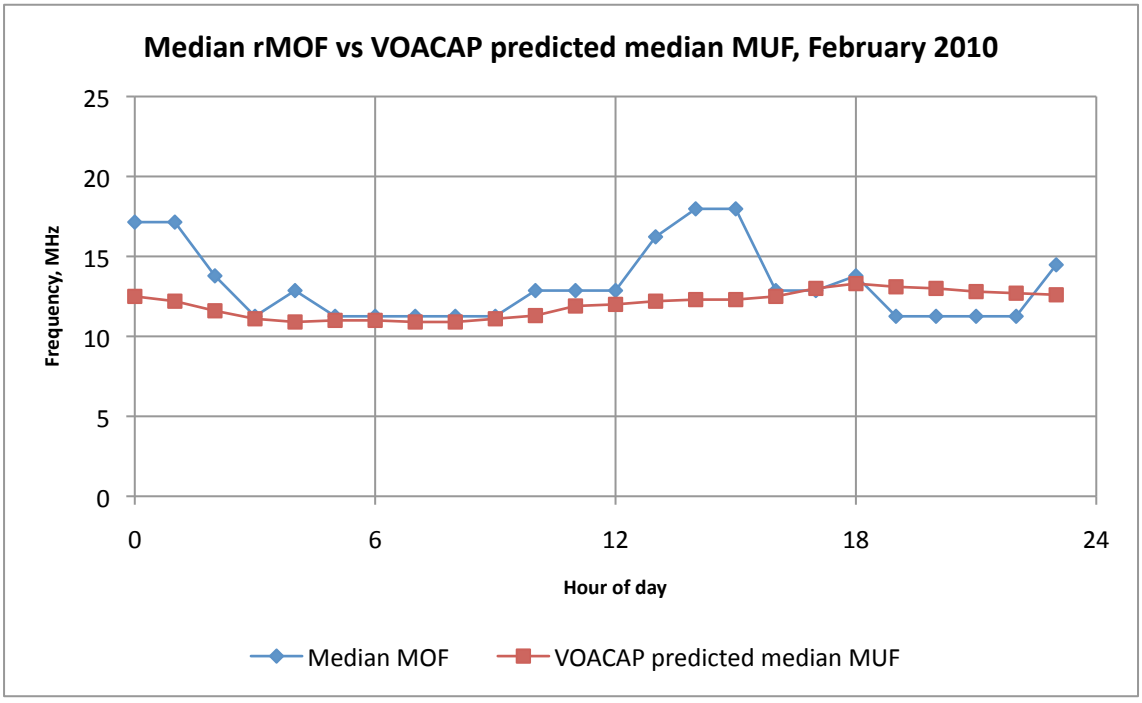

Figure 48 - Median rMOF vs VOACAP predicted median MUF for February 2010

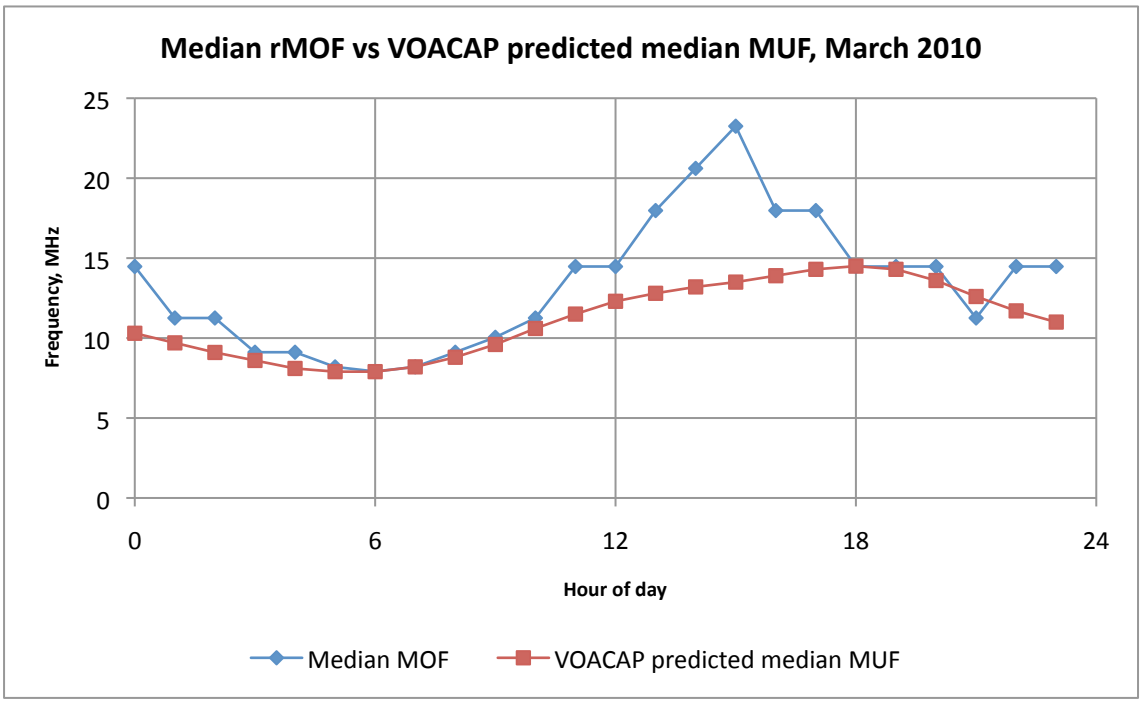

Figure 49 - Median rMOF vs VOACAP predicted median MUF for March 2010

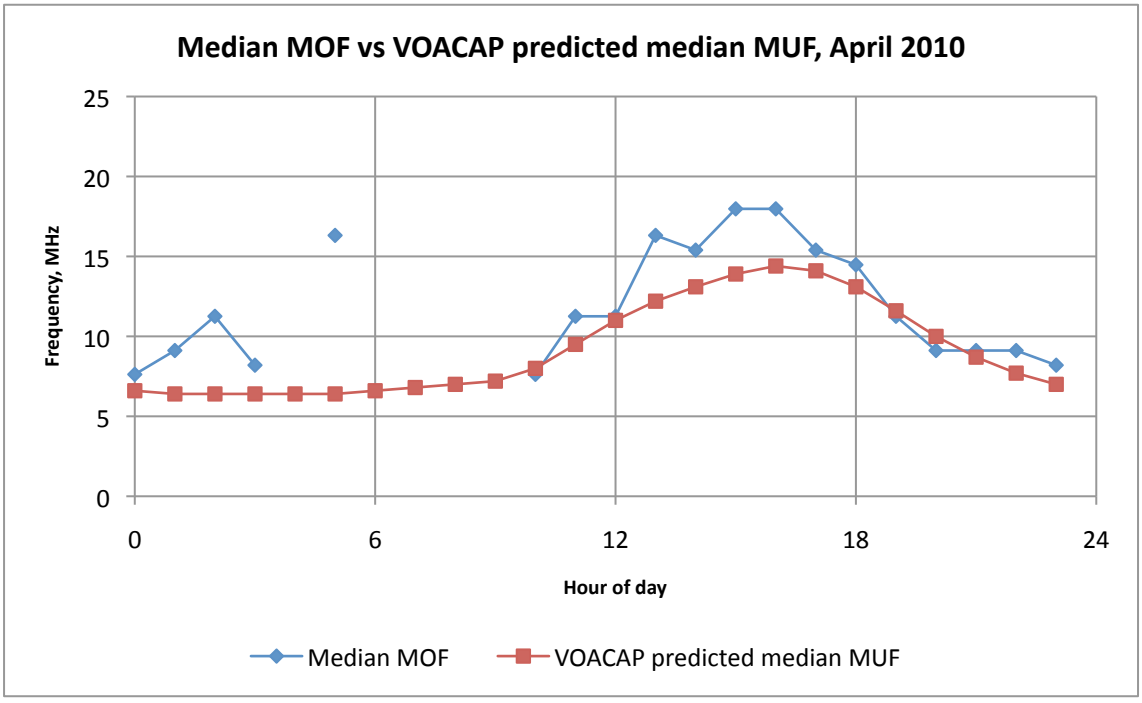

Figure 50 - Median rMOF vs VOACAP predicted median MUF for April 2010

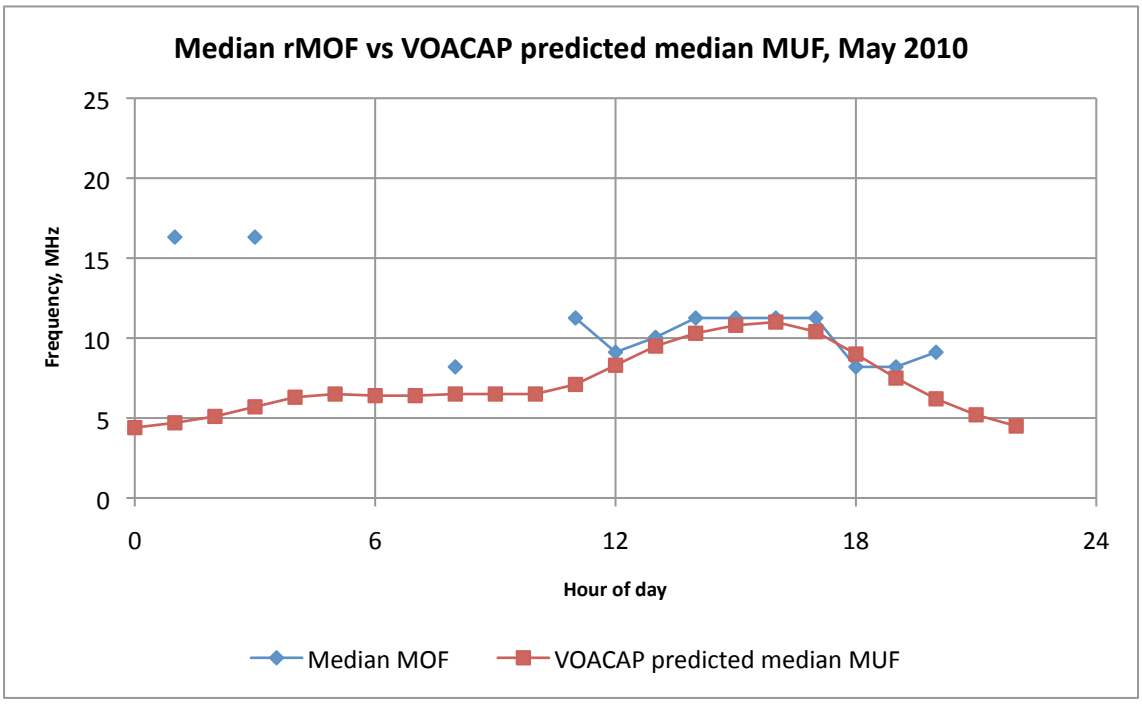

Figure 51 - Median rMOF vs VOACAP predicted median MUF for May 2010

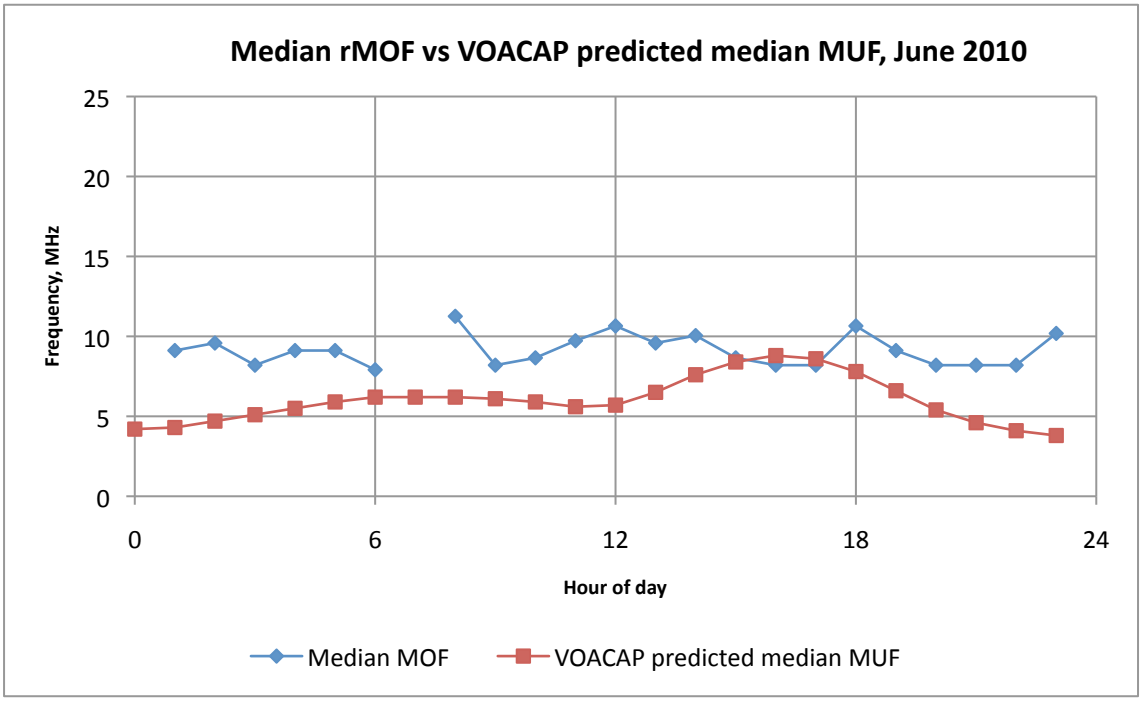

Figure 52 - Median rMOF vs VOACAP predicted median MUF for June 2010

6.3.6. Impulse response and spectrum

WinDRM provides a certain amount of diagnostic data in receive mode about the state of the incoming signal and the behaviour of the receiver algorithms. From September 2009 onwards, the version of WinDRM used on the Halley-Rothera experiment was modified to record the estimated impulse response of the signal (which is produced as part of the equalisation process) and also the received signal spectrum. The resolution of this data is quite coarse, and only limited conclusions may be drawn from it. The specrum data has a frequency (x-axis) resolution of ~23Hz per point, and so can be used to see large-scale effects such as frequency-selective fading, but cannot be used to determine the Doppler shift or spread affecting the individual carriers. Similarly, the impulse response data has a time (x-axis) resolution of ~0.5ms per point, meaning that only very coarse multipath effects may be seen. However, some illustrative example plots are included here to show the features of this dataset.

Figure 53 is an example of an impulse response, selected because it shows a distinct multipath effect. The spacing between the two peaks is around 1.7ms, which would correspond to a path difference for an EM wave in free space of around 500km. This kind of path difference on the 1600km Halley-Rothera circuit could be produced by 3-hop propagation, although in the absence of any ionosonde data this cannot be proven. The effect is, however, very short-lived – within a few seconds (see Figure 54) the distinctive second peak has disappeared. Some multipath activity is producing a broad peak in both responses, but the data lacks the resolution to distinguish between the individual propagation modes.

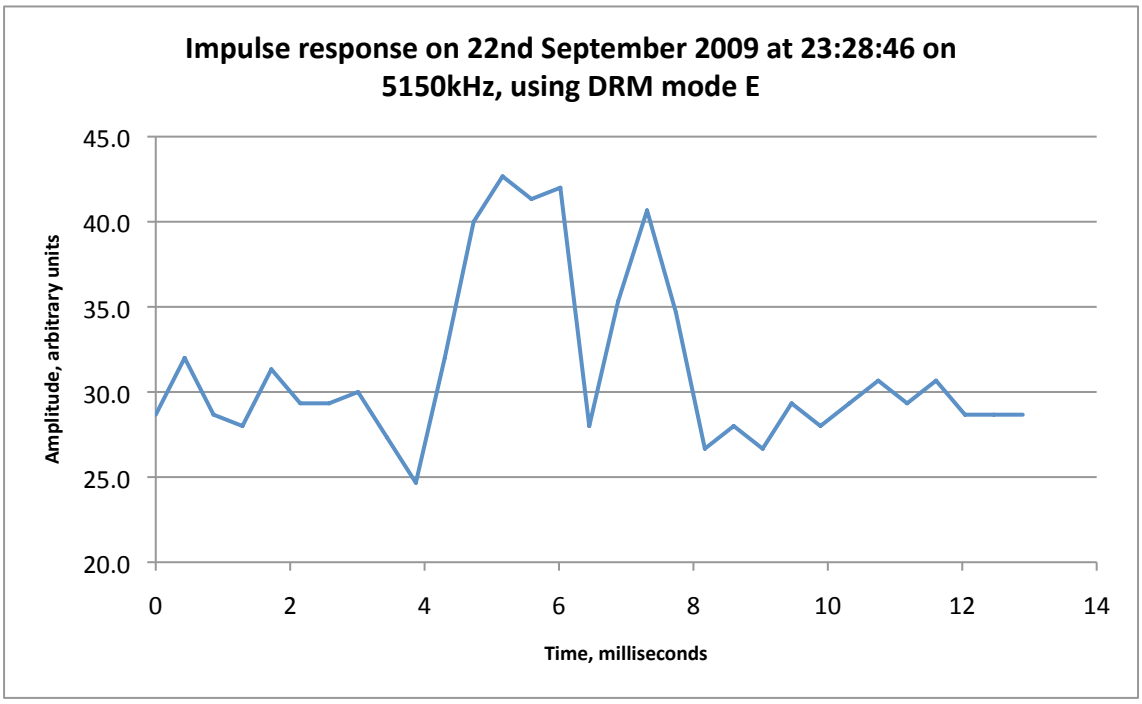

Figure 53 - an example impulse response where multi-hop propagation can be seen

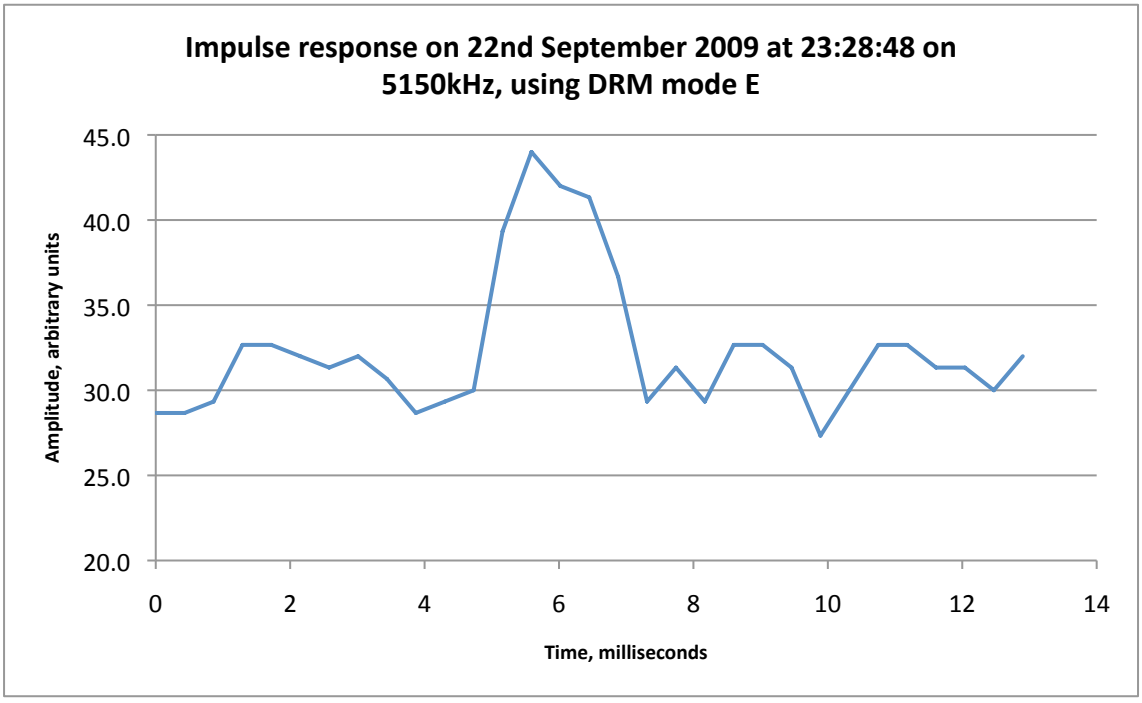

Figure 54 - the impulse response a few seconds later

An example of the spectrum data is given in Figure 55. In this particular example, the constant-amplitude "frequency pilot tones" can be seen clearly at 725, 1475 and 1850Hz. Note that the spectrum runs from DC to 3kHz, but the signal starts at 350Hz and finishes at 2850Hz. A more typical spectrum, where the frequency pilots are not clearly distinct from the modulated data carriers, is shown in Figure 56.

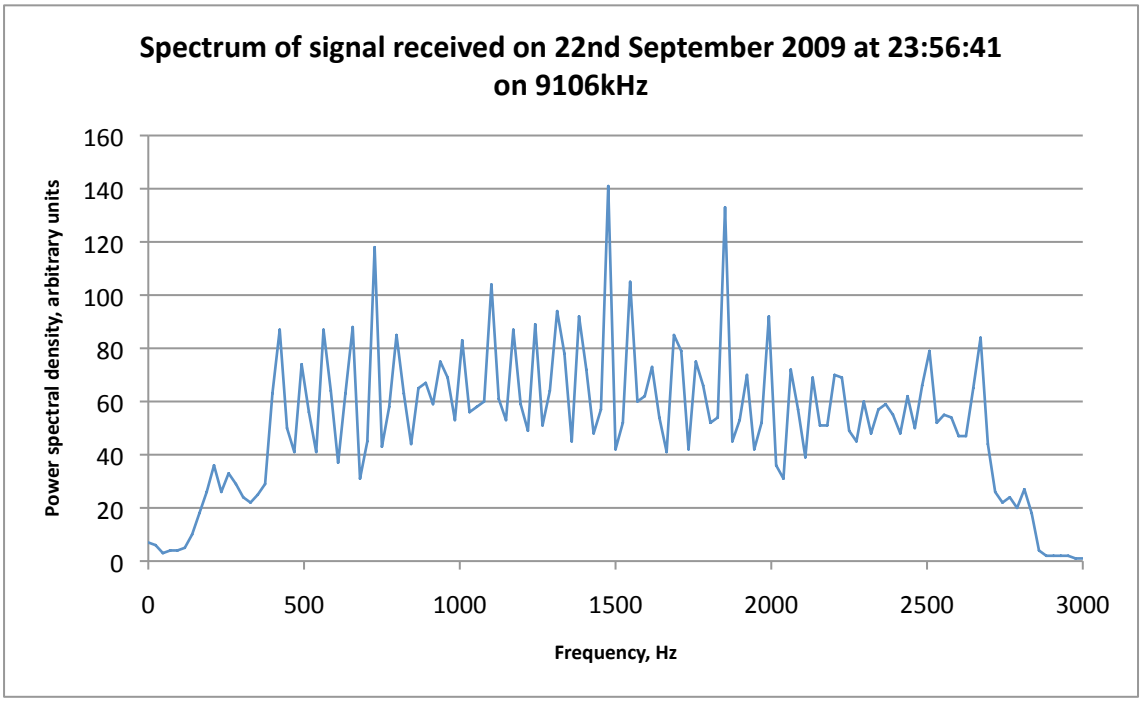

Figure 55 - spectrum received at Rothera, showing clearly the three frequency pilot tones at 725, 1475 and 1850Hz. The spectrum runs from DC to 3kHz, but the signal starts at 350Hz and stops at 2850Hz, giving a bandwidth of 2500Hz.

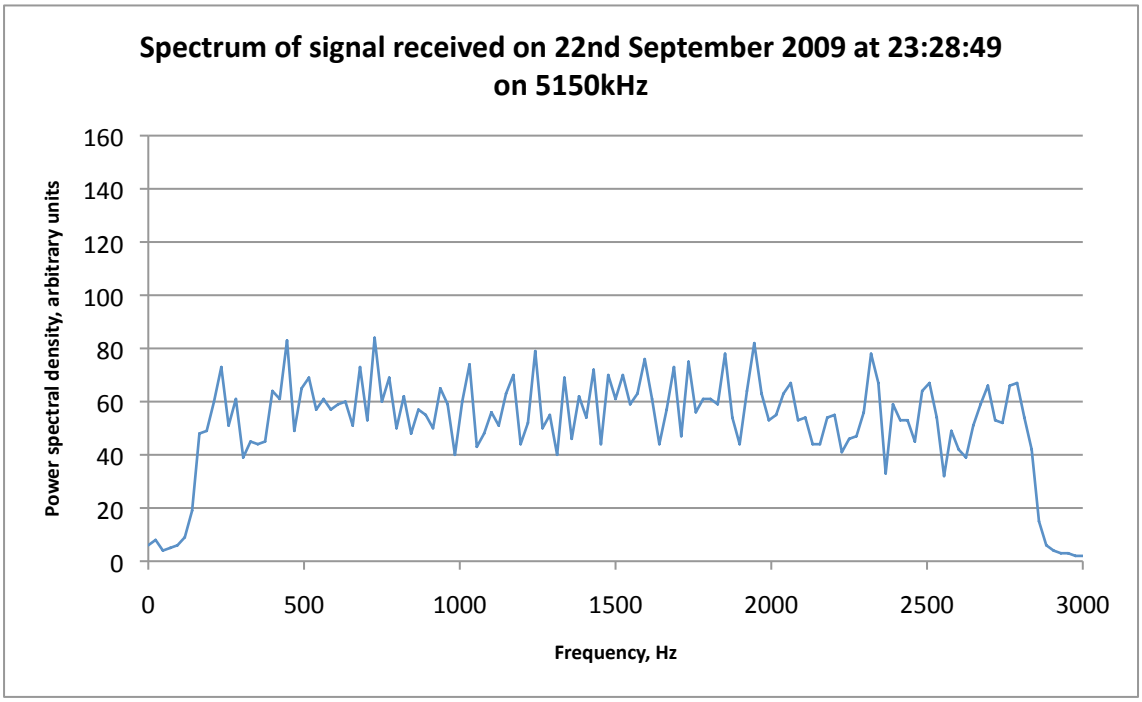

Figure 56 - a more typical received spectrum (this is the spectrum that corresponds to the impulse response in Figure 54). Note that the frequency pilots are not distinct from the modulated carriers.

6.4. Discussion

6.4.1. Data throughput

The results presented in Section 6.3 show that HF may be used to convey a useful volume of data over a significant distance in Antarctica. In particular, its performance exceeds that of the meteor-burst system mentioned in Section 2.2.4. The meteor-burst system achieved an annual data throughput of around 10MB, over a 1400km link using 150W transmitters. This compares with the 400MB that could be achieved (based on the estimates of Table 21) on HF over a similar range (1600km) and using less transmit power (100W PEP transmitters backed off to around 10W RMS).

Comparing with satellite, 400MB of airtime annually would have cost around $23,000 on Iridium dialup or $2,800 using Iridium OpenPort.

6.4.2. Implications for system design

The disparity between the very high throughputs available in the austral summer and the much lower volumes in the winter will mean that most instruments will need to change the way that they report depending on the time of year. In winter the instruments will have limited power availability, since battery capacity is reduced in the extreme cold and solar panels will be in darkness. Given that the propagation conditions are also poor during this period, many instruments may choose not to report at all, or only to report a brief "all systems OK" and perhaps a summary of their current data. Once the summer comes and power and propagation conditions are more favourable, the instruments can then start sending their backlog of data to the base stations. As a consequence, it may prove that enhancing the peak capacity in the austral summer (through the use of higher order modulation, for example) may actually make a much larger contribution to the usefulness of the system than attempting to increase the performance in wintertime.

6.4.3. Effect of the sunspot cycle

The sunspot cycle has a profound effect on the behaviour of HF communications systems: higher sunspot numbers around solar maxima are associated with increased levels of ionisation in the E and F regions, but also bring enhanced auroral activity and lead to more frequent occurrences of PCA events and other dynamic phenomena. The present measurements were made close to a solar minimum, and in fact close to one of the lowest solar minima in recorded history[13], so consideration should be given to how the system will perform over the full solar cycle.

The smoothed sunspot numbers for the period of the experiment are given in Table 23.

[13] The lowest smoothed sunspot number in 2009 was 1.7 – only three other solar minima have been lower since records began in 1749: 1913 (1.5), 1823 (0.1) and 1810 (0). Data from NOAA, see footnote to Table 23 for details.

Table 23 - Smoothed sunspot numbers for the period of the on-air tests. Data from NOAA[14].

Month	Smoothed Sunspot Number
June 2009	2.7
July 2009	3.6
August 2009	4.8
September 2009	6.2
October 2009	7.1
November 2009	7.6
December 2009	8.3
January 2010	9.3
February 2010	10.6
March 2010	12.3
April 2010	14
May 2010	15.5
June 2010	16.4
July 2010	16.7
August 2010	17.4

Predicting the performance of the system at other stages of the sunspot cycle is difficult given the lack of ionosonde data for the period studied. Increasing sunspot numbers should lead to higher electron densities in the ionosphere. This will allow higher operating frequencies and also the possibility of link availability during times of day that do not support propagation when the ionisation levels are low. With higher

[14] ftp://ftp.ngdc.noaa.gov/STP/SOLAR_DATA/SUNSPOT_NUMBERS/INTERNATIONAL/smoothed/

frequencies comes lower absorption and hence better SNR for the same transmit power. However, the effects of auroral region enlargement, more frequent PCA events and the increased dynamic behaviour in the ionosphere is likely to produce interruptions to communications and may also lead to increased levels of Doppler and multipath spread. To give some concrete examples, data is presented from the Halley ionosonde, collected during the solar maximum of 1970 and the solar minimum of 1976. The plots show the median MUF for a 3000km circuit centred on Halley: this is a standard analysis technique (K. Davies 1990, 172) based on applying the critical frequency and height of the F2 layer (FoF2) to the 3000km transmission curve (see section 3.2.4 for details of transmission curves).

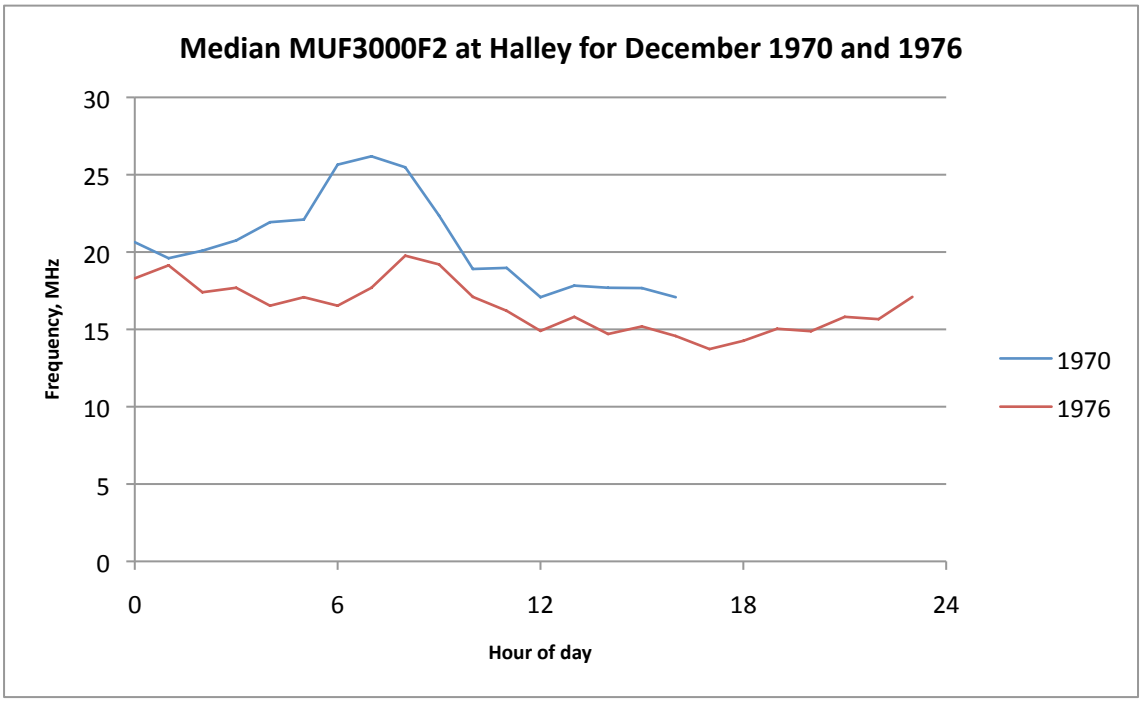

Figure 57 - Diurnal variation in median MUF3000F2 for December 1970 (sunspot maximum) and 1976 (sunspot minimum) at Halley

Figure 57 shows the plot for the month of December, the austral midsummer. It can be seen that the MUFs are much higher during the 1970 solar maximum than during the 1976 solar minimum, going as high as 26MHz in the mornings. The lack of data for the

later part of the day in 1970 is as a result of the ionograms being too complex to scale: the dataset contains FoF2 values for this period but no corresponding M3000F2 values. Since finding M3000F2 requires the virtual height of the F2 layer, it seems likely that range spread on the ionogram prevented the observer from finding the virtual height. This data suggests that an HF communications system operating in this region during the austral summer in a solar maximum year would benefit from the higher operating frequency (and hence SNR) in the early part of the day, but might suffer losses due to multipath and Doppler spread in the evening and overnight.

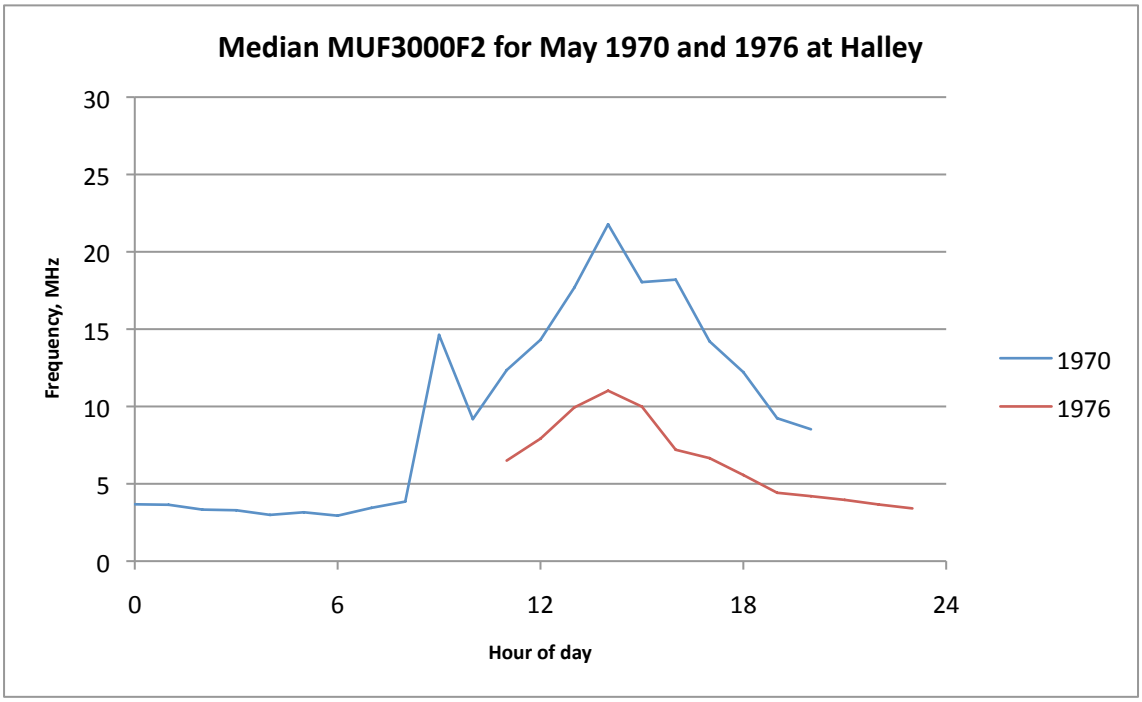

Figure 58 - Diurnal variation in median MUF3000F2 for May 1970 (sunspot maximum) and 1976 (sunspot minimum) at Halley

Now considering the austral winter, Figure 58 shows the data for the month of May. Again we can see much higher MUFs for the solar maximum year (1970), but in this case we can see that during the solar minimum year (1976), propagation only appears possible in the afternoon and evening of each day: the median FoF2 frequencies during this month are as low as 1 MHz in the late evening. Since ionosondes typically have a

minimum operating frequency of 1MHz, it may be that the FoF2 was too low to be measured by the ionosonde overnight and in the morning. By contrast, during the solar maximum year propagation was possible (albeit on very low frequencies) right through the night. Again, the gap in the 1970 data in the evenings after 2000 is caused by a lack of M3000F2 figures, again probably due to range spread on the ionograms.
It seems likely therefore that HF communications would be possible for longer each day during the austral winter at solar maximum than at solar minimum.

6.4.4. Implications for channel simulator design

The channel simulator described in chapter 5 is designed to show the performance of a modem in a set of channels with a range of different impairments. What it leaves out (quite deliberately) in its design is the largest factor affecting point-to-point HF communications: whether there is sufficient ionisation at the path midpoint to support communications on the circuit at any of the frequencies available for use. For a system where the data is not especially time-sensitive (most scientific telemetry falls into this category, with the notable exception of weather stations giving hourly reports to the World Meteorological Organisation), it is always possible to wait for a more favourable time of day in order to communicate, rather than to try and force a signal through a poor channel using the full panoply of sophisticated modulation and coding techniques (and quite possibly a great deal of transmit power).
A more detailed future study of HF communications in Antarctica could be conducted using oblique-sounding methodology, measuring Doppler spread and multipath directly in the manner of the DAMSON sounders described in section 3.2.8. This would be able to tie more closely into the existing channel simulator work than the on-air tests described in this chapter can, as without the Doppler and multipath spread

measurements, it is difficult to identify the channel conditions and correlate them to modem performance.

7. Conclusions and further work

7.1. Summary of outcomes

- A high-latitude HF channel simulator has been produced, drawing on existing work from the Radio Systems research group at Leicester, and used to conduct a series of modem performance tests.
- Military HF modem standards intended for use at mid-latitudes have been tested in the high-latitude simulator. MIL-STD-188-110B provides good performance on the majority of the simulator's channels at speeds of 1200bits/s and an SNR of 15dB.
- WinDRM, an OFDM-based software modem, was also tested in the simulator and found to perform satisfactorily but not as well as 110B under the same conditions. Its high peak-to-average-power ratio means that it will not be as power-efficient as 110B.
- On-air tests were conducted over a 1600km link between Halley and Rothera stations in Antarctica, using WinDRM. The results show that data can be transferred year-round, but the volume of data supported by the propagation conditions is very much higher in the austral summer.
- Estimates made from the results of the on-air tests suggest that an HF data communications system could handle a total annual throughput of around 400MB, which is considerably more than a meteor burst system operated under similar conditions. This is sufficient throughput to be useful in collecting data from autonomous instruments that produce a low volume of data, such as weather stations.

7.2. Recommendations

From an operational perspective it would seem that HF is best suited to serving multiple low-volume instruments (each producing <50MB/year), such as weather stations. Some of these low-volume instruments currently report via Iridum dial-up or ARGOS at considerable expense, so HF could result in significant cost savings. Anyone looking to rapidly implement an HF communications system would do well to consider buying off-the-shelf modems compatible with MIL-STD-188-110B.

For medium volume applications (<500MB/year), OpenPort may turn out to be a better choice. The OpenPort terminals are not particularly expensive (£3000) and can deliver much higher data rates than HF (up to 128kbit/s) while consuming about the same amount of power (100W). This permits a power-limited installation to complete its communications quickly and then power down the terminal, keeping power consumption (and hence battery and generating capacity) down. The cost of the OpenPort airtime would be offset by the reduction in demand for aircraft time, and the additional benefits of adding two-way communications of any kind to autonomous instruments are considerable:

- reduced uncertainty over instrument failure and hence reduced logistical costs
- instruments may be visited only when snow accumulation or faults require it, rather than every year, reducing costs and freeing aircraft time for other work
- the ability to process data as it comes in rather than as an annual block
- the ability to make changes to an instrument's configuration or firmware whilst deployed in the field

7.3. Future work

7.3.1. Channel simulator

The channel simulator has proved a useful tool, and it would be valuable to other members of the HF community. It would therefore be desirable to fully document it (independently of this thesis) and release it to the community under some form of free-for-non-commercial-use licence. It may also benefit from feature improvements. In particular, moving to a real-time architecture would make the simulator more versatile. This would permit an incoming waveform to be accepted as an audio stream and the output waveform generated as an audio stream in real time from the pre-calculated channel. Once this architecture is implemented, the simulator could then easily be made duplex, allowing the testing of modems with ARQ layers.

7.3.2. OFDM modes for polar HF circuits

Work on more rugged OFDM modes could certainly be continued, although the Halley-Rothera propagation study suggests that they might be of limited use on that circuit. However, the Halley-Rothera circuit is subauroral, and it may well be that more rugged modes are required for transauroral circuits (Halley – South Pole, for example).
It is clear from the results of the Halley-Rothera study that the bulk of the annual throughput is obtained in the austral summer (February alone makes up 30% of the annual total) and so making the best use of this period is clearly important. Faster and less robust modes should be tried, together with adaptive mode switching techniques in order to change mode based on the present state of the channel. It would also be of great value to try some of the peak-to-average-power ratio reduction strategies proposed in the literature to see what impact they have on the performance of OFDM in high-latitude HF channels.

7.3.3. FEC and ARQ

Another potentially valuable area of research is in FEC and ARQ techniques, something not touched on in this research, which is important in terms of keeping the link efficiency high. Both WinDRM and MIL-STD-188-110B use convolutional codes, whose performance has now been surpassed by Turbo-codes and low-density parity check (LDPC) codes, so research into implementing these codes on HF channels could potentially yield benefits in terms of higher throughputs or reduced power consumption. Improvements to ARQ would also be very valuable, since a lot of time may be wasted retransmitting packets in fading channels. In particular, switching to the use of a rateless code (such as the Raptor or Online codes) rather than the traditional cyclic redundancy check (CRC) would greatly simplify the ARQ process. Rateless codes can produce an arbitrary number of packets to be transmitted, and the receiver has to collect enough of them to decode the file. It does not matter exactly which packets are received, as long as there are a sufficient number of them. The overhead on Raptor codes is 0.2% (i.e. the receiver must receive 0.2% more data than the original file to be transmitted) and given the time overhead on turning around a half-duplex HF link, adding a few extra rateless code packets to any given transmission would improve link efficiency considerably. Rateless codes had been considered early in this project, but appeared to be subject to a great deal of secrecy and patent protection and so it was decided not to pursue them.

7.3.4. Propagation studies

Further propagation studies would be valuable, particularly on transauroral circuits such as Halley-South Pole, to give an indication as to whether more rugged modes are needed for these more demanding circuits. Since these experiments were carried out close to solar minimum, repeating the experiments as the sun becomes more active would also be very revealing.

Bibliography

Angling, M.J., and N.C. Davies. 1999. “An assessment of a new ionospheric channel model driven by measurements of multipath and Doppler spread.” In *Frequency Selection and Management Techniques for HF Communications (Ref. No. 1999/017), IEE Colloquium on*, p. 4/1-4/6.

———. 1997. “On an ionospheric channel simulator driven by measurements of multipath and Doppler spread.” In *Propagation Characteristics and Related System Techniques for Beyond Line-of-Sight Radio (Ref. No. 1997/390), IEE Colloquium on*, p. 4/1-4/6.

Angling, Matthew J. et al. 1998. “Measurements of Doppler and multipath spread on oblique high-latitude HF paths and their use in characterizing data modem performance.” *Radio Science* 33(1): p. 97–107.

Armstrong, J. 1999. “Analysis of new and existing methods of reducing intercarrier interference due to carrier frequency offset in OFDM.” *Communications, IEEE Transactions on* 47(3): 365-369.

Armstrong, J, P.M. Grant, and G. Povey. 1998. “Polynomial cancellation coding of OFDM to reduce intercarrier interference due to Doppler spread.” In *IEEE GLOBECOM 1998, 8-12 Nov. 1998*, IEEE GLOBECOM 1998 (Cat. NO. 98CH36250), Sydney,NSW, Australia: IEEE, p. 2771-6. http://dx.doi.org/10.1109/GLOCOM.1998.776492.

Blasi, L, and M de Simone. 1992. “A Short Wave Automatic System for Data Transmission Between Rome and the Italian Antarctic Base.” In *Proceedings of the 5th Symposium on Antarctic Logistics and Operations*, San Carlos de Bariloche, Argentina: Council of Managers of National Antarctic Programmes, p. 318-345.

Byrd, Richard E. 1931. *Little America*. G P Putnam's Sons.

Cannon, P. S. 1989. “Morphology of the high latitude ionosphere and its implications for HF communications systems.” *Communications, Speech and Vision, IEE Proceedings I* 136(1): 1-10.

Cannon, P. S. et al. 2000. “Damson HF channel characterisation-a review.” In *MILCOM 2000. 21st Century Military Communications Conference Proceedings*, p. 59-64 vol.1.

Chapman, S. 1931. “The absorption and dissociative or ionizing effect of monochromatic radiation in an atmosphere on a rotating earth.” *Proceedings of the Physical Society* 43(1): 26-45.

Cherry-Garrard, Apsley. 1922. *The worst journey in the world*. Constable and Company Ltd.

Davies, Kenneth. 1990. *Ionospheric Radio (IEE Electromagnetic Waves Series, Vol. 31)*. The Institution of Engineering and Technology.

Dudeney, J.R., R.I. Kressman, and A.S. Rodger. 1998. “Automated Observatories for Geospace Research in Polar Regions.” *Antarctic Science* 10(02): 192-203.

Elias, Peter. 1955. “Coding for Noisy Channels.” In *IRE Convention Record*, p. 37-46.

ETSI. 2009. “ETSI ES 201 980: Digital Radio Mondiale (DRM) system specification.” http://www.drm.org/uploads/media/es_201980v030101p.pdf (Accessed December 16, 2009).

Fischer, Volker. 2001. “Dream DRM Receiver” http://sourceforge.net/projects/drm/ (Accessed August 7, 2009).

Fischer, Volker, and Alexander Kurpiers. 2002. “Frequency Synchronization Strategy for a PC-based DRM Receiver.” In *7th International OFDM Workshop, 2002.* Hamburg.

Gherm, V. E. 2005. “HF propagation in a wideband ionospheric fluctuating reflection channel: Physically based software simulator of the channel.” *Radio Science,* 40, RS1001, doi:10.1029/2004RS003093

Gillespie, A. F.R, and S. E Trinder. 2006. “Analysis of multiple frequency HF networks versus single frequency token ring networks.” In *Ionospheric Radio Systems and Techniques, 2006. IRST 2006. 10th IET International Conference on*, p. 157 - 161.

Han, Seung Hee, and Jae Hong Lee. 2005. “An overview of peak-to-average power ratio reduction techniques for multicarrier transmission.” *Wireless Communications, IEEE* 12(2): 56 - 65.

Hargreaves, J. K. 1995. *The Solar-Terrestrial Environment: An Introduction to Geospace - the Science of the Terrestrial Upper Atmosphere, Ionosphere, and Magnetosphere*. Cambridge University Press.

Haselgrove, J. 1955. “Ray Theory and a New Method for Ray Tracing.” In Cavendish Laboratory, Cambridge: The Physical Society, London, p. 355. http://adsabs.harvard.edu/abs/1955phio.conf..355H (Accessed April 17, 2011).

Hunsucker, R. D., and J. K. Hargreaves. 2003. *The High-Latitude Ionosphere and its Effects on Radio Propagation*. 2nd ed. Cambridge University Press.

International Association of Geomagnetism and Aeronomy et al. 2010. “International Geomagnetic Reference Field: the eleventh generation.” *Geophysical Journal International* 183(3): 1216–1230.

ITU. 2000. “ITU-R Recommendation F.1487 : Testing of HF modems with bandwidths of up to about 12 kHz using ionospheric channel simulators.”

ITU-T. 1994. “ITU-T Recommendation X.200 : Information technology - Open Systems Interconnection - Basic Reference Model: The basic model.” http://www.itu.int/rec/T-REC-X.200-199407-I/en.

Jeffreys, Harold, and Bertha Jeffreys. 2000. *Methods of Mathematical Physics*. 3rd ed. Cambridge University Press.

Jorgenson, M.B., and K.W. Moreland. 1999. “HF Serial-Tone Waveform Design.” In *RTO IST Symposium on Tactical Mobile Communications*, Lillehammer, Norway: NATO RTO MP-26.

Kadokura, Akira et al. 2008. “Unmanned magnetometer network observation in the 44th Japanese Antarctic Research Expedition: Initial results and an event study on auroral substorm evolution.” *Polar Science* 2(3): 223-235.

Kierans, Peter, and Kerry Hanson. 2004. “New HF/MF digital maritime mobile systems.” In Geneva: ITU-R. http://www.itu.int/oth/R0A0E000023/en.

Lane, G. 1993. “Voice of America Coverage Analysis Program (VOACAP).”

Lanza, Francesco. 2004. “DRM mode "HAM" specification.” http://www.qslnet.de/member/hb9tlk/drm_h.html (Accessed December 16, 2009).

MacKay, David J. C. 2003. *Information Theory, Inference and Learning Algorithms*. 2007 ed. Cambridge University Press.

Mastrangelo, J.F. et al. 1997. “A new wideband high frequency channel simulation system.” *Communications, IEEE Transactions on* 45(1): 26-34.

Mawson, Douglas. 1914. “Australasian Antarctic Expedition, 1911-1914.” *The Geographical Journal* 44(3): 257-284.

Meyers, Michael. 2010. *CompTIA A+ Certification All-in-One Exam Guide, Seventh Edition*. 7th ed. McGraw-Hill Osborne.

Mlynarczyk, Janusz. 2011. Personal correspondence. “Ionospheric ray tracing algorithm and homing-in method.”

———. 2010. Personal correspondence. “Observation and modelling of Ismaning-Krakow DRM broadcasts.”

Mukumoto, Kaiji et al. 2005. “VHF data transmission experiments using MBC equipment conducted during the period from JARE-43 to JARE-45.” *Advances in Polar Upper Atmospheric Research* 19: 89-105.

NATO. 1989. “NATO STANAG 4285: Characteristics of 1200/2400/3600 bits per second single tone modulators/demodulators for HF radio links.”

NATO. 2000. “STANAG 5066 ‘Profile for Maritime High Frequency (HF) Radio Data Communication’.”

Otnes, R., and V. Jodalen. 2001. “Increasing the availability of medium data rates at high latitude HF channels.” In *Military Communications Conference, 2001. MILCOM 2001. Communications for Network-Centric Operations: Creating the Information Force. IEEE*, p. 437-441 vol.1.

Owren, L et al. 1959. “Arctic Propagation Studies at Tropospheric And Ionospheric Modes of Propagation.”

Panta, K. R., H. A. Suraweera, and J Armstrong. 2004. “Performance of PCC-OFDM in multipath fading channels.” In *Proc. 5th Australian Communications Theory Workshop (AusCTW 2004)*, Newcastle, Australia, p. 118-121.

Peco, C. et al. 2009. “On the diversity in multiantenna HF communications.” In *Ionospheric Radio Systems and Techniques, 2009. (IRST 2009). The Institution of Engineering and Technology 11th International Conference on*, p. 1-4.

Raab, F. H et al. 2002. “HF, VHF, and UHF systems and technology.” *Microwave Theory and Techniques, IEEE Transactions on* 50(3): 888 -899.

Rose, M.C., D.J. Maxfield, and J Junyent. 2009. “Performance of some environmental power systems in Antarctica.” *Geophysical Research Abstracts* 11(EGU General Assembly 2009).

Rishbeth, H. 1988. “Basic physics of the ionosphere: a tutorial review.” *Electronic and Radio Engineers, Journal of the Institution of* 58(6): S207 -S223.

Seaton, K.A., and J. Armstrong. 2000. “Polynomial cancellation coding and finite differences.” *Information Theory, IEEE Transactions on* 46(1): 311-313.

Smith, N. 1939. “The Relation of Radio Sky-Wave Transmission to Ionosphere Measurements.” *Proceedings of the IRE* 27(5): 332-347.

Storey, J. W. V., M. C. B. Ashley, and M. G. Burton. 1996. “An automated astrophysical observatory for Antarctica.” *Publications of the Astronomical Society of Australia* 13(1): 35-38.

Stott, Jonathan. 1998. “The how and why of COFDM.” *EBU Technical Review* (278): 43-50.

Strangeways, H. J., V. E. Gherm, and N. N. Zernov. 2002. “Simulating the digital HF multipath wideband ionospheric channel.” In *Getting the Most Out of the Radio Spectrum*, IEE Two Day Conference, London, UK: IEE, p. 42-1.

Strangeways, Hal J. 2000. “Effect of horizontal gradients on ionospherically reflected or transionospheric paths using a precise homing-in method.” *Journal of Atmospheric and Solar-Terrestrial Physics* 62(15): 1361-1376.

Strom, C., and A. Kunze. 1959. “Development Trends in USAF Global Communications Systems.” *Communications Systems, IRE Transactions on* 7(4): 241-248.

Titheridge, J. E. 1985. *Ionogram analysis with the generalised program POLAN*. Report UAG-93. University of Auckland.

Tsunoda, Roland T. 1988. “High-latitude F region irregularities: A review and synthesis.” *Reviews of Geophysics* 26(4): PP. 719-760.

Turner, J. F. 1968. “The development of the ionospheric index T”, IPS Series R Report R11.

US Marine Corps. “TRC-170 Student Handbook.” http://www.armymars.net/ArmyMARS/MARS.../Intro%20to%20TRC-170%20Student%20Handout.pdf (Accessed April 9, 2011).

Viterbi, A. 1967. “Error bounds for convolutional codes and an asymptotically optimum decoding algorithm.” *Information Theory, IEEE Transactions on* 13(2): 260-269.

Vogler, L.E., and J.A. Hoffmeyer. 1993. “A model for wideband HF propagation channels.” *Radio Science* 28(6): 1131-1142.

Warrington, E. M., A. J. Stocker, and D. R. Siddle. 2006. “Measurement and modeling of HF channel directional spread characteristics for northerly paths.” *Radio Science* 41: RS2006. doi:10.1029/2005RS003294.

Watterson, C., J. Juroshek, and W. Bensema. 1970. “Experimental Confirmation of an HF Channel Model.” *Communication Technology, IEEE Transactions on* 18(6): 792-803.

Wilkins, Hubert. 1929. “The Wilkins-Hearst Antarctic Expedition, 1928-1929.” *Geographical Review* 19(3): 353-376.

Wright, J. W., P. E. Argo, and M. L. V. Pitteway. 1996. “On the radiophysics and geophysics of ionogram spread.” *Radio Science* 31(2): 349-366.

Yates, Peter. 2008. Personal correspondence. “Digital HF Communications in Antarctica.”

Zaalov, N. Y., E. M. Warrington, and A. J. Stocker. 2003. “Simulation of off-great circle HF propagation effects due to the presence of patches and arcs of enhanced electron density within the polar cap ionosphere.” *Radio Science*, 38, 1052, doi:10.1029/2002RS002798